2017-08-18

Optimizing Industrial Consumer Demand Response Through DIsaggregation, Hour-Ahead Pricing, and Momentary Autonomous Control

Ahmed Abdulaal
University of Miami, a.abdulaal@umiami.edu

UNIVERSITY OF MIAMI

OPTIMIZING INDUSTRIAL CONSUMER DEMAND RESPONSE THROUGH DISAGGREGATION, HOUR-AHEAD PRICING, AND MOMENTARY AUTONOMOUS CONTROL

By

Ahmed Abdulaal

A DISSERTATION

Submitted to the Faculty
of the University of Miami
in partial fulfillment of the requirements for
the degree of Doctor of Philosophy

Coral Gables, Florida

August 2017

UNIVERSITY OF MIAMI

A dissertation submitted in partial fulfillment of
the requirements for the degree of
Doctor of Philosophy

OPTIMIZING INDUSTRIAL CONSUMER DEMAND RESPONSE THROUGH DISAGGREGATION, HOUR-AHEAD PRICING, AND MOMENTARY AUTONOMOUS CONTROL

Ahmed Abdulaal

Approved:

_____ Shihab Asfour, Ph.D. Professor and Associate Dean College of Engineering	_____ Murat Erkoc, Ph.D. Associate Professor of Industrial Engineering
_____ Ramin Moghaddass, Ph.D. Assistant Professor of Industrial Engineering	_____ Moataz Eltoukhy, Ph.D. Assistant Professor of Kinesiology and Sport Sciences
_____ Osama Mohammed, Ph.D. Professor and Director of Energy Systems Research Laboratory Florida International University	_____ Guillermo J. Prado, Ph.D. Dean of the Graduate School

ABDULAAL, AHMED (Ph.D., Industrial Engineering)

Optimizing Industrial Consumer Demand Response Through Disaggregation, Hour-Ahead Pricing, and Momentary Autonomous Control (August 2017)

Abstract of a dissertation at the University of Miami.

Dissertation supervised by Professor Shihab Asfour.
No. of pages in text. (129)

The work in this study addresses the current limitations of the price-driven demand response (DR) approach. Mainly, the dependability on consumers to respond in an energy aware conduct, the response timeliness, the difficulty of applying DR in a busy industrial environment, and the problem of load synchronization are of utmost concern. In order to conduct a simulation study, realistic price simulation model and consumers' building load models are created using real data. DR action is optimized using an autonomous control method, which eliminates the dependency on frequent consumer engagement. Since load scheduling and long-term planning approaches are infeasible in the industrial environment, the proposed method utilizes instantaneous DR in response to hour-ahead price signals (RTP-HA). Preliminary simulation results concluded savings at the consumer-side at the cost of increased supplier-side burden due to the aggregate effect of the universal DR policies. Therefore, a consumer disaggregation strategy is briefly discussed. Finally, a refined discrete-continuous control system is presented, which utilizes multi-objective Pareto optimization, evolutionary programming, utility functions, and bidirectional loads. Demonstrated through a virtual testbed fit with real data, the new system achieves momentary optimized DR in real-time while maximizing the consumer's wellbeing.

ACKNOWLEDGEMENTS

I would like to thank my advisor, Dr. Shihab Asfour, for his encouragement, guidance, financial, and emotional support. I would also like to thank Dr. Osama Mohammed and Dr. Ramin Moghaddass for guiding my work and for their constructive inputs.

I must also thank my coworker and dear friend, Jaime Buitrago, for his friendship, technical assistance, and emotional support.

My appreciation also extends to the U.S. Department of Energy for funding the University of Miami Industrial Assessment Center (MIIAC), which provided my doctoral assistantship and made available all the equipment and data used in my studies.

My deepest thanks go to my family; my parents Reda Abdulaal and Fatma Elbaghdady, my sister Sarah Abdulaal, and my wife Yuliya Krauchuk, for their exceptional patience, love, and unconditional support. Without them, my achievements would not have been possible.

Finally, I am very thankful to many of my friends, coworkers, students, and teachers who I could not have mentioned all their names, but they have impacted my life during the past few years with priceless knowledge and joyful experiences.

TABLE OF CONTENTS

LIST OF FIGURES

Page

LIST OF TABLES

Page

Chapter 1: Introduction

Demand-Supply Nature and Problems

The demand for electricity fluctuates widely from summer to winter (Figure 1.1-a), from workday to holiday (Figure 1.1-b), throughout the day from hour to hour (Figure 1.1-c), and even within the hour from minute to minute. These acute demand fluctuations are difficult to predict, yet it must be matched with generation with tight tolerances in real time. Utility providers respond by continuously ramping generation up and down relying on fossil fuel run peaker plants due to their high responsiveness. However, these sources are inefficient, harmful to the environment, and impact the future supply of energy.

In response to the risks and harms caused by the current electricity demand nature, governments and utilities are investing in two quasi-independent solutions: One solution targets the generation side is to increase the reliance on clean and renewable energy sources. The second solution targets the demand side and takes the forms of policies, rates, and other load control strategies known as demand response (DR) or demand side management (DSM) programs.

However, these solutions are challenging. For example, renewable energy supply is characterized by being of an unstable nature causing the power supply system to become even less adaptable to high load variations. Therefore, what we need today are smart grids capable of using digital information and control technology to improve the efficiency of the electric system. Nearly all the existing electric transmission and distribution infrastructure in the US was built prior to 1965. Power is generated and distributed by utilities with fairly little communication between utilities and consumers in terms of how to get more out of the system [1].

With advances in the smart grid technology, distributed energy systems, and the vehicle-to-grid integration, there will be a shift from a centralized, producer-controlled to a distributed consumer-interactive system. The smart grid should enable the real-time communication between the consumer and the utility, to allow consumers tailoring their energy consumptions on the basis of individual preferences like price and environmental concerns [1].

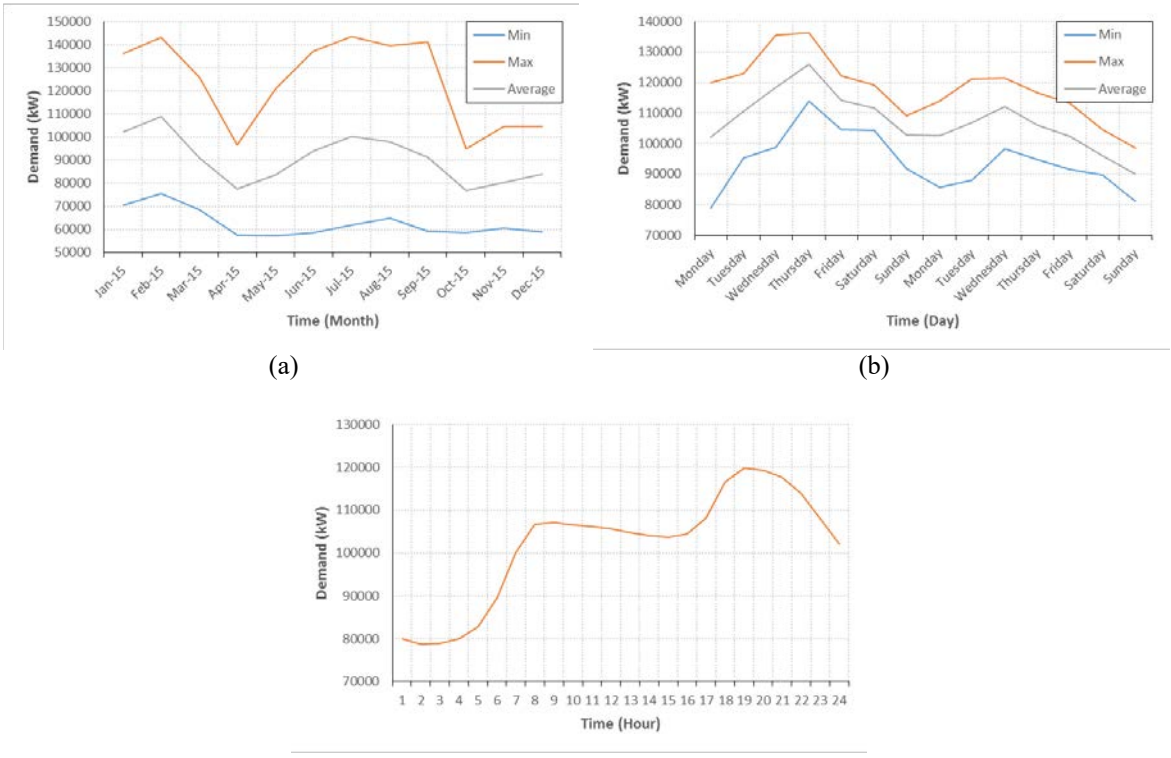

Figure 1.1. Electricity demand fluctuations. (a) by month. (b) by day. (c) by hour. Sampled data downloaded from PJM RTO for the year 2015 [2].

Motivation

As briefly mentioned, the increasing penetration of renewable energy to the grid makes the power supply system less adaptable to load variations. A large fluctuation in demand may lead to stability problems, power quality problems, and even an entire

system collapse. Therefore, there is a significant need for preeminent control systems to optimize scheduling and supply-demand matching in real time [3-6].

Tariffs and RTP

One direct and efficient approach considered by policymakers to control demand variations, reduce peak demand, and meet utility-load obligations through increased consumer communication, is the implementation of the Real Time Pricing (RTP) tariffs [7]. Under RTP, consumers are charged hourly-varying prices for electricity consumption that reflect the contemporaneous marginal supply costs. Typically, consumers are notified of the new hourly energy rates one day or less in advance. Relying on available information about the hourly cost of energy in the short period, consumers can choose to reduce, increase, or shift their energy consumption from a higher priced hour to a lower one. Further description of the different tariff types is provided in chapter 3.

While this approach is argued to be the most direct and efficient, there are several reliability issues questioning the performance of RTP to ultimately affect energy demand as intended; mainly, the extent and consistency of a diverse consumer population to respond to these varying prices, and the accuracy of forecasted demand when assigning real time price rates. Therefore, the current trend in research focuses on transforming the RTP system from a one-way, utility-to-consumer, communication system to a two-way, utility-consumer information exchange system, which increases the utilization of advances in the smart-grid like integrated smart meters - controllers distributed along the grid nodes. In addition, the increase in electric vehicles (EVs) usage is expected to play a substantial role in the RTP environment where vehicles can be used as means of energy storage and trading as well as load mitigation using complex charge-scheduling.

For utilizing tariffs in DR, most researches made targeted residential consumers, like in [8-35]. Fewer research efforts addressed commercial and industrial consumers as in [36-44]. Most of the DR applications in research were limited to HVAC loads. For example, some researchers introduced automated controllers to short-term schedule the on/off cycles of residential HVAC units and the operation of other home appliances in response to information available about RTP rates in the upcoming short term period [9, 13, 14, 18, 20, 22, 23, 29-32]. Other researchers, [10, 11, 27, 28, 33, 39, 42]. introduced controllers to continuously adjust the temperature settings for HVAC units in accordance to rises or declines in the RTP rates while considering the consumer's comfort-tolerance level.

From a thorough literature review, several challenges impeding the full utilization and global-scale adoption of RTP-driven DR were identified. These challenges are summarized as following:

- The accuracy of predicting and setting a price for energy to reflect the actual cost of generation in real time [20, 45], particularly with the growing grid-penetration by renewable energy sources, where the supply cost function becomes more complex due to the intermittency nature of renewable resources.
- The financial and power implications for policymakers and regulators [7, 8, 20], particularly, due to allowing increased control at the customer-side. Regulators have higher incentive for profit-generation and risk avoidance than for energy conservation or customer-expense minimization. To regulators, risks like system failure from overloads, blackouts, or slow response to

demand peaks, are avoided by increasing system security and maintaining high base-generation levels. Their strategy is to use a large and stable generation capacity to supply a large and static portion of demand while connecting/disconnecting smaller peaker generators as needed for the peaking portions. The challenge is in designing a system capable of providing attractive profitability and security measures sufficient to motivate policymakers and regulators.

- The elevated difficulty in predicting demand due to the co-dependency between price and demand [20, 46, 47]. The challenge is in developing highly intelligent and adaptive demand-forecasting algorithms accounting for changes in demand resulting from changes in price.
- The dependency on consumers to consistently follow price changes and react in an energy-aware conduct remains an obstacle due to the lack of knowledge and diverse nature of human behavior [7, 8, 10, 20, 32].
- In addition to the lack of knowledge among consumers, the lack of effective building automation systems is a major barrier to fully utilizing the benefits of RTP [10, 18].
- Load synchronization [7, 18, 20, 27, 47]; if load-shifting is achieved via automatic controllers responding to price changes for all the consumers in the network simultaneously, then a large demand spike would occur during the cheaper periods which threatens the system's stability. This may require a special price-setting strategy like adopting Inclining Block Rates (IBR) [18,

47] or assigning different prices to different consumers or to different locations [20, 46, 48].

Research Objectives

The work discussed in this dissertation aims at improving the power supply and demand system through a proposed DR scheme. The work is to consider and overcome the aforementioned obstacles currently associated with DR and energy pricing. This is accomplished in three research segments: Designing an autonomous DR controller concept to be installed at the individual consumer site, proposing a strategy for disaggregating consumers' demand by classifying and grouping consumers according to their demand profiles, then a further micro-optimization of the DR control system in order to achieve momentary real-time action, enable special load types (e.g. bidirectional loads), and maximize consumer's wellbeing.

Research Scope and Reasoning

Although the concepts of the work done in this research can be applied to any type of load, this research's main targets are commercial and industrial consumers in the state of Florida. In contrast to most research reviewed, where residential consumers were the target of concern, commercial and industrial consumers are chosen for the following reasons:

First, industrial and commercial buildings account for the majority of the total energy consumption in the United States as shown in (Figure 1.2).

Second, industrial consumers have high demand and each consumer independently can have a sizeable effect on the overall load shape, while in the case of residential

consumers, demand has to be aggregated among several individuals as each individual's contribution to energy demand is very insignificant.

Third, while real time residential demand management approaches have showed significant savings at the customer side, actual savings at the utility side were difficult to assess since each consumer is different and contributes by very little. Therefore, residential demand response under RTP is unattractive for many utility companies due to the reliability issues associated with the unpredictable nature of the consumer.

Fourth, In contrast to large industrial equipment, most demand-consuming appliances for residential consumers utilize single speed motor systems which cycle at low frequencies. For example, a traditional air conditioning unit can only operate on full power. While For industrial use, the larger equipment can operate at variable loading levels or cycle at various frequencies through Pulse-Width Modulation (PWM) controllers providing opportunities for load management approaches under RTP.

Fifth, large buildings are expected to host large scale of employee EVs, commercial EVs, renewable energy generators, and bulk storage systems, which provides opportunities for industrial consumers to utilize load shifting for DR, yet viable approaches are currently limited in published research.

Sixth, data availability; Real consumption data for many industrial facilities, equipment, and potentials for energy savings specific to each consumer have been collected and evaluated. The data were obtained from energy assessments conducted by the Industrial Assessment Center (IAC) program at the University of Miami (MIIAC) for facilities in the state of Florida and in Puerto Rico. These data are used in this research as both input data and for simulation parameter verification.

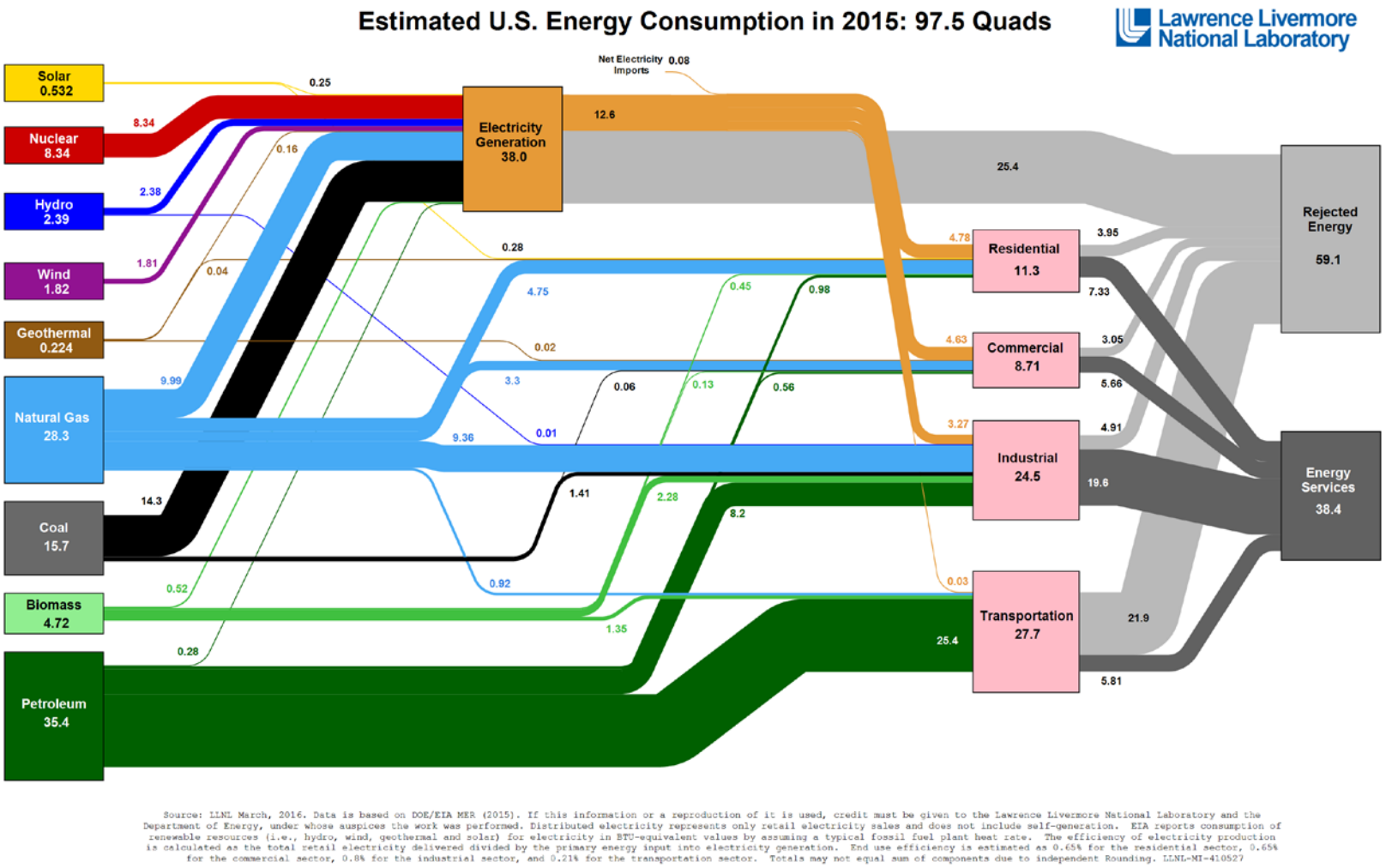

Figure 1.2. Estimated energy flow in the US for the year 2015. Source: Lawrence Livermore National Laboratory [49].

Research Vision

The effort is spent in this research with the hope of providing supporting research evidence, which could encourage regulators to allow the consumer's subjection to prices set by control algorithms. This shall be achieved through demonstrating the robustness and profitability of such systems using theory validated by both simulation and experiment.

Chapter 2: Literature Review

RTP in Residential DR

The majority of articles available in literature discussed methods for residential demand management under RTP or other dynamic pricing schemes [9-14, 18, 20, 27-35]. In [11], the author presented a price responsive intelligent thermostat for use in local load management. He proposed a technique for treating the single speed compressor of the home air conditioning unit as a variable power unit via an alternative thermostat design using low frequency PWM, thus, enabling the control of power consumption with tunable saturation limits by means of a linear control design triggered by fluctuations in price. In his research, he aggregated the load from small independent residential consumers into a larger load group to have a sizeable effect on load generation. The main two limitations to his work were in modeling his power reference and in estimating profitability; because the controller is not suited for time-varying energy sources, the author assumed stable and known power reference in contrast with the reality of energy supply. Moreover, the author did not address revenue and profitability implications of his method which is the main concern of both users and regulators.

Focusing on the same load type, the authors in [10] and [27] proposed controller strategies for reducing energy cost by assigning residential HVAC temperature setpoints to price ranges based on consumer's discomfort tolerance. In contrast to using the RTP system similar to [10] or [11], the authors in [27] argued that retail electricity priced on a 15-minute basis provides more precise control than hourly-based pricing. Their argument is supported by the findings in [7].

While demand management techniques through controlling HVAC load intensity were discussed in [11] and [20], the authors in [18] targeted other residential equipment by presenting an automated optimization-based load scheduler for the operation of household appliance. They considered the trade-off between minimizing electricity cost under RTP tariffs and minimizing waiting time. Similarly, the authors in [12] provided an optimization model for adapting the consumer's hourly load level in response to RTP tariffs through the addition of ramping up/down constraints in their model. Their method works with the energy management system (EMS) of a house or small building. However, their work was theoretical and lacked description of the load-consuming equipment or how they can be used in DR. They assumed that a minimum daily building consumption is pre-known and that the daily load can be spread across the 24 hour period with fixed hourly ramp up and ramp down limits. While their assumptions are adequate for assessing the usefulness of smart metering and RTP, their method cannot be implemented realistically. Moreover, limitations to their method include the uncertainty associated with an extended energy planning horizon of up to 24-hour period when hourly price knowledge is available for only 2 hours. The authors also described a framework for the bidirectional communication between the utility and the consumer.

The authors in [20] disaggregated domestic load profiles and used a simulation methodology based on the price-demand elasticity levels for consumers to drive the load-shifting response in a grid supporting renewable energy penetration by means of automatic smart meter/controllers. Their method is limited to the strength of demand-forecasting and price-setting strategies. Methods for managing photovoltaic (PV) panels

and energy storage units including thermal, battery storage, and EVs for residential DR were suggested in [9, 13, 18, 22, 32].

RTP in Industrial DR

While it is easier for residential consumers to respond to price variations by adjusting heating, ventilation and air conditioning (HVAC) loads or by scheduling the operations of household appliances, it is difficult for industrial consumers to respond in a similar manner due to the stresses imposed by just in time (JIT) manufacturing and market competition. Nevertheless, HVAC systems in commercial buildings offer high potential for responding to DR events [50]. Moreover, HVAC systems in commercial buildings can provide frequency regulation services to the grid and fine-tune the balancing between supply and demand [42, 51-59]. Different than most approaches in savings estimation, The analysis in [42] includes the demand charge factor in the objective of optimizing HVAC loads in response to day-ahead RTP and frequency regulation price signals.

In [42, 60], the authors considered demand shifting while utilizing the commercial buildings' thermal storage in precooling. They noted that precooling reduces the deviation from thermal comfort levels in DR periods. The authors in [39] divided the day into four segments with assigned optimized discrete thermostat setpoints. They relied on prediction of price and weather variables. While prices vary by the hour, their approach is limited to assigning four setpoints to four time periods rather than assigning setpoints for each hour and thus, increase the utilization of RTP.

As for non-thermostatic DR, the authors in [41] presented a scheduling approach for commercial buildings. Their method relies on long-term price and renewable generation predictions. However, their work does not explicitly define the types of schedulable loads

in a commercial building and their impact on the consumer. Therefore, their simulation may not be realistically applicable for the busy and competitive environment of commercial buildings. In [38], the authors presented an energy management approach for industrial consumer with a cogeneration plant under multiple pricing schemes including time-of-use (TOU) pricing and RTP. Their approach accomplished DR by managing the cogeneration plant output versus the energy purchase from the grid. The only work targeting industrial production processes for DR is in [44]; The authors scheduled manufacturing processes in a steel powder plant relying on price prediction model for the production day. However, their proposal considers a high degree of uncertainty where manufacturers would be reluctant to adopt it due to the profitability risks, specifically for JIT industrial processes. Moreover, their work is specific to industries with consecutive manufacturing processes where resources can be shifted from one process to another without significantly impacting the overall throughput.

It is noted that all of the researchers mentioned above assumed price knowledge for 24 hour periods or longer which is required for the successful managing of industrial HVAC loads or scheduling of residential loads. Mainly, authors relied on the day-ahead price (DAP) availability, TOU rates, or price prediction approaches.

Financial Implications and Price Setting in RTP

The work in [20] included the assessment of financial implications on consumers and utility. They noted that, under RTP, customers are able to use more energy over the year while paying less for it. Similarly, researchers in [8, 26, 61, 62] examined the economic advantages of RTP. They showed RTP can produce significant gains in economic efficiency in the long run while similar price models, like TOU, Critical-Peak Pricing

(CPP), and DAP, only capture a portion of the high efficiency gains RTP offers. The author in [8] expressed that regulated electricity retailers are less inclined to adopt RTP as their financial gains are positively proportional to increased energy usage.

However, the utility gains from RTP are highly dependent on the accurate price setting; the researchers in [45] proposed a method of finding a set of consistent prices with the actual output of resources. Although their method produces consistent prices with the actual response of resources, the prices are not set with the purpose of signaling a customer/controller response behavior in real-time demand management system. Whereas in [47], the authors presented price-setting algorithms for RTP aiming to minimize the Peak to Average Ratio (PAR) in electricity demand by taking into account the co-dependency between price and demand, and considering the effect of users' Energy Consumption Scheduling (ECS) systems effect on load profile.

Environmental Impact of RTP

The environmental impacts of RTP were examined in [63]. The authors estimated the effect of load variation on SO2, NOx, and CO2 emissions and concluded that, depending on the region, RTP may increase or decrease emissions. In particular, RTP is greener in regions where peak capacity is supplied by fossil generation and less green in regions where peak capacity is supplied by renewable energy generation like hydroelectric.

Load Synchronization

Many authors drew attention to that their methods may result in simultaneous shifting of loads to a cheaper time across all consumers which would cause a new demand spike higher than any spike under the fixed price system. In [48], locational-based pricing were suggested which could mitigate the load synchronization effect from

the use of load-shifting controllers. Likewise, the authors in [18, 47] argued that IBR tariffs may result in avoiding the high demand spikes from synchronization of loads. The work in [54] show how the aggregation of large collection of on/off loads can provide ancillary services to the grid and avoid load synchronization through a randomized control strategy.

Remarks from Reviewed Literature

In general, it is concluded that the residential sector has attracted more research in DR than the industrial or commercial sectors. Moreover, the majority of research concerning non-residential DR is limited to small office buildings or campus buildings but no significant work has been dedicated to large manufacturing facilities.

HVAC loads provided the researchers-preferred potential for DR in all sectors. Moreover, EMS and the thermal storage capacity of larger buildings can increase the utilization of HVAC loads in DR while accounting for the impact on the consumer's comfort level.

RTP as a method of peak load mitigation is essentially environmentally and financially rewarding in areas where fossil generation is depended upon, however, almost all DR methods discussed in literature were justified using arbitrary or empirical assumptions of consumer loads and utility prices in the near future, while in reality, load and prices may fluctuate wildly and unexpectedly from hour to hour, making the scheduling approaches in DR impractical. It is also noted that price-driven DR in literature utilized the established DAP, TOU, or RTP system paired with price forecast approaches. While some researchers suggested alterations to the aforementioned systems

by including IBR or CPP, design and investigation of novel pricing schemes were hard to find in DR literature.

Finally, the synchronization of loads is a critical challenge impeding the wide-scale implementation of automated DR methods. This challenge calls for the restructuring of the whole pricing system or for an increased communication among all supplying and consuming entities in the grid.

Chapter 3: RTP Tariff Modeling

Chapter Introductory Remarks

Purpose of RTP

In contrast to the traditional flat rate energy tariff, which is fixed for duration of a billing cycle, typically a month, RTP tariffs are more dynamic, where the energy rates fluctuate in various frequencies within the billing cycle. The frequency of rate adjustments depends on the applied RTP system. Ideally, the purpose of a dynamic tariff is to reflect the combined costs from the contemporaneous wholesale market price of fuel, running costs of generation, and transmission costs, where such costs increase or decrease as demand fluctuates. These tariffs are usually communicated to the consumer a day ahead or less in advance for demand planning purposes.

Deregulated vs Regulated Markets

The RTP approach became feasible following the deregulation electricity markets and the introduction of smart-metering. Electricity deregulation started taking place in the United States following the passing of the Energy Policy Act of 1992. The purpose of electricity deregulation is to allow competition in the wholesale market of electricity which, as a result, encourages a more efficient production of electricity and better consumer service. However, as of 2014, only 16 states have deregulated electricity markets, the remaining states are yet to participate in electricity deregulation. This resistance to a nation-wide participation in electricity deregulation is attributable to concerns about negatively impacting states' economies and consumers' use. For example, the spike in electricity prices after deregulation in some states and the famous California blackout in 2000 are some of the incidents exposing the weaknesses of electricity

deregulation. Nevertheless, implementation of RTP has been only feasible in the deregulatory environment, because in regulated markets the pricing strategy targets cost recovery from capital expenditures and long term-operation. Therefore, the goal in regulated markets is far from efficient pricing. Moreover, regulated markets utilities face attractive opportunities to grow through increased earnings and capital investments with high ROI [8].

Types of Dynamic Tariffs

The most common types of these tariffs are:

- Time of use (TOU): The most commonly used in regulated markets as an optional alternative to the flat rate. TOU is the least dynamic form of RTP tariffs and the closest to the flat rate system. TOU provides higher reliability and reduces the costs of forecasts errors, which the utility would incur, if a different RTP system was used. In TOU, only two or three sets of flat rates are charged to the customer throughout the day, where the day is divided into two or three segments; off-peak, shoulder, and on-peak. Then, like the flat tariff, rates may be adjusted in future billing cycles.
- Critical peak pricing (CPP): The closest in concept to the TOU system, however, the peak period is event driven and mostly limited to no more than several hours in an event day. Also, there is a limit on the number of events in a year. The purpose of CPP is to drive a stronger demand response during critical events where reducing peak demand is vital to the utility. The peak rate would be much higher than most rates and the consumer is incentivized to participate in CPP by reduced energy rates during all other periods. In this

system, the consumer would be notified a few hours before the peak event in order to take the necessary measures and reduce demand.

- Day-ahead pricing (DAP): A less volatile form of RTP where the deregulated market participants commit to buying or selling energy from the wholesale market one day ahead of the operating day. As a result of the buy and sell bids, demand forecasts are performed and cost-efficient generation is optimized accordingly. Consequently, an hourly price is cleared for the upcoming operating day. This system encourages the optimization of ancillary services, including DR, in order to commit to the original bids. One advantage of this system is that it mitigates the risk of high price volatility in real-time. For the consumer in DAP, the hourly energy rates only for a 24 hours period are obtainable one day ahead of time. In DAP, the supplier handles more uncertainty risks than the consumer, where suppliers remain subjected to the risks of price volatility when the amounts committed from successful biddings fall short of the actual demand in real time. In order to supply or manage excesses in demand or supply, Suppliers are forced to buy or sell wholesale electricity in the highly volatile real time market.
- Real-time pricing (RTP): The most volatile tariff for energy pricing where the deregulated market participants buy and sell energy during the course of the operating day. Specifically, the energy which deviates from their original day-ahead commitments. Typically, the price is updated every few minutes according to buy and sell bids then the final hourly price is settled based on deviations from the Day-ahead market. RTP reflects the actual real-time

demand and production costs of energy. This tariff settlement is for market participants and seldom available as a billing rate option for end-consumers. However, very few companies offer this rate option for consumers who can then follow the energy prices on hourly basis and make demand-planning decisions. This rate is usually called hour-ahead real time pricing (RTP-HA) [7, 41, 64-67]. RTP-HA is less common due to the difficulty of consumer adaptation and load scheduling within a one-hour notice, although it is advantageous to the supplier who can mitigate the costs of long term forecast errors and inefficient bidding in the wholesale energy market, in contrast to the DAP system. In order for the RTP-HA to prevail, intelligent, instantaneous, momentary, and autonomous DR controller technologies are needed.

Chapter Objective and Motivation

The objective in this chapter is to develop a price-simulation model to mimic realistic prices in the real time environment. This step is needed in order to obtain a virtual load network where the proposed DR method in chapter 4 can be tested and validated. Moreover, the model contributes to research as an available tool for utilization in DR and other energy-related research which requires realistic real time market volatility models. The tool has been published in [68].

Data Collection

During energy assessments, The MIIAC team implements a data-logging strategy to capture actual client's consumption. The MIIAC uses the logged data for making decisions and calculations in energy saving recommendations. Usually, the logging

period extends from one week to a few months with data captured at 1 second, 15 seconds, or 1 minute intervals. Sometimes, the team gets involved with other projects which require logging for prolonged periods from several months to more than a year. From the MIIAC archive, eight companies from different industries were selected for the analysis. The companies were selected from assessments conducted in the hot season between the years 2010 and 2014. The companies' locations and average demand are shown in Table 3.1. These companies are assumed to be supplied by the same distribution substation in the distribution network for the purpose of this simulation study.

1 week period of data logged on 1-minute intervals were extracted for each company. The data represents the 3-phase current amperage drawn by each company as measured from the main service entrances (MSEs). MSEs are the main building supply breakers used for metering and billing the consumption by the utility provider. Knowing the voltage used at each company and assuming a power factor of 0.9, the demand in kW was computed for each data point extracted, then the results were averaged over each 60 min data points as an approximation of the actual demand for each hour. The computed data were used to simulate the load in our simulation system as shown in Figure 3.1.

It is clear from the data plots that the total system demand has an increasing behavior in the mid-day period and is generally lower during weekends than weekdays. Almost all entities in the system follow the same trend in energy demand with exception of three entities; MI0198, MI0246, and MI0265, where their energy demand is stable throughout the recorded period. This could be attributed to that some facilities work at full load for 24/7 period or to the necessity for keeping some type of loads, like cooling loads used for freezing processes, constantly on due to the products' storage requirement.

Table 3.1. Companies selected for the simulation model.

Company codename	Industry	Location	Average demand (kW)
MI0189	Aerospace products and parts manufacturing	Miami	153.9761
MI0197	Marinas	Miami	30.1444
MI0198	Aerospace products and parts manufacturing	Medley	225.6109
MI0234	Cosmetics and skin care products manufacturing	Hialeah	131.1498
MI0246	Chemical manufacturing	Miami	401.3903
MI0265	Flower wholesaler	Miami	404.0479
MI0267	Food wholesaler	Doral	534.1631
MI0268	Sign manufacturing	Hialeah	683.9466

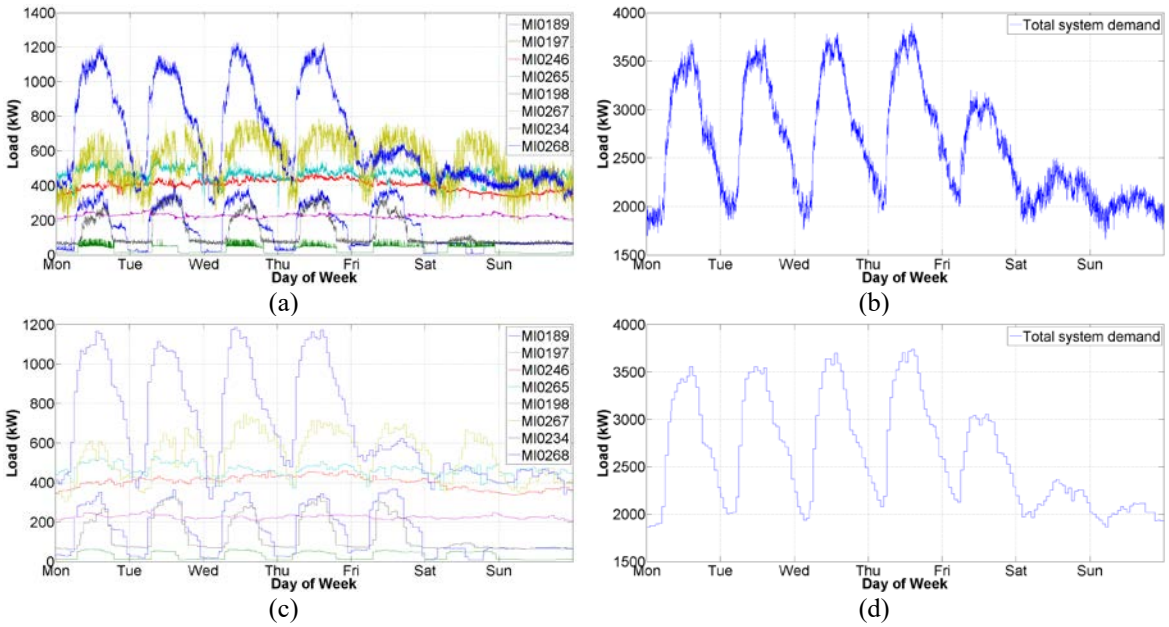

Figure 3.1. System load in kW used in the simulation model. (a) 1-minute load per consumer. (b) 1-minute total system load. (c) Hourly average load per consumer. (d) hourly average total system load.

Modeling Demand Forecast

Currently, Energy demand forecast across the nation for planning purposes and tariff adjusting is performed on a state-wide basis [69], meaning that the load data is aggregated from numerous entities in the system. Because demand forecast techniques are not of concern in this research, we simulate forecasted data for a given period from the actual data obtained. A simulated forecast data point is computed as the inverse of the normal cumulative distribution function with the real data point as the mean, the error as

the standard deviation, and at a corresponding random probability. The errors in demand forecasting are selected from literature as 1.40% and 2.06% for the hour-ahead and day-ahead forecasts [70]. The hourly load data is used to simulate the forecasted data using the NORMINV function in MATLAB. The SIMULINK block diagram in Figure 3.2 shows how the forecasted data were simulated for the DAP system-wide forecasted load. Figure 3.3 shows a plot of the forecasted demand along with the actual demand on the same axis. The same technique was repeated to obtain the forecasted data in RTP settings.

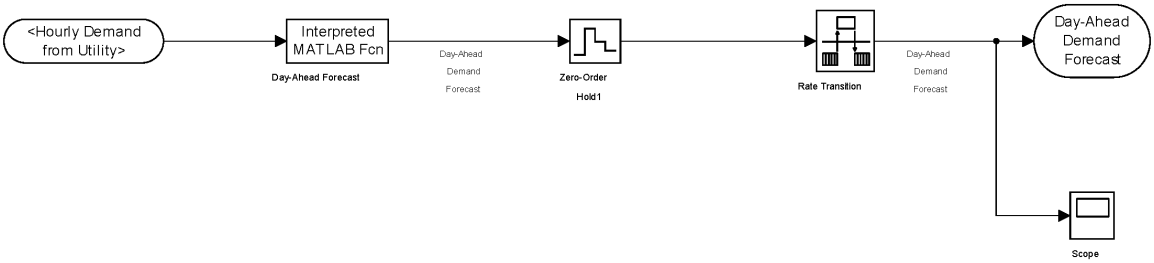

Figure 3.2. SIMULINK block diagram for generating forecasted demand from actual demand data in day-ahead forecasting.

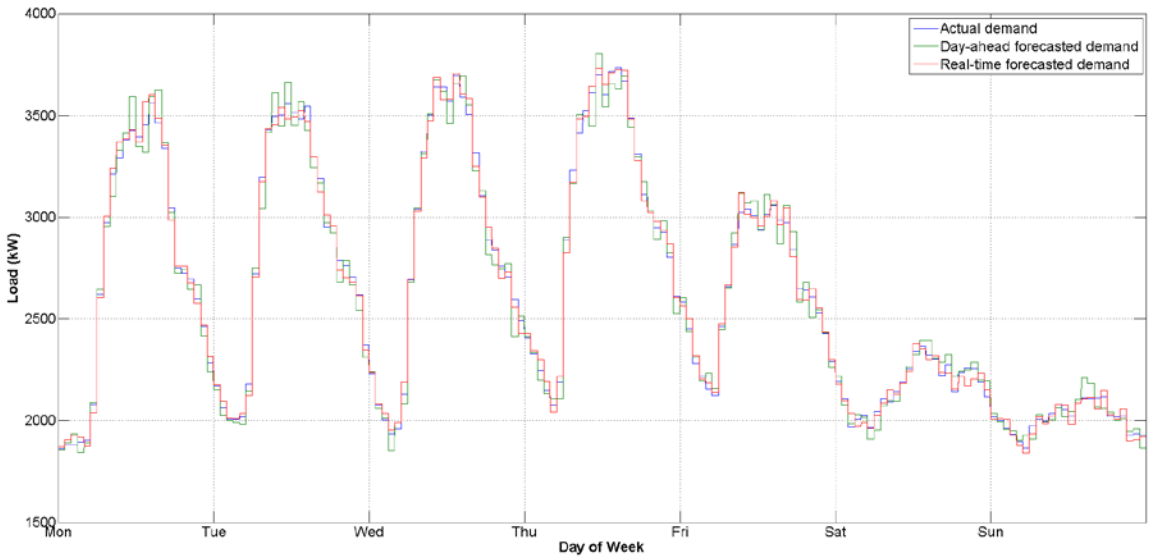

Figure 3.3. Actual demand and simulated forecasted demands.

Modeling RTP Tariff

In general, energy tariffs are designed of either a bundled one-part or an unbundled multi-part architecture. In brief, the difference between these classifications is that the bundled tariffs do not directly relate demand, energy, and customer charge costs to generation, transmission and distribution costs, while the unbundled does. The one-part tariffs use only one volumetric charge ($/kWh) to recover both the fixed and the variable costs while the multi-part has more than one rate component [7]. Typically, a separate peak demand rate ($/kW) is charged to the consumer in the unbundled rate structure. The demand charge is more popular in regulated markets as a mean to mitigating peaks in the system by penalizing consumers for their highest demand reached every month, while its existence alongside DAP and RTP tariffs is diminished since these tariffs vary by the hour and drive DR by doing so. Therefore, the simulated system in this study is based on the bundled rate structure.

The RTP tariff of interest in this study is the hour-ahead tariff (RTP-HA), where the tariff is adjusted and notified to the consumer one hour ahead of time. Generally, all RTP tariffs reflect the marginal cost of energy production and therefore, these tariffs vary as the expected load varies. Fuel and variable operation cost derive the marginal cost of energy production. Five approached for estimating the marginal cost were explained in [7]. The most two commonly used approaches are the system lambda and the power pool approaches. In the first approach, the marginal cost is calculated as the incremental cost of the generation unit operating above the base level. The incremental cost is obtained from the utility's dispatch model. In the latter approach, the marginal cost is calculated as the spot market clearing price in the regional power pool.

Data Acquisition

Due to the limitation of the information available about generating units, the power pool approach is selected in this study. The spot market energy prices from historical data is available and obtained from the Pennsylvania, Jersey, Maryland Power Pool (PJM) Interconnection LLC [2]. The real-time prices of energy in a typical summer 2-week period in the Mid-Atlantic region, starting July 14th 2014, along with load data were obtained. The obtained data were used to build a price estimation model using IBM SPSS software and SIMULINK. Using cross-validation, the model was used to simulate a realistic RTP scenario for the load network in this study.

Model Formulation

Using curve estimations in SPSS and after several regression tests, with price as the dependent variable (DV) and all of the time of the day, day of the week, and the peak-to-average ratio (PAR) as independent variables (IVs), we concluded a cubic relationship between the DV and both of the time of the day and day of the week. Also an exponential relationship with the load was observed. From regression and mediation tests, we concluded that both the hour of the day and the day of the week have an indirect effect component on the price that is mediated through the load. Therefore, the model can be depicted by the path diagram shown in Figure 3.4 and the real-time market price of fuel can be estimated using the following regression equation:

$$\lambda_t^{fuel} = \varphi_1 + \varphi_2 \cdot h_t + \varphi_3 \cdot {h_t}^2 + \varphi_4 \cdot {h_t}^3 + \varphi_5 \cdot d_t + \varphi_6 \cdot {d_t}^2 + \varphi_7 \cdot {d_t}^3 + \varphi_8 \cdot e^{\varphi_9 \cdot PAR_t^{total}} \tag{3.1}$$

where λ_t^{fuel} is the real-time market price of fuel expressed in \$/MWh at time t, $\varphi_{1:9}$ are the constant and coefficients obtained from the regression analysis., h_t and d_t are the

hour of the day and the day of the week during the simulation time instant t, and PAR_t^{total} is the peak to average ratio, which is calculated as:

$$PAR_t^{total} = \frac{D_t^{total}}{\overline{D}_t^{total}} \tag{3.2}$$

where L_t^{total} is the lumped system demand at time t.

Like many time-varying parameter regression models, this model helps in predicting the systematic and periodic portion of variability in the spot electricity price, however, a large share of variability remains missing. According to price prediction models in previous literature, forecasting for this variability is proven to be unattainable and inconsistent [71]. Therefore, some of the price volatility cannot be simulated by (3.1) alone. We solve this by artificially accounting for the remaining volatility by adding the following sinusoidal component to (3.1):

$$\varphi_{10} \cdot e^{\left(PAR_t^{total\varphi_{11}}\right)} \cdot \sin\left(\varphi_{12} \cdot h_t + \varphi_{13} \cdot PAR_t^{total\varphi_{14}}\right) \tag{3.3}$$

where $\varphi_{10:14}$ are auxiliary coefficients which aid in simulating the remaining variability in the model unaccounted for by (3.1).

Model Parameter Estimation

For estimating the parameters in (3.1) and (3.2), we utilized tools from two software packages; the global optimization toolbox in SIMULINK and nonlinear regression analysis in SPSS. We identified the pattern search method as the optimal in finding acceptable coefficients, which would be in the optimal or suboptimal region. We then refined the solution using the Levenberg–Marquardt algorithm in SPSS, which finds local optimal solutions.

The 2-week summer price and load data from PJM are utilized for the parameter estimation process, which also means that the model is tested for its ability to simulate price data matching those of the PJM market. We concluded that the addition of the sinusoidal error component denoted by (3.3) increases the coefficient of determination to 0.6, which is considered satisfactory given the difficulty in predicting real-time price as mentioned in literature. Table 3.2 presents the optimized model coefficients and Figure 3.5 indicates the resemblance between price volatility from the actual PJM data and the price simulation model. It is important to note that the objective of this model is to simulate realistically volatile RTP tariffs given any real or assumed load network. This model is not to be mistaken as an approach for the accurate prediction of future prices. Therefore, accounting for overfitting error is neglected in this model.

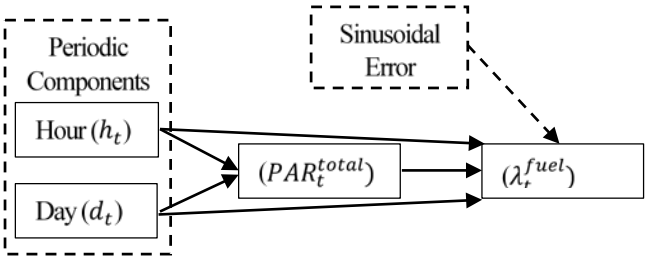

Figure 3.4. Path diagram for price prediction model.

Table 3.2. Optimized coefficients of the spot market fuel price formulation model.

Coefficient	Value	Coefficient	Value
φ_1	2.78	φ_8	15.67
φ_2	-1.39	φ_9	1.03
φ_3	0.19	φ_{10}	0.73
φ_4	-0.01	φ_{11}	2.91
φ_5	-9.92	φ_{12}	64.27
φ_6	1.62	φ_{13}	76.13
φ_7	-0.05	φ_{14}	0.05

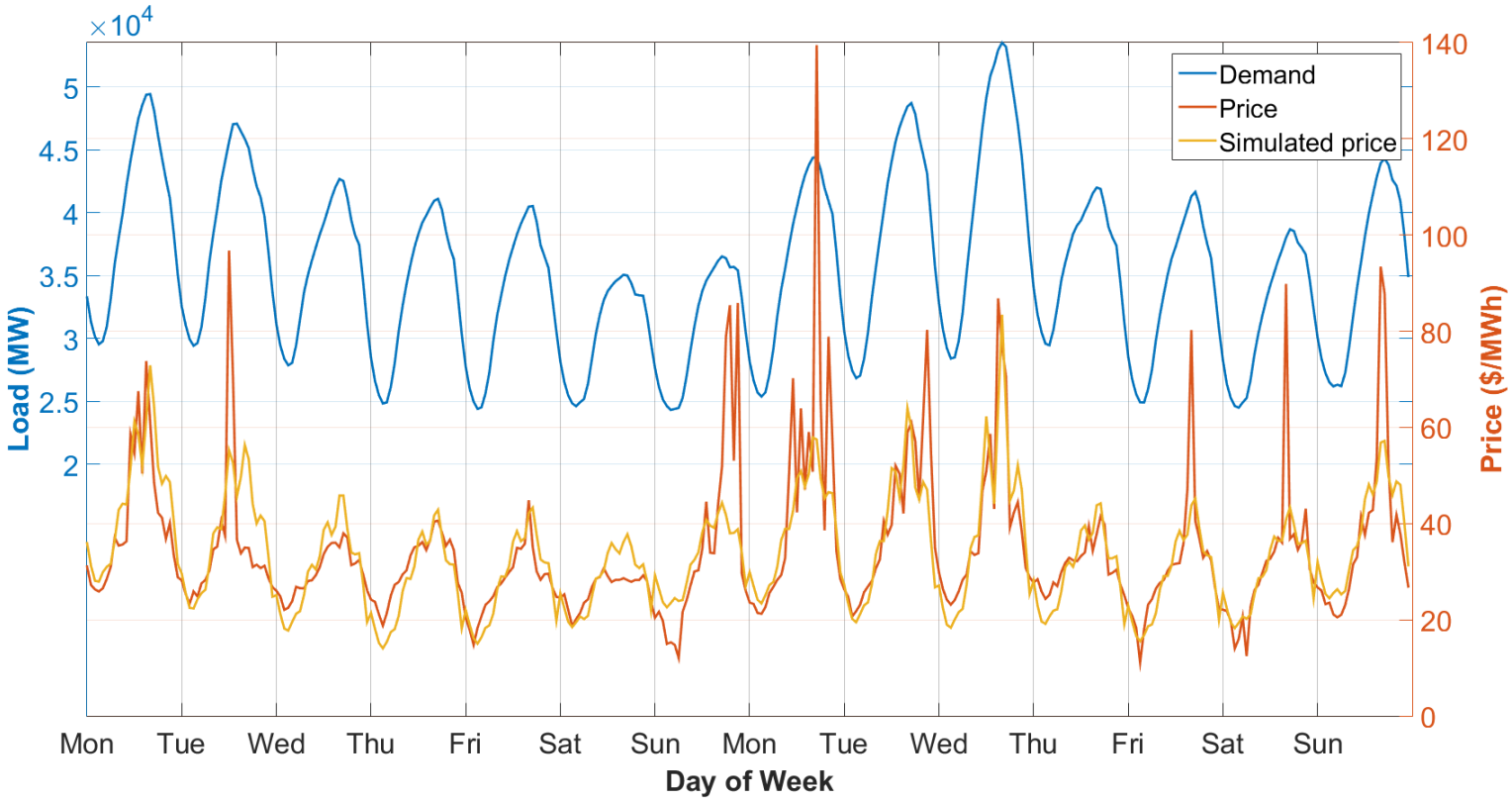

Figure 3.5. Load, actual, and simulated spot market prices (Mid-Atlantic region data for two weeks starting 7/14/2014).

Chapter 4: Autonomous Linear Demand Control in Real-Time

Chapter Introductory Remarks

In reviewed literature regarding DR for residential consumers, achieving demand control using RTP tariffs was easily modeled as functions of tradeoffs between a consumer's comfort level, price elasticity, and tolerance to waiting in the cases of scheduling home appliance operations. Such methods assumed price knowledge for a day ahead of time or longer. However, the same methods cannot be realistically applied to industrial and commercial consumers due to the throughput and time constraints imposed by JIT systems and market competition. Therefore, Industrial consumers are inflexible to rescheduling production lines operations or other machinery simply in response to changes in energy tariffs. Nevertheless, from the results of energy audits conducted by the MIIAC in Florida, it was observed that almost all industrial facilities waste energy through using lower thermostat settings than recommended for cooling, excessive lighting, higher than required compressed air pressure, and operating AC motors at full capacity, when partial loading is attainable. All of which are controllable wastes which could be eliminated, except that industrial consumers tend to neglect these wastes for the purposes of maintaining high comfort and security levels. For example, an industrial consumer may use higher than required compressed air pressure because they prefer having a surplus in compressed air to facing shortages if a new air leak is to occur. A proposed methodology for addressing the consumer's comfort, security, or convenient constraints with respect to DR optimization is discussed in chapter 6.

Chapter Motivation

Due to the conflicting goals of being energy efficient and maintaining a high comfort and security levels, a trade off would be to temporarily trim energy wastes through automatic, price-triggered control systems. However, the pricing schemes adopted in previous DR studies do not maximize the advantage for the utility provider nor are they fully applicable to the industrial consumer. As discussed in the previous chapters, these methods either rely on price forecasts, which is associated with errors and uncertainty, or on less volatile price models, like DAP or TOU, which do not reflect the actual contemporaneous cost of supply and provide less efficiency gains than RTP. Moreover, even if price optimization is achievable for a full day ahead of time, the feasibility of load scheduling strategies remains a challenge for busy industrial consumers. What is needed is a DR strategy to work with the spot-market price volatility as in RTP-HA.

Currently, many industrial consumers utilize EMS which allow for more than monitoring of energy consumption of various equipment. For example, intelligent EMS allow users to set the operation capacity of equipment, schedule the on and off cycles of HVAC systems or other equipment, control motor speeds through variable speed drives (VSD), control compressed air storage tanks, and set lighting levels. Moreover, the data collected from EMS can be used in intelligent prediction models like artificial neural networks (ANN) or can be used in model predictive controls (MPC) to estimate the future state of equipment.

Chapter Objective

The objective of this chapter is to propose a design for a control system operating in integration with the EMS of industrial and commercial consumers. A simplified linear

control algorithm is developed, which is capable of the autonomous adjustment of operation setpoints for controllable industrial and commercial use equipment in response to real time price variations. Therefore, the aims of the proposed method is to utilize the real spot market energy prices while omitting the needs for price forecasting, long-term planning, or equipment scheduling approaches. In addition, the proposed method is to minimize the impact on the industrial consumer's comfort and security levels through utilizing momentary load shifting rather than load shaving which may be considered extreme in the workplace.

Operation Scheme

The proposed method's operation scheme is such that load is shifted instantaneously and momentarily as the price is updated in the RTP-HA market. Two strategies for demand shifting are utilized: The planned demand is shifted from an upcoming higher price hour to a current lower price hour, or from a current higher price hour to an upcoming lower price hour. We name the first process as "backward demand shifting" (BDS) and the latter as "forward demand shifting" (FDS). The schematic representation of the proposed operation scheme is shown in Figure 4.1 and Figure 4.3. A onetime user input is required for defining minimum, maximum and preferred equipment operation setpoints using the EMS interface, in addition, the user defines a reference energy price for the controller. On its part, the controller receives projected load data from the EMS and transmits the optimized equipment load levels to the EMS. A regulator is required to manage the communication and information flow between EMS, proposed controller, and ultimately process the operation signals for the controllable equipment's use. At each time increment, the controller sends two signals; one for the current operation setpoint

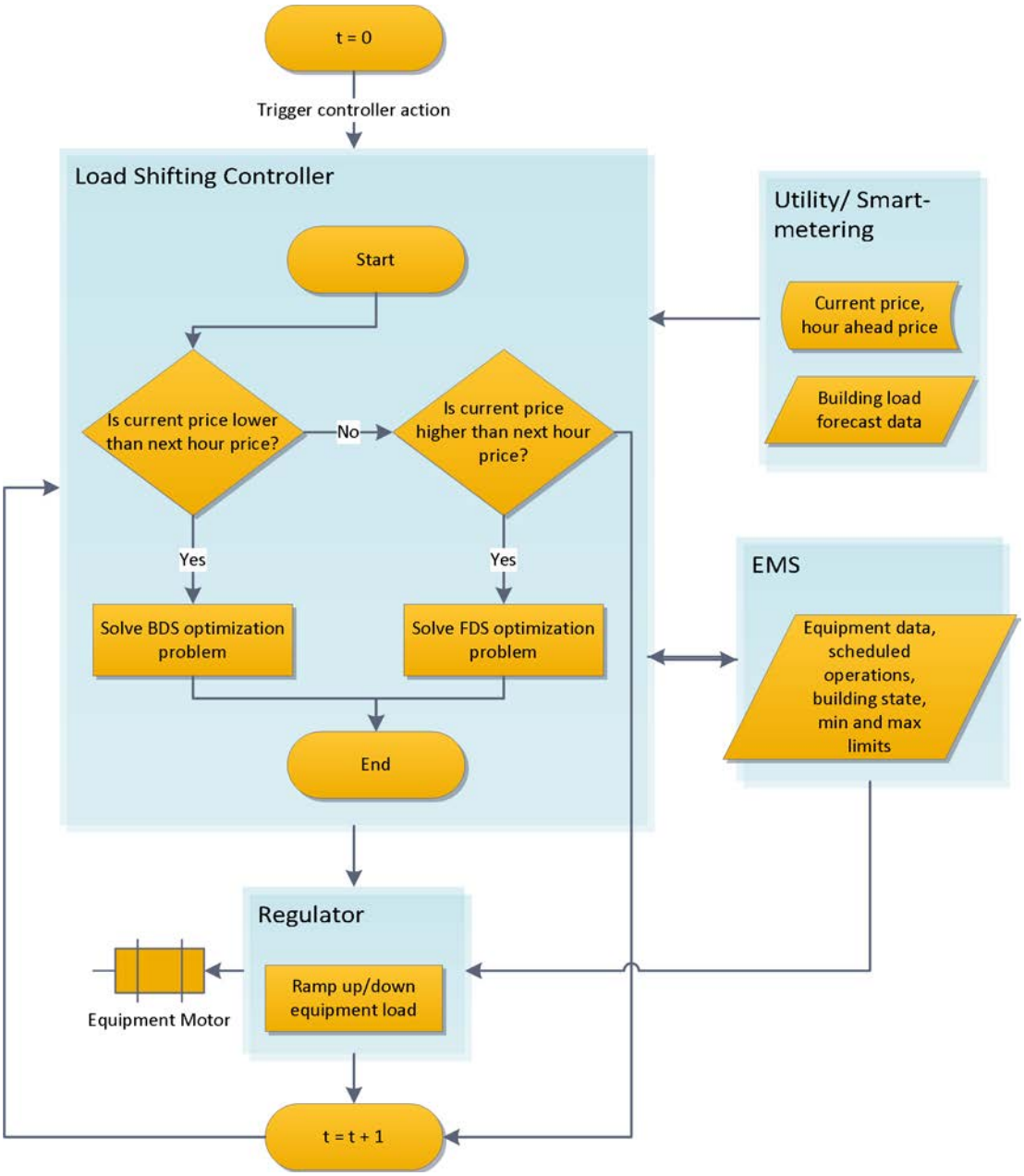

Figure 4.1. Flow chart of demand shifting controller in a RTP-HA scheme where price information are available for the current hour and the following hour only.

and the second signal is delayed for the following time increment operation setpoint, thus achieving demand shifting.

For example, in the case of a thermostat load, the output of the controller is a real number representing the optimal amount of energy required for shifting. The regulator then processes the control signal and matches it to a temperature thermostat setpoint. The

matching process is executed through a pre-defined table of assigned setpoints to different energy ranges. This procedure is schematically represented in Figure 4.4. Simultaneously, the EMS monitors the energy level and makes necessary adjustments utilizing the EMS to controller input channel.

In the case of the HVAC example above, the demand shifting approach insures minimal impact to the preferred comfort conditions through increasing the buildings' thermal inertia prior to the temporarily reduction in HVAC loads. This goal would not be achievable if the demand shaving approach was chosen.

Mathematical Formulation

The mathematical optimization model concept is based on minimizing the sum of the squared deviation of energy costs from two consecutive hours along a reference datum, where the energy costs are only available for the two consecutive hours through the RTP-HA system and the reference datum is the one-time user input value. Detailed formulations of the model are explained in the following subsections.

BDS Model Mathematical Formulation

Using time step increments of 1 hour, if the current energy rate at time t is cheaper than that of the upcoming time step increment, $t+1$, then the BDS approach is triggered, and the controller output signal is determined through the following algorithm:

$$\underset{e_{t+1}^{loss}=e_t^{gain}+\varepsilon}{argmin} \left\{\left[\lambda^{FR}.D_t - \lambda_t^{DR}.\left(D_t + e_t^{gain}\right)\right]^2 + \left[\lambda^{FR}.D_{t+1} - \lambda_{t+1}^{DR}.\left(D_{t+1} - e_{t+1}^{loss}\right)\right]^2\right\} \tag{4.1}$$

Subject to:

$$e_{t+1}^{loss} \leq e_{t+1}^{max} \tag{4.2}$$

$$e_t^{gain} \leq e_t^{free} \tag{4.3}$$

$$e_{t+1}^{loss}, e_t^{gain} \geq 0 \tag{4.4}$$

$$e_{t+1}^{loss} = e_t^{gain} + \varepsilon \tag{4.5}$$

where D_t is the consumer's expected (forecasted) demand at current time increment, e_{t+1}^{loss} is the optimal amount of load to be shifted from the upcoming time increment to the current one by becoming e_t^{gain} at the current time increment, thus, constraint (4.5) is applied. ε is an arbitrary value set by the user to identify whether to enforce a complete load shifting or to allow for partial load shifting. In this chapter, we assume complete load shifting and thus ε is set to 0. Later in chapter 6, we propose a strategy for considering tradeoffs and flexibilities in load shifting. λ^{FR} and λ_t^{DR} are the user-defined reference price and the available dynamic rate in the RTP-HA system, e_{t+1}^{max} is the maximum limit for the energy reduction during the upcoming time increment, e_t^{free} is the unutilized load capacity, which can be added to the current load at the current time increment.

D_t and D_{t+1} are approximated from smart metering and EMS data through the use of intelligent forecast methods and information about building state from EMS. e_{t+1}^{max} and e_t^{free} are determined from EMS using the user-set tolerance limits and information about the building state. λ^{FR} remains constant for all DR processes until the user decides to interfere and adjust his reference price. λ_t^{DR} and λ_{t+1}^{DR} are communicated to the controller through the utility-to-controller channel. These two sets of prices are updated at each time increment in the RTP-HA, where λ_{t+2}^{DR} and later prices are unknown at time t. e_{t+1}^{max} is computed from:

$$e_{t+1}^{max} = \sum_{i} {e_{t+1}^{max}}_{i} \tag{4.6}$$

where ${e_{t+1}^{max}}_{i}$ is the maximum amount of energy which can be reduced from equipment i during the upcoming time period $t+1$. ${e_{t+1}^{max}}_{i}$ and ${e_{t}^{free}}_{i}$ are calculated from EMS data using the user's tolerance levels and other parameters in the system depending on the type of load. For example, for cooling loads, as demonstrated by the diagram in Figure 4.3, ${e_{t+1}^{max}}_{i}$ may be expressed as:

$${e_{t+1}^{max}}_{i} = f\left(R^{TOL}, T_{t+1}^{out}, T_{t+1}^{in}, c_i\right) \tag{4.7}$$

where ${e_{t+1}^{max}}_{i}$ is a function of the maximum temperature given by the consumer's tolerance level R^{TOL}, the outside temperature T_{t+1}^{out}, the indoor temperature T_{t+1}^{in}, and the measured energy demand for equipment i at full load c_i.

FDS Model Mathematical Formulation

In contrast to BDS, FDS is triggered when the current energy rate at time t is more expensive than that of the upcoming time step increment $t+1$. The algorithm for computing the controller output signal thus becomes:

$$\underset{e_{t+1}^{gain} = e_t^{loss} - \varepsilon}{argmin} \left\{ \left[\lambda^{FR}.D_t - \lambda_t^{DR}.\left(D_t - e_t^{loss}\right)\right]^2 + \left[\lambda^{FR}.D_{t+1} - \lambda_{t+1}^{DR}.\left(D_{t+1} + e_{t+1}^{gain}\right)\right]^2 \right\} \tag{4.8}$$

Subject to:

$$e_t^{loss} \leq e_t^{max} \tag{4.9}$$

$$e_{t+1}^{gain} \leq e_{t+1}^{free} \tag{4.10}$$

$$e_t^{loss}, e_{t+1}^{gain} \geq 0 \tag{4.11}$$

$$e_{t+1}^{gain} = e_t^{loss} - \varepsilon \tag{4.12}$$

where e_t^{loss} is the optimal amount of load to be shifted from the current time increment to the upcoming one by becoming e_{t+1}^{gain} at the upcoming time increment. D_t, ε, λ^{FR}, and λ_t^{DR} are defined in the previous subsection. Similar to our assumption in BDS, ε is set to 0., e_t^{max} is the maximum limit for the energy reduced during the current time increment, e_{t+1}^{free} is the maximum available capacity for load increase at the current time increment (i.e. unutilized load capacity).

Model Linearization

Instantaneous DR in real time requires solving the optimization algorithm in a timely manner, however, in the case of BDS, the objective function (4.1) is nonlinear. Linearization of the model is achievable by substituting the quadratic components, $\left(D_t + e_t^{gain}\right)^2$ and $\left(D_{t+1} - e_{t+1}^{loss}\right)^2$, of (4.1) with the two new variables y and z correspondingly. Constraint (4.5) can be used to eliminate the nonlinear components ${e_t^{gain}}^2$ and ${e_{t+1}^{loss}}^2$ through solving for $y - z$ and adding the new set of constraints (4.17), (4.18), and (4.20). The first two constraints eliminate the minimization bias by insuring that the optimal solution is not achieved such that the chosen values of e_{t+1}^{loss} or e_t^{gain} cause y and z to be zeroed. The linearized model is formulated as:

$$\underset{e_{t+1}^{loss}=e_t^{gain}}{argmin} \Big\{-2 \cdot \lambda^{FR} \cdot \lambda_t^{DR} \cdot D_t \cdot e_t^{gain} + 2 \cdot \lambda^{FR} \cdot \lambda_{t+1}^{DR} \cdot D_{t+1} \cdot e_{t+1}^{loss} + {\lambda_t^{DR}}^2 \cdot y + {\lambda_{t+1}^{DR}}^2 \cdot z - 2 \cdot \lambda^{FR} \cdot \left(\lambda_t^{DR} \cdot {D_t}^2 + \lambda_{t+1}^{DR} \cdot {D_{t+1}}^2\right) + {\lambda^{FR}}^2 \cdot \left({D_t}^2 + {D_{t+1}}^2\right)\Big\} \tag{4.13}$$

Subject to:

$$e_{t+1}^{loss} \leq e_{t+1}^{max} \tag{4.14}$$

$$e_t^{gain} \leq e_t^{free} \tag{4.15}$$

$$e_{t+1}^{loss}, e_t^{gain}, y, z \geq 0 \tag{4.16}$$

$$y \geq {D_t}^2 + 2 \cdot D_t \cdot e_t^{gain} \tag{4.17}$$

$$z \geq {D_{t+1}}^2 - 2 \cdot D_{t+1} \cdot e_{t+1}^{loss} \tag{4.18}$$

$$e_{t+1}^{loss} = e_t^{gain} \tag{4.19}$$

$$y - z = {D_t}^2 - {D_{t+1}}^2 + 2 \cdot e_{t+1}^{loss} \cdot (D_t + D_{t+1}) \tag{4.20}$$

The BDS model becomes linear and can be solved using linear programing solvers. Similarly, the linearized FDS model formulation becomes:

$$\underset{e_t^{loss}=e_{t+1}^{gain}}{argmin} \left\{2\lambda^{FR} \cdot \lambda_t^{DR} \cdot D_t \cdot e_t^{loss} - 2.\lambda^{FR} \cdot \lambda_{t+1}^{DR} \cdot D_{t+1} \cdot e_{t+1}^{gain} + {\lambda_t^{DR}}^2 \cdot y + {\lambda_{t+1}^{DR}}^2 \cdot z - 2 \cdot \lambda^{FR} \cdot \left(\lambda_t^{DR} \cdot {D_t}^2 + \lambda_{t+1}^{DR} \cdot {D_{t+1}}^2\right) + {\lambda^{FR}}^2 \cdot \left({D_t}^2 + {D_{t+1}}^2\right)\right\} \tag{4.21}$$

Subject to:

$$e_t^{loss} \leq e_t^{max} \tag{4.22}$$

$$e_{t+1}^{gain} \leq e_{t+1}^{free} \tag{4.23}$$

$$e_t^{loss}, e_{t+1}^{gain}, y, z \geq 0 \tag{4.24}$$

$$y \geq {D_t}^2 - 2 \cdot D_t \cdot e_t^{loss} \tag{4.25}$$

$$z \geq {D_{t+1}}^2 + 2 \cdot D_{t+1} \cdot e_{t+1}^{gain} \tag{4.26}$$

$$e_t^{loss} = e_{t+1}^{gain} \tag{4.27}$$

$$y - z = {D_t}^2 - {D_{t+!}}^2 - 2 \cdot e_t^{loss} \cdot (D_t + D_{t+1}) \tag{4.28}$$

Both the BDS and FDS models can then be solved optimally using linear programing solvers. The model linearization proves the practicality of the proposed controller application through permitting timely response in the real time setting. In chapter 6, we

introduce a single nonlinear algorithm combining BDS and FDS and solve it in real time, without linearization. We also introduce a consumer utility concept in chapter 6, which allows for higher flexibility in load shifting.

Case Study: Industrial Facility Air Handling System

Case Description

In this section, we demonstrate through simulation the load shifting process for the industrial building MI0189. From the energy audit for consumer MI0189, Five components in the HVAC system were identified as candidates for load control; air duct fans, direct expansion (DX) compressors, DX air handlers, exhauster fans, and the Roof Top Units (RTUs). Utilizing an EMS permits the consumption control of fan motors and RTUs through VSDs and automatic control of thermostat settings. From the audit, it was recorded that the thermostat settings were set to between 68◦F and 72◦F during production hours while the recommended range is from 68◦F to 76◦according to the OSHA standards [72]. Moreover, the exhauster, air handler and duct fans were running at full or close to full capacity when turned on. The weekly consumption of these components compared to the overall consumer's demand is shown in Figure 4.2. The data indicates that the five candidate components account for roughly 30% of the peaking demand during workdays. We demonstrate the operation scheme of the controller on the inline duct cooling/ventilation systems since they account for significantly large amount of the building's energy consumption.

Simulation Parameters

Simulation of the building and the EMS operation was feasible due to the availability of real time-interval data. Such data were captured for a 1 week period as part of the

energy audit process by utilizing programmable data loggers, current transducers, indoor and outdoor temperature sensors, and airflow meters. Using the parameter estimation toolbox in SIMULINK, a realistic thermal model for the building was developed. The estimated parameters for the thermal model represent both the heat gains as a linear function of the ambient temperature due to the building's thermal resistivity, and the periodic nonlinear heat gains due to solar loading, machine operation, and human traffic. The validation step proved that the simulation model produces energy and temperature outputs matching the actual measured data. The MATLAB/SIMULINK framework for the proposed controller is shown in Figure 4.3.

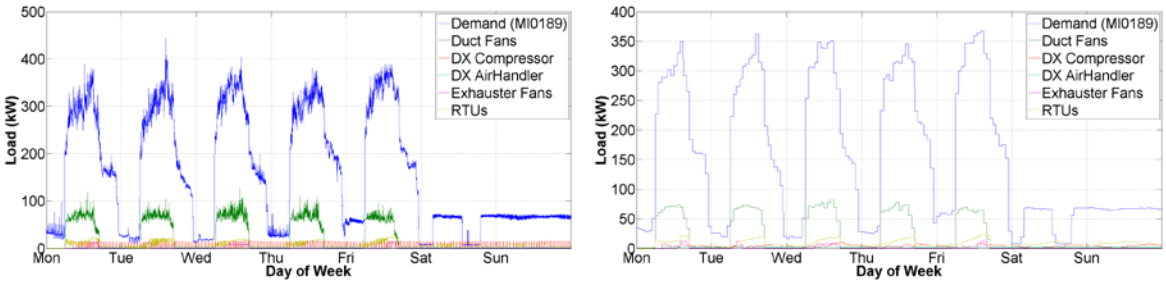

(a) (b)

Figure 4.2. Building MI0189 1-week demand profile with 5 candidate HVAC components for demand control: (a) 1-minute logged demand and (b) hourly averaged demand.

In this example, it is assumed that the one-time user input to the controller sets his reference price to \$0.1/kWh and his lower and upper limits for temperature to 70◦F and 78◦F, respectively. The controller then solves the optimization functions for BDS and FDS for each time step and outputs the proposed amount of energy to trim or add for the current and forthcoming time steps. The regulator processes the controller's output by translating it to thermostat set points and to on/off signals. The on/off signals dictate the cycling between the parallel systems. The two SIMULINK block schemes for the regulator functions are shown in Figure 4.4 and Figure 4.5.

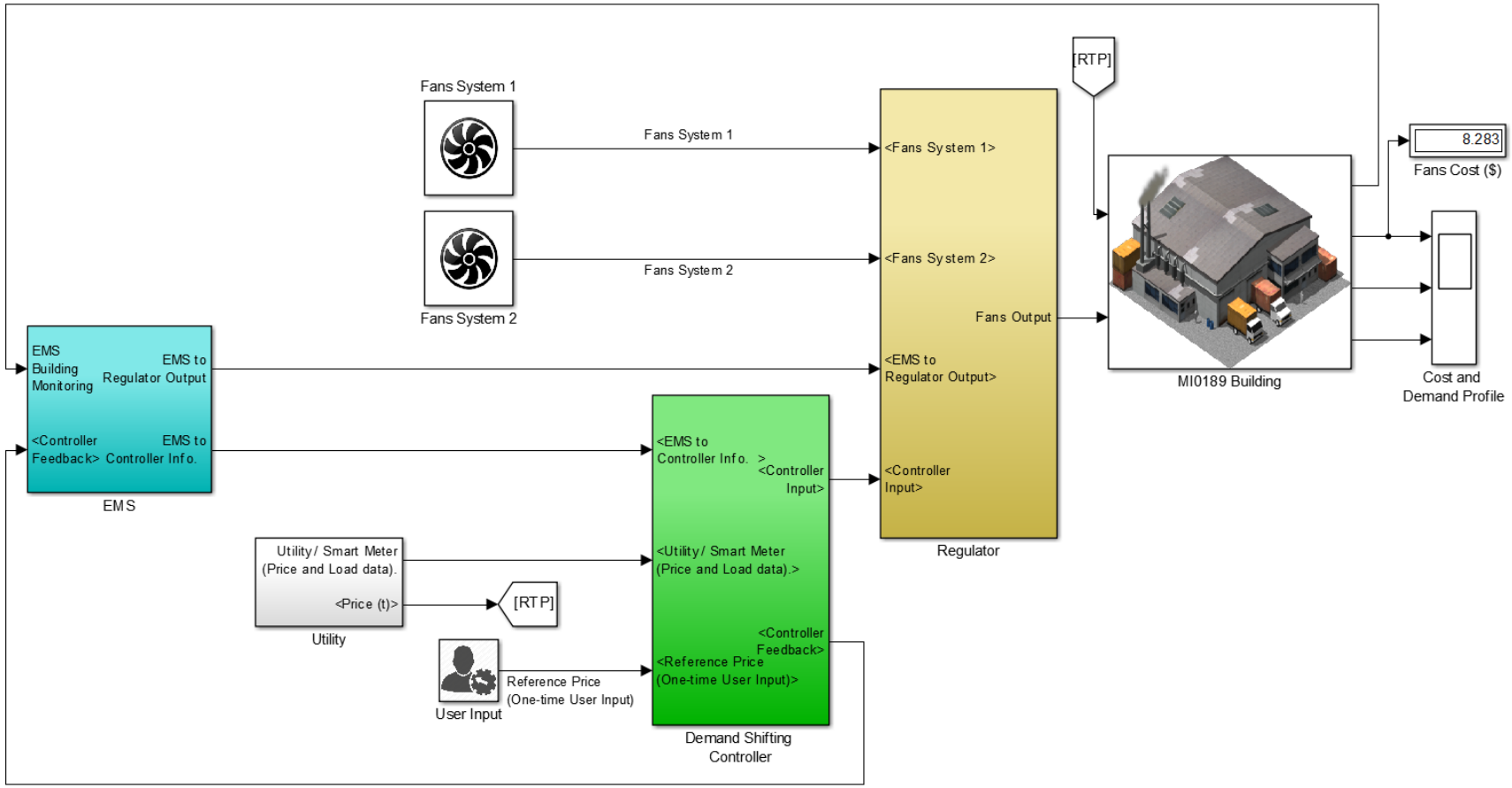

Figure 4.3. The Proposed controller and regulator system framework in SIMULINK for an industrial building with EMS and controllable cooling/ventilation load.

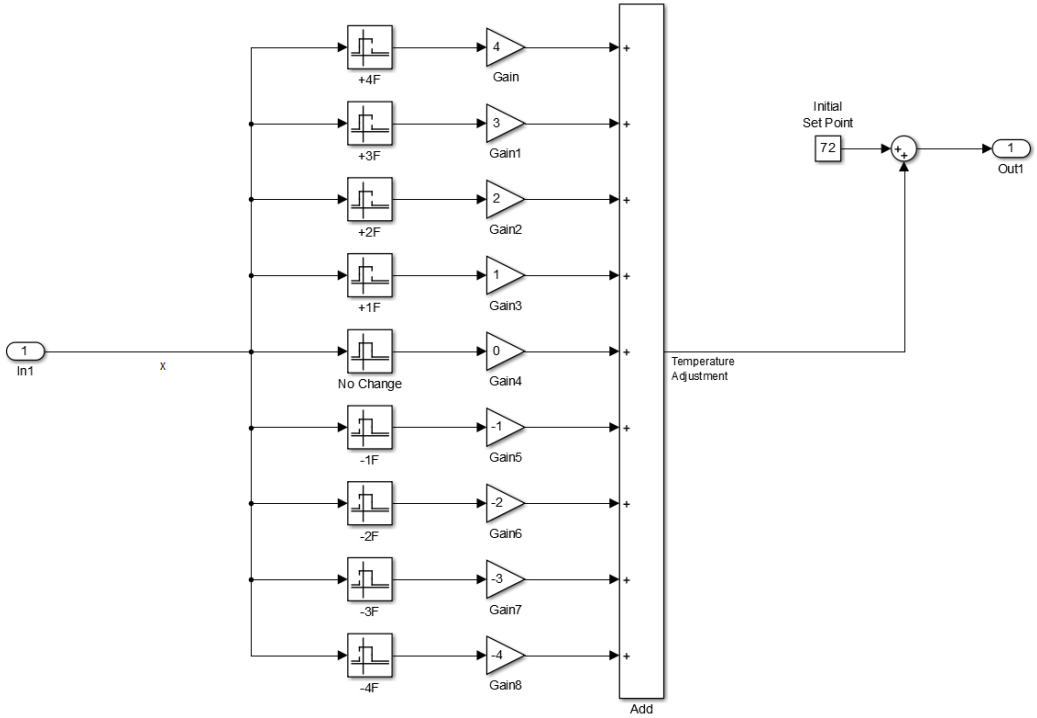

Figure 4.4. Regulator SIMULINK block schema for adjusting thermostat setpoints based on controller signal (e).

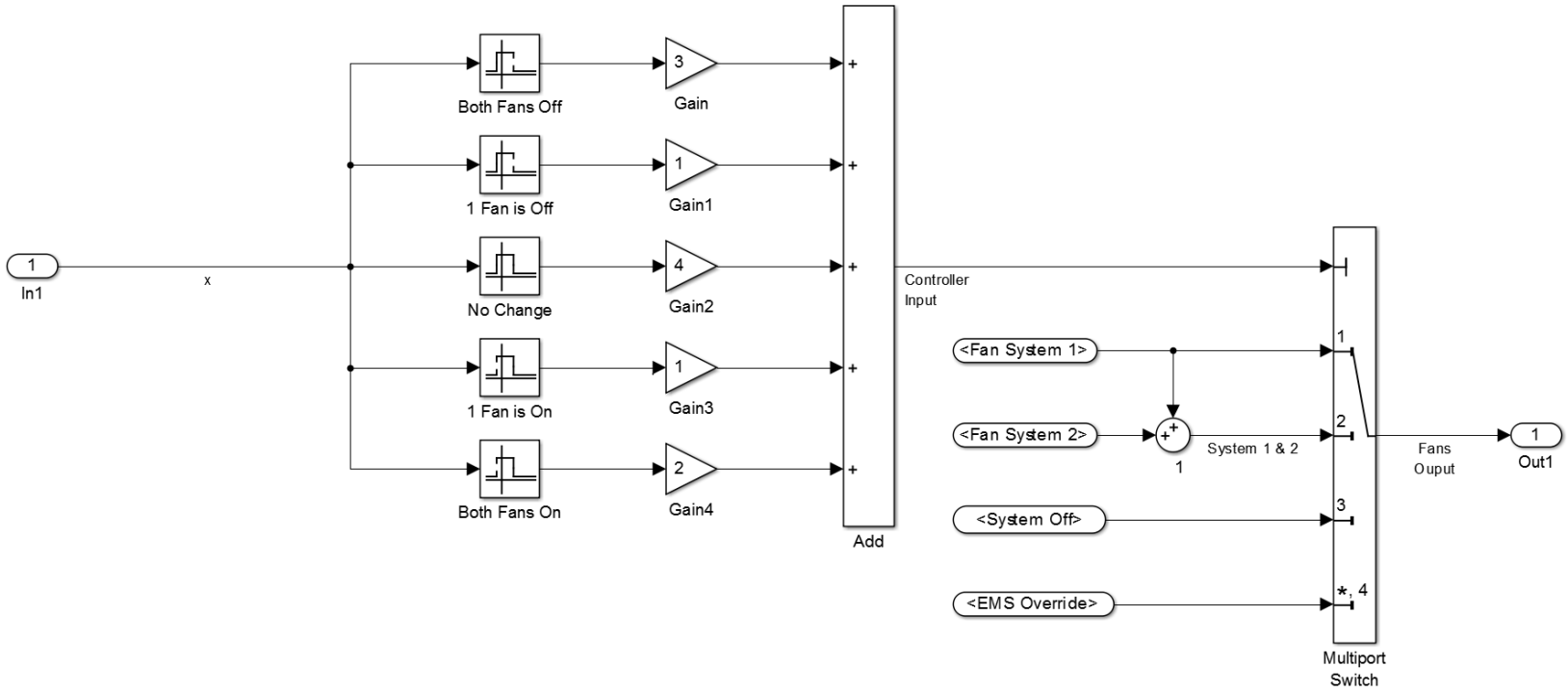

Figure 4.5. Regulator SIMULINK block schema for cycling between parallel HVAC units based controller signal (e)

Simulation Results

A simulation model was run for a 1 week period utilizing the simulated RTP-HA system discussed in chapter 3. Comparison of the demand profiles for the duct system before and after the implementation of the proposed algorithm is shown in Figure 4.6. The new demand profiles indicate the shifting, and sometimes shaving, of 50% and 100% of the duct system's demand away from the certain peak periods as triggered by the RTP-HA. The calculated savings are 17.9% in HVAC energy costs from the duct system alone and 10.2% savings in HVAC energy consumption which was achieved despite that only load shifting was intended for by the controller. As for the impact to the consumer with respect to the thermal comfort level, Figure 4.7 shows that the changes in the indoor climate conditions were minimal and insignificant. The minimal changes in indoor climate are attributed to the shifting of cooling energy which, as a result, increases the building's thermal inertia prior to demand reduction intervals.

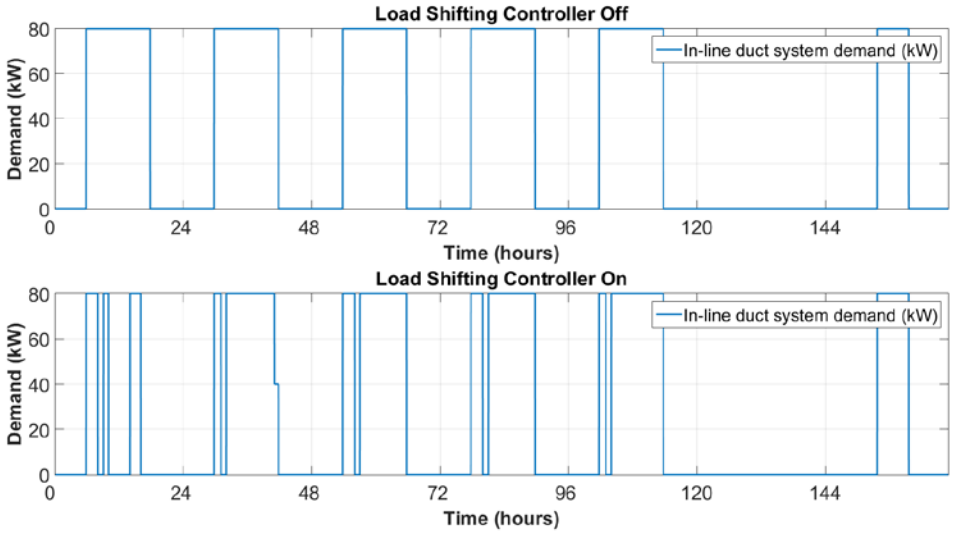

Figure 4.6. Duct system demand profiles before implementing the proposed controller (top) and after (bottom).

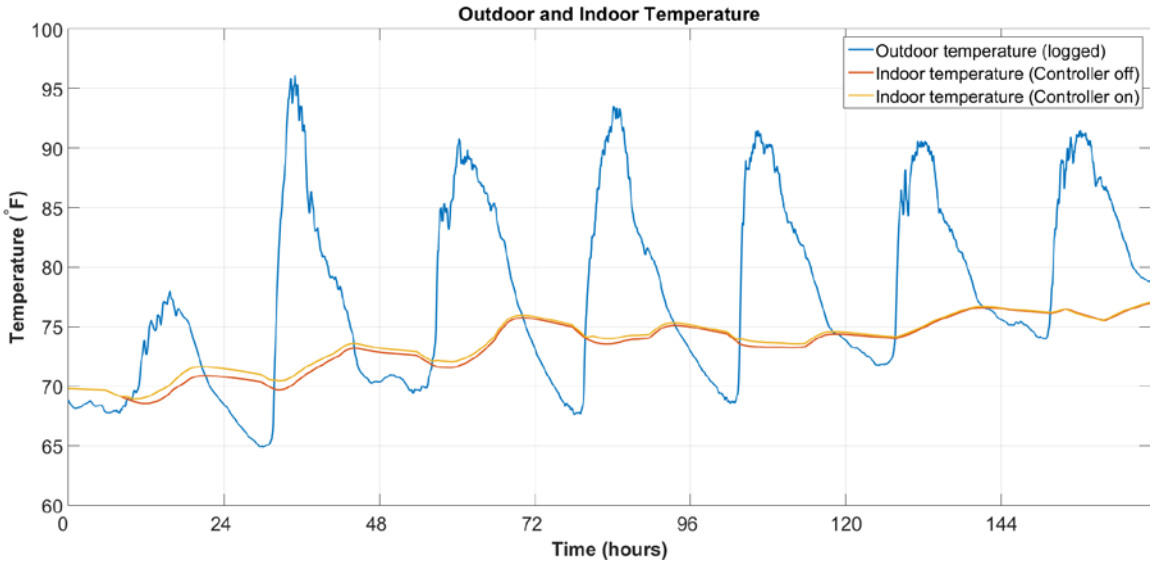

Figure 4.7. Comparison of the indoor climate conditions before and after controller implementation.

Results and Discussion

Model Assumptions

In order to confidently validate the functionality of the proposed load shifting controller method, we assumed conservative conditions when running the simulation; Different than the case study discussed above, it is assumed that no reduction in energy will be allowed and only complete load shifting is forced, even if the buildings' state monitoring system does not show necessity for accepting significant demand increase as a result of load shifting. This can be regarded as the worst-case scenario or the case of storing energy for use during the more expensive time periods.

Consumer-Side Impact

The results were obtained from simulations runs in SIMULINK. The obtained results indicated reductions in HVAC and compressed air systems costs for all eight consumers in the RTP-HA environment. The equipment energy costs savings are provided in

Table 4.1. A Comparison of the demand profiles for each of the eight consumers before and after applying the controller is shown in Figure 4.8. Figure 4.9 shows the

change in each building's equipment energy demand when the load shifting controller is applied. The drops and spikes shown in both figures indicate the magnitude of the load being successfully shifted in response to price signals from the utility. This results in energy cost savings for the consumers. For example, a reduction of HVAC energy costs for consumer MI0189 by 3.06% was achieved. Which is equivalent to annual dollar savings of $1029.6. The savings are obtained from controlling the cycles and operation of the duct fans, DX compressor, DX air handler, and the air conditioning RTUs. Building MI0268 showed the highest savings of 4.52%, which is equivalent to $22,100 savings in annual energy bills for that building. Building MI0268 savings are achieved from controlling the building's air compressors and air conditioning RTUs. The equipment utilized in each building for the building's energy demand shifting are listed in Table 4.2.

Table 4.1. Equipment energy cost savings when applying the demand shifting controller method.

Consumer	MI0189	MI0197	MI0246	MI0265	MI0198	MI0267	MI0234	MI0268
Savings (%)	3.06%	1.08%	0.41%	2.41%	0.30%	0.48%	2.69%	4.52%
Equivalent annual savings ($)	$1,039.6	$327.6	$572	$7,436	$260	$988	$535.6	$22,100

Table 4.2. Equipment utilized per building as candidates for demand shifting.

Building	**Equipment types for demand shifting**
MI0189	Duct fans, DX compressors, DX air handlers, RTUs
MI0197	Air compressors, DX compressors. DX air handlers
MI0198	Air compressors, chiller systems, RTUs
MI0234	Air compressors. DX compressors, DX air handlers
MI0246	Air compressors, chiller systems, DX air handlers, RTUs
MI0265	Air compressors, chiller systems, production water chillers, cooling tower fans
MI0267	Chiller systems, RTUs, water coolers
MI0268	Air compressors, RTUs

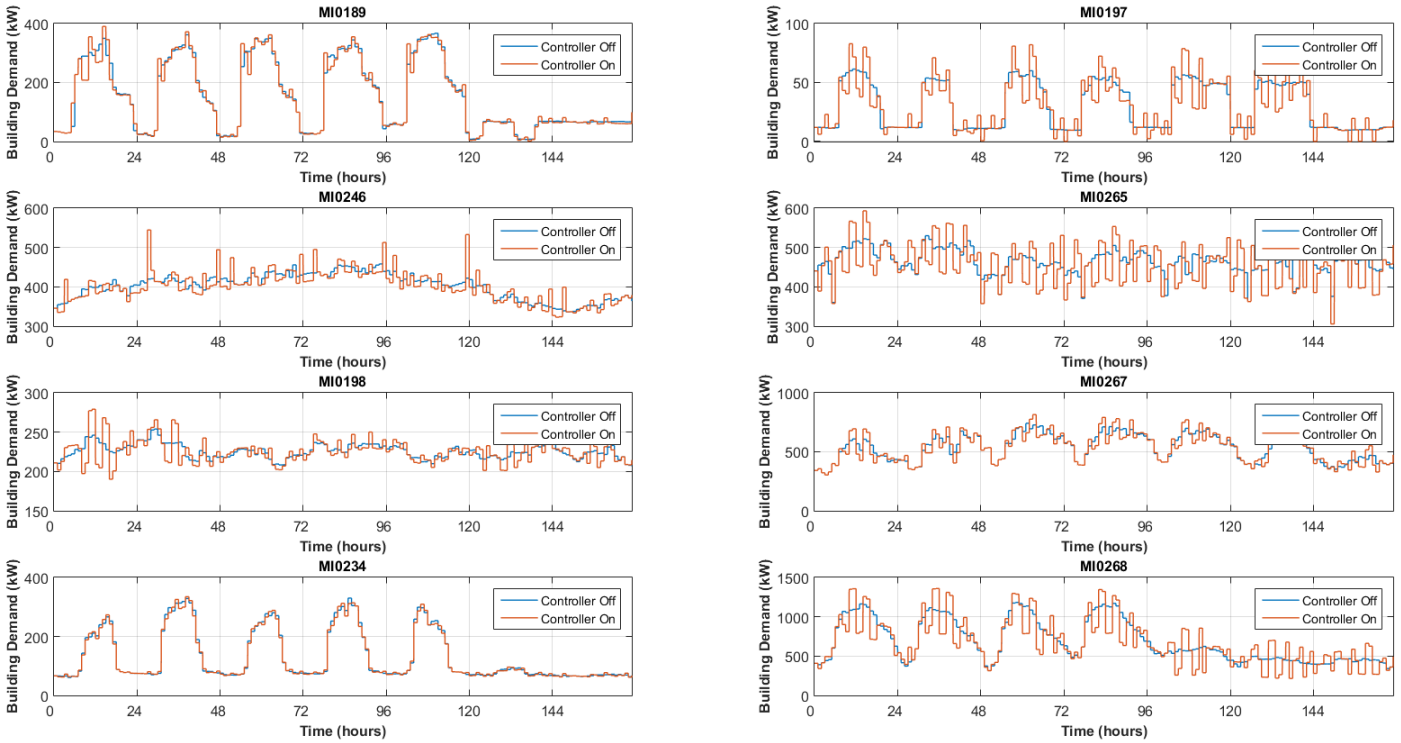

Figure 4.8. The eight consumers' demand Profiles prior and Post to demand shifting in the RTP-HA scheme.

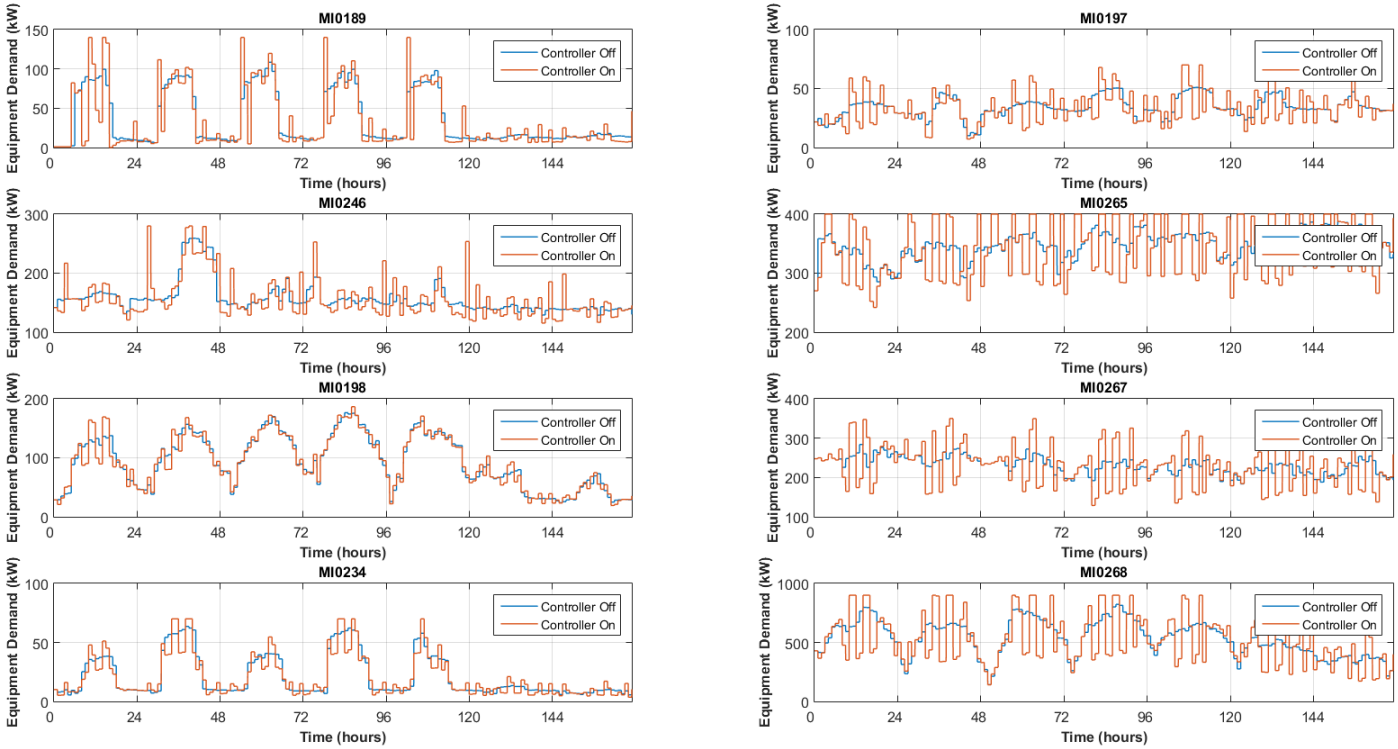

Figure 4.9. The change in the lumped equipment load profiles for the eight due to load shifting in RTP-HA scheme.

Supplier-Side Impact

The impact to the utility can be studied from the lumped simulation results for each consumer; When all buildings in the system follow the proposed demand shifting method guided by the RTP-HA scheme, the new aggregated load impacts the utility by creating new load spikes away from the expected peak hours as shown in Figure 4.10. This load synchronization occurs as all consumers shift a portion of their loads to the cheapest hours. The new aggregated peak in the one week simulation data becomes 3999 kW instead of 3737 kW before implementing DR. This corresponds to a 7% increase in the PAR, which, in result, would threaten the stability of the system and invalidate the purpose of demand controlling through imposing dynamic tariffs. A mitigation of this problem would be offsetting the controller triggers, either at the building level or the equipment level, in order to start at different time instances from each other. The resulting outcome is shown in Figure 4.11. Moreover, a finer RTP system can aid in this issue where new prices are generated every 15 min instead of every hour.

Utility cost analysis was performed using the simulation results. We calculated a drop in utility cost of generation by 0.3% as a result of large load reductions during peak hours. The drop would be higher if load synchronization is avoided. The utility revenue using a RTP system becomes 3.4% higher than when using the conventional flat rate tariff. Therefore, we conclude that all parties benefit from switching to RTP system guiding an effective load shifting method like the one proposed in this chapter. This 3.4% expresses the maximum amount of reduction in the RTP tariff, which the utility can apply as a form of incentives without affecting their expected revenue achieved, had they been using the flat tariff system.

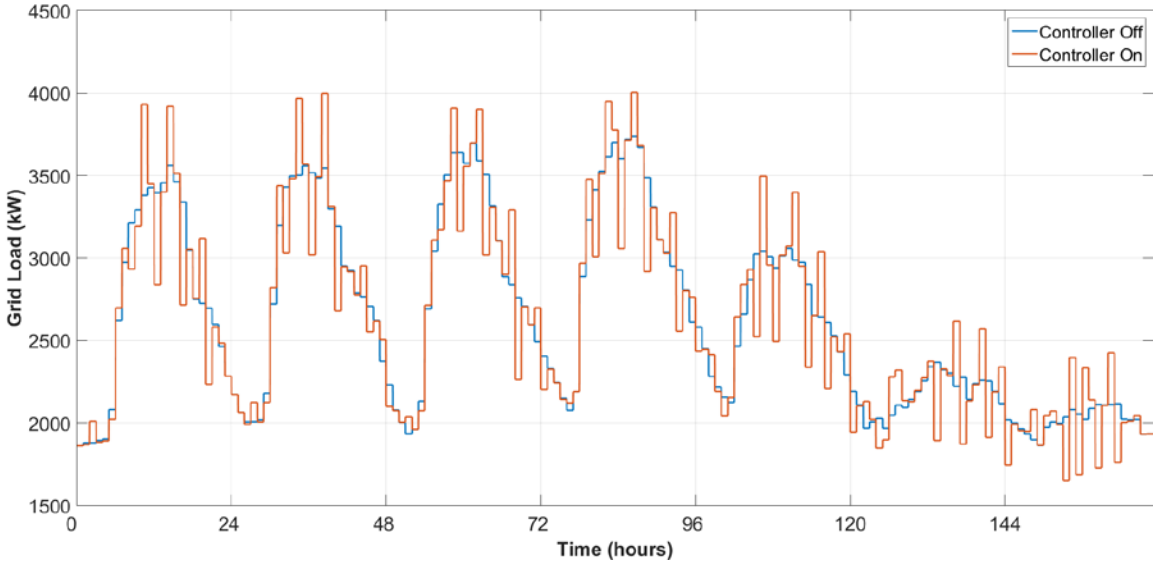

Figure 4.10. New load synchronization peaks when all consumers use demand shifting controllers at the exact same time instances following the RTP-HA signals.

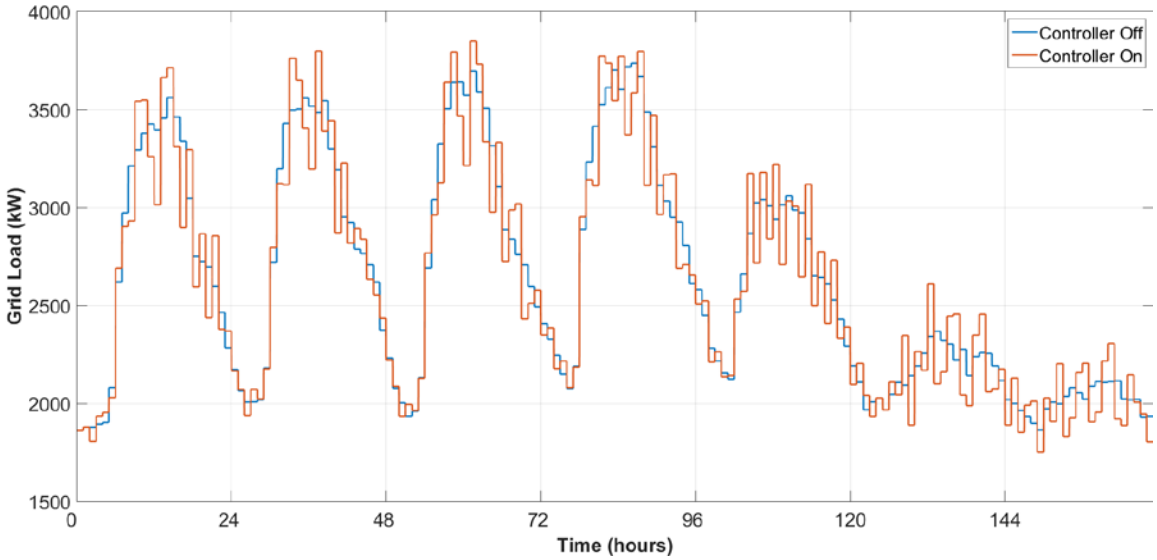

Figure 4.11. Reduction in load synchronization peaks when consumers use demand shifting controllers at randomly offset time instances.

Discussion

In an effort to understand the discrepancies in achieved savings between different consumers, an interesting conclusion was drawn out from the analysis of simulation results; there is an evident relationship between a consumer's load profile and the saving potentials from applying DR. For instance, buildings with higher volatility in the demand profile (e.g. MI0268) achieve higher savings from the reduction of peaks during

expensive hours than buildings with less volatile demand profiles (e.g. MI0246). It is also noted that the price volatility in real time is a significant factor which affects the utilization of the proposed method.

Although the model considered only industrial and commercial consumers, it is predicted that the proposed DR method would produce much higher savings for residential consumers due to their higher flexibility compared to commercial and industrial consumers, where goals like productivity, throughput, and the requirements of JIT manufacturing limit the flexibility in scheduling energy demanding operations. Thus, many researchers target the residential sector as a good candidate for demand shifting or shaving. In this study, the industrial consumer's inflexibility was accommodated for by assuming that only a modest portion of the demanded energy, such as that consumed by HVAC systems or compressed air systems, can be shifted only between two consecutive hours, either by increasing the utilization at one hour on the expense of the following or preceding hour, or through storage systems use.

The proposed method emphasizes load shifting, although, realistically, demand shaving can be achieved by impacting the comfort level during peak demand periods. The simulation results indicate that costs can be reduced by HVAC's demand shifting methods driven by the real time tariffs. However, as shown in Figure 4.8 and Figure 4.9, the RTP as a DR method does not necessarily result in reducing high demand peak, instead, peak demand is shifted to a cheaper hour and may even become higher during that hour, without any penalty forms as in IBR for instance. Even if IBR is applied as some researchers had argued, the aggregate effect of having many consumers concentrate a portion of demand, with or without a limiting penalty, to a certain period would

produce high demand spikes. It should be noted that load shifting and peak load shaving are two contrasting objectives, however, both objectives can be merged. The main focus of the proposed method was on the former objective.

The results proved a critical limitation with the existing pricing systems as drivers for DR. Improvement of the current pricing policies is required. For example, a less aggregated or a consumer-customized method for determining dynamic tariffs is required in order to avoid the load synchronization effect. Although the consumer-side DR is the main focus of this dissertation, in the following chapter, we develop machine learning approaches for load disaggregation and briefly discuss their relevance to the load synchronization problem. The other problem witnessed in the results is the co-dependency between price and demand which is not accounted for when generating new prices each hour. These problems lead to further research opportunities with the goal of developing new, adaptive algorithms for generating near-optimal prices with the purpose of reducing the PAR accounting for the consumer's response.

Chapter Conclusive Remarks

This chapter proposed a control schema and an algorithm for the instantaneous shifting of controllable loads. The controller receives price signals set an hour in advance by the RTP-HA tariff system and instantaneously plans loads for the current and following hour in coordination with an existing EMS. The algorithm is transformed to a linear problem, which does not require realizable computational time, making it practical for use in a fast-pace real time environment. The model is tested using real data from 8 industrial and commercial buildings in Florida during the summer period.

The results indicated instantaneous DR can be achieved successfully while omitting the need for longer planning horizons as done in previous research. Additionally, the results showed minimal impact to the consumers' comfort standards. Following the proposed method, it can be concluded that utilizing RTP-HA price signals results in lowering consumption costs for consumers.

As with all DR approaches, the model raises the issue of load synchronization. While mitigation of load synchronization may be possible by applying DR signals of less than an hour (15 or 30 minutes), it is evident that the existing pricing systems can benefit from restructuring or new policies need to be implemented.

Chapter 5: Load Disaggregation

Chapter Introductory Remarks

Currently, utility providers and regulators rely heavily on the system's aggregate demand information for setting energy tariffs, deploying DR programs, and planning supply generation for both baseline and peaking loads. However, this approach may result in efficiency losses for DR applications and may even yield counterproductive responses as with the case of load synchronization. Therefore, disaggregation of consumers' loads, by clustering and classifying consumers exhibiting similar consumption patterns, can result in better DR performance, where energy rates are diversified according to each cluster of consumers. Previous work had proven that clustering of load profiles (LP) yields better tariff design [73-75], demand forecast [76-78], production planning [73, 79-87] and even addresses smart meter data forgery and security problems [84, 88].

Clustering is the unsupervised process of machine learning, where unlabeled consumers are partitioned according to their similar features, without a priori knowledge of the clusters' structure. Classification is the process of assigning new consumers to existing and known clusters.

Chapter Motivation

In the previous chapter, the aggregate system simulation results showed a negative impact of load synchronization, which motivated the discussions in this chapter. While the virtual consumers had benefited from utilizing the proposed load shifting methodology, the utility provider had suffered higher spikes due to the synchronization of loads in the low energy price periods. Optimizing the consumer-side DR is the major

topic of this dissertation, however, we had conducted additional work in the topic of consumer load profile disaggregation for better utility-side managing of DR. This discussion is part of the work published in [89-91].

Chapter Objectives

The goal of this chapter is to address new approaches for consumer load profile clustering and classification with the objective of designing customized and more efficient RTP-HA rates, which would reduce the impact of load synchronization. The clustering segment is guided by the objective of determining similar periodic behaviors among consumers. In addition, a new classification algorithm is proposed with the objective of outperforming classical methods in accuracy, faster adaptation to changing consumer behaviors, and faster labeling of new consumers.

Data for Disaggregation

Laboratory archived data were mined to study the similarities in consumption among various consumers. The archived data were collected over the course of 14 years from manufacturing and commercial consumers. From the data, 15-minute interval time-series demand readings were extracted for 60 consumers.

In order to prepare raw data for disaggregation, first, we applied a smoothening algorithm, which combines multiple regression models in a k-nearest-neighbor based meta-model. This step helps in removing noise from the data (i.e. random variations). Second, we normalized each data entry on the {1,0} scale in order to achieve comparativeness among the population individuals. This step is important since, in disaggregation, we are interested in comparing individuals based on their consumption patterns and not their consumption sizes.

Clustering Load Profiles

The next step in the load disaggregation process is to identify unique clusters of consumers. There is no optimal strategy to clustering data, since the assessment of a clustering quality is subjective to the user and highly depends on his objectives. Previous load clustering studies were concerned about identifying typical daily load profiles among a group of consumers [74, 79, 80, 82, 83, 85-87], who were mostly residential. However, typical daily load profile clusters do not identify, and accordingly distinguish, the periodic consumption behaviors among consumers. In the context of industrial consumers, their consumption behaviors are characterized by being periodic and consistent across the production seasons. For example, a typical manufacturing facility may run 2 shifts and 5 days a week, resulting in identical waves of energy consumption during the 5 days followed by static, close to zero, consumption during the weekends. Then the same behavior is repeated for every week in the season. The same cannot be stated about the residential consumer, who is characterized by having a more random and unpredictable behavior. Therefore, in contrast to research in literature, our work argues that the successful disaggregation of industrial consumer load profiles for DR objectives is based on the typical weekly profiles. We have addressed the weekly load profile typification using two approaches:

The Wave Function Approach

In the first approach [90, 91], we argued that the repetitive behavior of an industrial consumer can be fitted, by a set of parameters, to a wave function. Accordingly, the parameter values act as features for cluster identification. We defined three main parameters, where each parameter uniquely contributes to a feature of the shape

variability in the consumer's weekly load profile. Furthermore, the combination of two or more parameters aid in identifying to identifying unique clusters. The first parameter, α, explains the intra-day variability, the second parameter, ω, represents the inter-day variability, and the third parameter, β, represents the intra-week variability. The three are parameters of the wave function described by:

$$f(t) = \alpha \cdot \sin(\omega \cdot t + \beta) + \gamma \tag{5.1}$$

where γ is an added calibration parameter. For the 60 consumers unlabeled data, we estimated the parameters using the Nelder-Mead simplex algorithm [92]. Because the algorithm requires unconstrained optimization, we added a post-processing function for scaling the optimized parameters, without affecting the shape generated by the periodic function (5.1). Finally, the K-means algorithm [93] was used to identify clusters of the three main parameter combinations in the 3-dimensional space as shown in Figure 5.1. The clustered data using this approach are shown in Figure 5.2. We chose the number of distinctive clusters as 6 using the elbow method with the plot of the error.

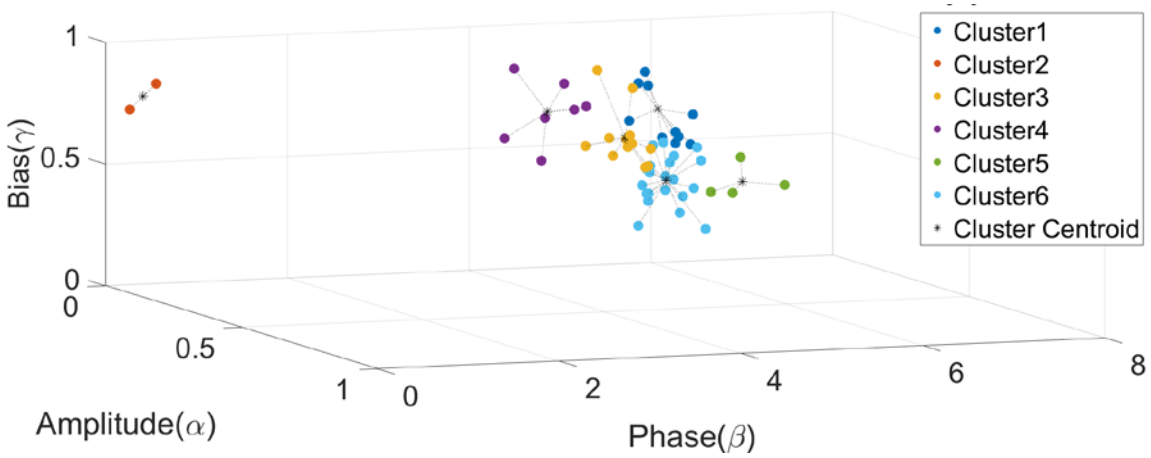

Figure 5.1. Data clusters and cluster centroids using the wave function approach.

The Time-Series Approach

In this approach, we find distinctive and continuous K-means computed across all the time intervals of the available data. The clustering problem dimension becomes as large

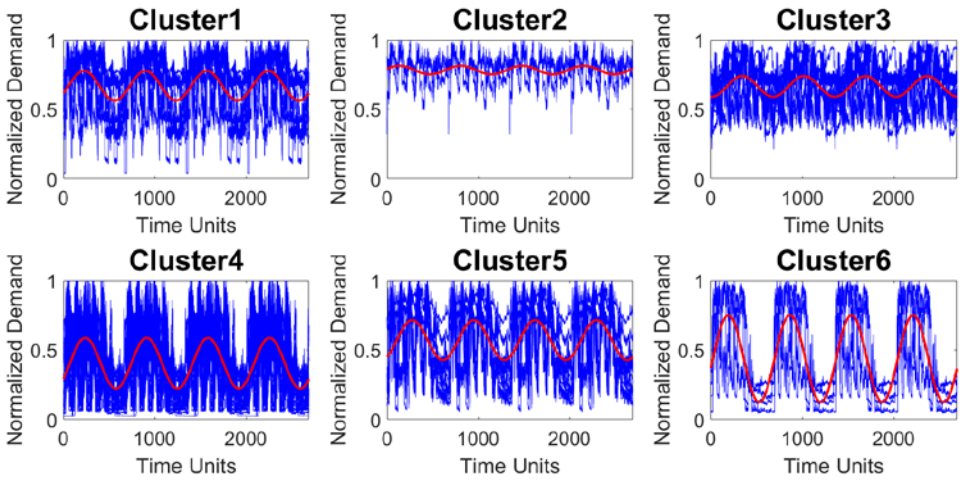

Figure 5.2. Clustered 1-month data plotted against their representative cluster wave function.

as the length of the data. The clustering optimization process becomes more memory exhaustive than in the previous case, where the clustering dimension is only 3, however, substantial amount of time is saved, since no parameter optimization is needed in this approach. The K-means objective in this approach become a function in time, which can be mathematically formulated as:

$$\min \sum_{k \in K} \sum_{j \in N} \left\| D_j(t) - \bar{C}_k(t) \right\|^2 \tag{5.2}$$

where K is the set of distinctive cluster centroids, N is the set of consumers, $D_j(t)$ is the demand-time function of consumer j and can be regarded the same as D_{t_j} for simplification, and $\bar{C}_k(t)$ is the centroid of cluster k, which is also a function of time. Using the same recursive procedure of the K-means algorithm, the clusters, represented by Figure 5.3, were identified. Different than the previous approach, we relied on the Silhouette analysis [94] to identify the number of clusters. However, the Silhouette analysis concluded that 6 is a good number of clusters, in line with the conclusions drawn from the method used in the previous approach. An extension of this work is available in

[89]. For the remainder of this chapter, we utilize clusters formed using the time-series clustering approach.

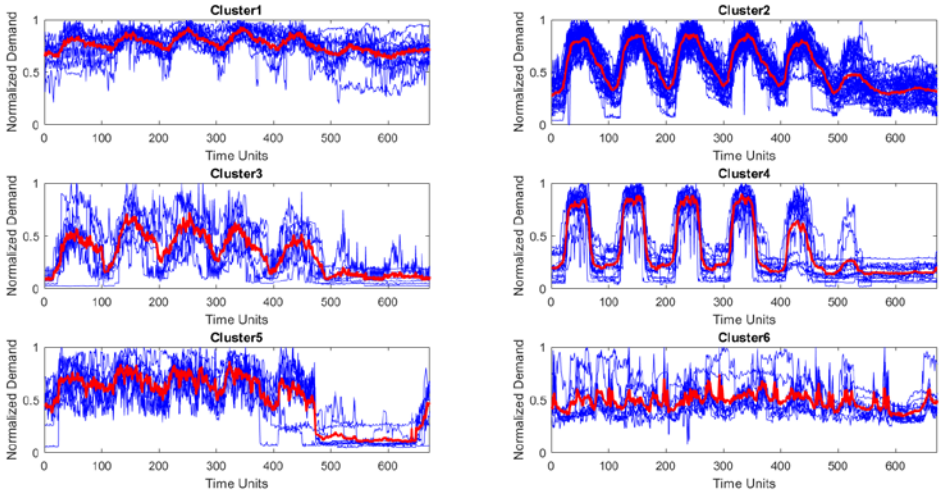

Figure 5.3. Clustered 1-week data plotted against their representative cluster centroid using the time-series approach.

Classification of DR Model Data

For the study data presented in the previous chapter, we disaggregate loads according to their proximity to the distinctive clusters. This process is known as classification. Classification is a supervised process of machine learning, where classes are defined *a priori*. Classifiers are trained using a data set of predictors and a response vector (i.e. previously clustered data), then a function is learned, which can assign new unobserved data (e.g. DR model data) to existing clusters.

The high dimensionality of the unobserved data imposes challenges to the classification process, when the time-series approach is sought. Our study in [89] concluded that even the best-known classification methods in machine learning do not guarantee quality for the very high dimensional (i.e large number of features) load profile data. Therefore, we proposed a unique classification method combining techniques from

optimization theory, fuzzy logic, and evolutionary computation. This method is presented in the following section.

The Fuzzy Genetic Algorithm for Classification

We developed the Fuzzy Genetic Algorithm (FGA) classifier to robustly assign high dimensional load profile data to clusters, where the centroid function $\bar{C}_k(t)$ is known. The algorithm applies fuzzy relationships, where the load profile is initially and iteratively given degrees of membership to more than one cluster. The genetic algorithm (GA) carries out this fuzzy process during the evolution stages until a single membership is determined. In GA, an initial population of individuals (i.e. chromosomes) is created following some specified rules, then the individuals are modified in order to produce children for the next generation. Individuals are assigned scores (i.e. fitness) in each generation. Based on the scores, individuals are selected for passing on to the next generation as elite, mutation, or crossover children. Generations are repeated until a specified termination criteria is met. The parts of the FGA are described in the subsections below:

Fitness Function

The FGA fitness (i.e. objective) function is defined as the ratio between the consumer's load-time function (i.e. load profile) proximity to the assigned cluster centroid and its remoteness from the other clusters' centroids. Proximity and remoteness are measured in squared Euclidean distances. This function is expressed as:

$$\underset{k\in K}{\operatorname{argmin}} \sum_{g\in K \mid g\neq k} \sum_{t\in R \mid R\subset H} \frac{\left\| D_j(t) - \bar{C}_k(t) \right\|^2}{\left\| D_j(t) - \bar{C}_g(t) \right\|^2} \tag{5.3}$$

where R is a vector of randomly chosen scattered time increments over which the proximity is assessed and H is the complete time set (e.g. $H = 672$ for 1-weak 15 minute interval data).

Termination Criteria

In contrast to the classical GA, where termination is met by assessing the change in fitness values or through a generation limit, the FGA uses the fitness values only for elite and crossover individual selection, but not for termination. In this context, the fitness scores are not recorded in memory for each generation. This is essential since new scores at each generation are computed using new randomized values for R. Finally, the termination is met when either of the following conditions satisfies: The same individual remains elite after a specified number of generations or the strongest crossover child maintains its chromosome structure after successive crossovers.

Chromosome Coding

The chromosomes (i.e. individuals/ consumers/ load profiles) for the initial population are coded such that each chromosome represents a unique cluster k as a candidate solution. Thus, the initial population's chromosomes are binary coded, where the location (i.e. column number) of the 1 elements constitutes the individual's k. The binary values are then allowed to vary during the successive steps using the fuzzy logic.

Crossover Permutation

Different than the classical crossover function of the GA, we implement the Fuzzy logic in the crossover permutation of the FGA; During crossover, the child (i.e new individual) is allowed to belong both its parent clusters with degrees of membership on the range $\{0,1\}$. Using a recursive process, the degrees of membership are adjusted by

assuming new dummy parent centroids for each recursion. Each dummy centroid is weighted by the degree of membership as in the fuzzy C-Means algorithm [95], however, the proposed FGA is different than the fuzzy C-Means, where the FGA centroids, $\bar{C}_k(t = R \subset H)$, are functions of randomly selected time increments, which are randomized in each generation. Finally, the crossover child is assigned to the cluster of the parent with the largest membership value.

Mutation Permutation

In the FGA, mutation is given the last order of execution after elite and crossover selections. The remaining chromosomes are mutated by randomly switching the binary values. The initial chromosome coding, crossover, and mutation process are explained schematically in Figure 5.4.

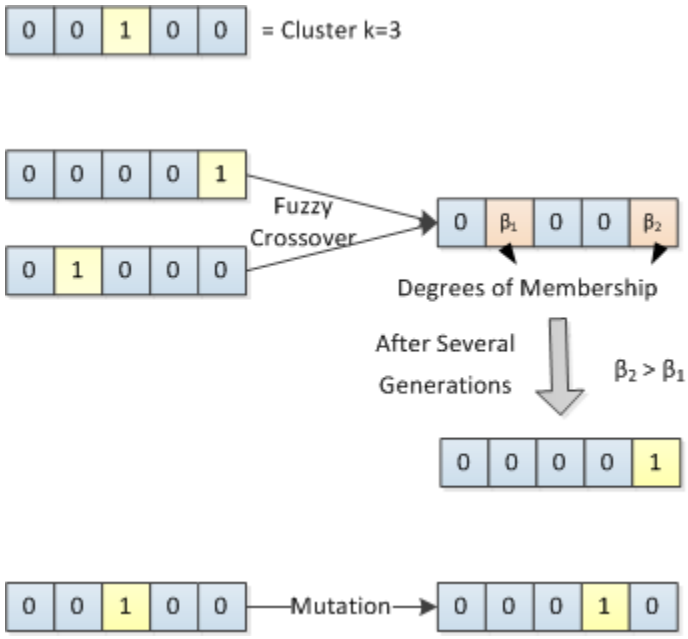

Figure 5.4. Schematic representation of the FGA evolution processes.

Conclusions and Remarks for Application to DR

Following the discussed clustering strategy, the simulation model's load in the previous chapter can be disaggregated through classifying the 8 consumers. We identified

that the consumption behaviors of the 8 consumers can be classified into 4 clusters as following:

- Cluster 1: MI0246, MI0265, and MI0267.
- Cluster 2: MI0189, MI0197, and MI0268.
- Cluster 3: MI0198.
- Cluster 4: MI0234.

In agreement with the suggestions of many researchers in literature, the successful clustering can be utilized to help improve the utility operations. One way to utilize this information is to study and propose cluster-specific DR policies. Currently, many utility providers apply policies, which discriminate between consumers according to their peak demand sizes. However, the value of the consumer's peaking demand is not an indication of his consumption behavior. Thus, we argue that the way in which a consumer uses energy is what should define his energy rate structure, rather than his single time demand quantity. The next step in such research progression should be to construct and optimize RTP-HA tariffs and policies for each consumer cluster. However, the utility-side impact is not the main focus of this dissertation. To strengthen our analysis, we used the price simulation model in chapter 3 to simulate independent prices for each of the 4 clusters, then we run the simulation model discussed in Chapter 4 with the new prices. We observed that the new lumped load pattern demonstrates less variability and fewer instances of load synchronization spikes, which increases the benefit for the utility-side. These results are plotted in Figure 5.5 which demonstrates the gains when compared to Figure 4.10, which shows the effect of the aggregated RTP-HA system.

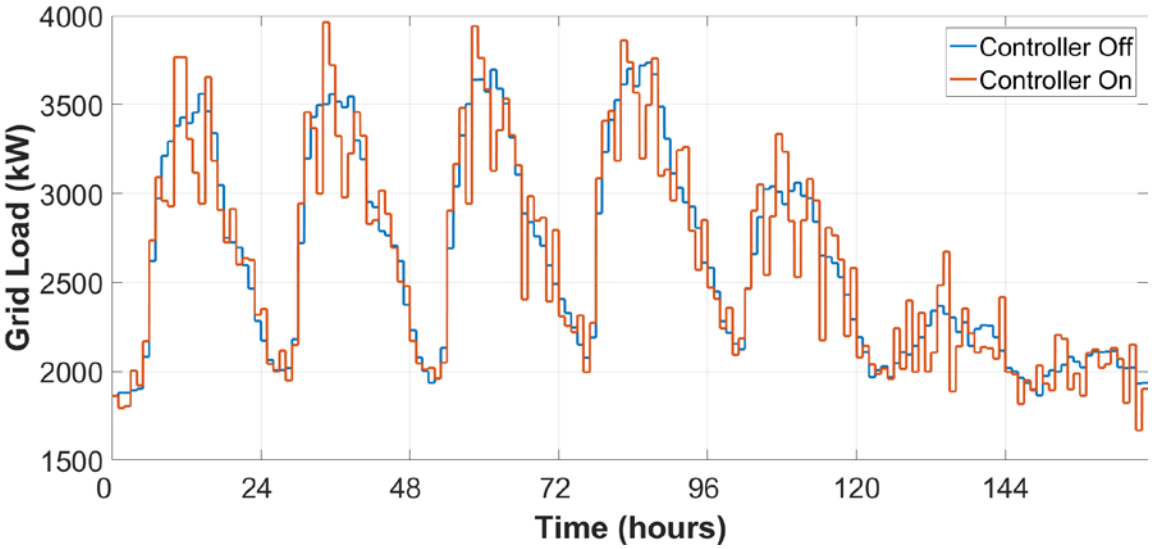

Figure 5.5. Less variability and fewer load synchronization peaks when all consumers use demand shifting controllers at the exact same time instances following the cluster-disaggregated RTP-HA signals.

Chapter 6: Continuous Multi-Objective Demand Response to Discrete Controller Signals

Chapter Introductory Remarks

In chapter 4, an autonomous controller was proposed, which outputs real numbers at discrete intervals. The outputted numbers represent the optimal amount of load to be shifted between two successive hours in the 2-hour planning period. These outputs were transformed into machine operation signals through a simple regulator methodology, which transfers the output values to a set of relays and switches. We extend the work discussed in chapter 4 by proposing a more pragmatic and intelligent way to manage the real-time operation of the discrete DR controller. First, the discrete DR algorithm is modified and solved without linearization. Second, a continuous controller is added to manage the operation in real time while considering a true multi-objective scenario of cost savings and consumer utility. We integrate additional dimensions into the industrial consumer's autonomous DR problem. These dimensions are paramount to the practicality of the proposed system and to accommodate higher flexibility and the realistic requirements of the future. We discuss these dimensions in the subsections below.

Nonlinear Objectives

In the reviewed literature, the DR problem was modeled as a mixed-integer linear programming problem (MILP). Some researchers suggested a nonlinear problem but relied on linear approximations methods. The problem discussed in chapter 4 was unique in considering real, non-integer, variables, which better identify optimal levels for energy consumption. Nevertheless, the problem was solved through linear approximation assumptions. In this chapter, we utilize more complex solution methods like quadratic

programming or evolutionary programming, which provide opportunities for formulating large scale and complex DR problems with large number of variables.

Two-Stage Discrete-Continuous DR

The load shifting optimization problem, which we introduced in chapter 4 and later modify in this chapter, aims at finding optimal demand values to shift between two successive hour subject to two different energy rates. Therefore, the solutions are identified for discrete time steps (i.e. every hour). However, satisfying these discrete load shifting targets requires dynamic optimization in real time (i.e online optimization. Therefore, we introduce a 2-stage hierarchical approach to the complete consumer-side DR problem, where the first stage solution is completed in discrete intervals, while the second stage solution is updated in continuous time. In response to discrete-events such as hourly price signals, the first stage identifies target load amounts using real decision variables (DVs), while the second stage attempts to satisfy the first stage targets though managing the operation of controllable loads using integer DVs.

Consumer Utility Functions

In most of the literature reviewed, some indicator of the consumer's utility for the managed loads was included as a factor in the DR objective. Depending on the type of DR approach, whether it is HVAC temperature control or load scheduling, this indicator was measured as a comfort index or a wait time. The notion of utility function is however adopted in quasi-independent research efforts, which targets the supplier-side (i.e. utility-side) operations, whether for price setting or load dispatch planning [96-98]. In this context, utility functions were used to model the consumer's price elasticity behavior. Therefore, the utility function commonly used defines the consumer's response in

operating different loads with regard to different energy prices [99]. Different than previous DR research, we integrate utility functions in the DR problem, where loads are managed depending on its utility value for the consumer. We derive utility functions uniquely for each load type. We utilize these functions for computing inputs to a new DR objective function, which updates solutions in continuous. Accordingly, equipment operations are managed depending on both utility values and the load shifting targets identified in discrete-time.

Multi-Objective Optimization

All of the reviewed literature described a multi-objective DR problem, mainly the two objectives of energy cost minimization and consumer comfort maximization. However, these objectives were given weights and added in a single DR objective function. This approach is questionable where there is no clear definition of how weights are determined, how they impact the solution, and whether there should be constraints on weights. Differently, we utilize a controlled Pareto optimization scheme, where several feasible solutions satisfying both objectives are investigated.

Consumer as a Prosumer

The previously discussed DR strategy considers the one-way flow of energy; from the utility supplier to the consumer. However, today's industrial consumers utilizes building-integrated energy sources like a fuel generators, solar panels, or battery storage system. Therefore, we introduce a comprehensive DR problem which includes DVs regarding the consumer-side energy sources.

Chapter Motivation and Objectives

The practicality of the DR controller proposed in chapter 4 is what motivates the work presented in this chapter. First, the previous problem assumed a complete load-shifting scenario, while this may not be possible in real-life situations as higher flexibility is desired by the consumer. Second, the problem had ignored potential opportunities available for the industrial consumer, which can increase the efficiency gains of participation in DR. These opportunities include the management of bulk energy storage systems, utilizing EV battery capacity, or managing consumer-owned fuel-run generators. Third, the previous problem did not include a function for measuring, and adapting to, the consumer's time-dependent and task specific comfort requirements. Therefore, our objective is to develop a comprehensive, autonomous, and adaptable solution to the consumer-side DR problem, which provides higher flexibility to the consumer and increases the utilization of DR benefits for the consumer.

Stage 1: Load Shifting Targets Optimization in Discrete Time

Mathematical Formulation

In the first stage, we combine the two problem (4.1) and (4.8) then modify the problem to become:

$$\underset{e}{argmin}\{[\lambda^{FR} \cdot B_t - \lambda_t^{DR} \cdot (B_t + e)]^2 + [\lambda^{FR} \cdot B_{t+1} - \lambda_{t+1}^{DR} \cdot (B_{t+1} - e)]^2\} \tag{6.1}$$

Subject to:

$$-C \leq e \leq C \tag{6.2}$$

$$e_t = max(0, e) \tag{6.3}$$

$$e_{t+1} = max(0, -e) \tag{6.4}$$

where, different than the problem formulation of chapter 4, B_t is the base load, which is the consumer's non-controllable (i.e. non-schedulable and can't be shifted) load for the hour t. B_t covers the lumped load of production operations, lights, industrial refrigerators, computers and servers, etc. In this context, e is the target load shifting amount between the time steps t and $t+1$ from the additional, non-base loads (i.e. controllable loads), such that $e_t = e$ and $e_{t+1} = -e$. If approximately M controllable loads are registered in the system between t and $t+1$, then C represents their lumped capacity. The objective function aim to identify an optimal the amount of energy to be added to, or subtracted from, a given hour while reversing this action during the following, or preceding, hour. The optimal value for e is further processed to form two quasi-dependent solutions for the two hours through (6.3) and (6.4).

The problem's modification in this chapter is valid due to the interdependency between e and the overall building's load, which would affect the forecast reliability. Therefore, separation of the base load, B_t or B_{t+1}, from the overall load is necessary where B_t can be forecasted with higher accuracy. Thus, accounting for the interdependency between price signals and consumer's expected demand can be achieved from the utility-side planning, when separate logged data are available for B_t and C.

Stochastic Form

The problem formulated above relies on the predictability of B_t and B_t. Alternatively, if the consumer's base load was characterized of having a high degree of uncertainty (i.e high forecast error), then the problem can be reformulated to a stochastic form, however, this is seldom for the industrial consumer whose load profile is characterized of having a predictable periodic behavior as shown with data in chapter 5. The stochastic form is:

$$\underset{e}{argmin} \sum_{p^{D_t}} \sum_{p^{D_{t+1}}} \left\{ P_{p^{B_t}}^{t-1:t} \cdot \left[\lambda^{FR} \cdot B_{t,p^{B_t}} - \lambda_t^{DR} \cdot \left(B_{t,p^{B_t}} + e \right) \right]^2 + P_{p^{B_{t+1}}}^{t:t+1} \right.$$
$$\left. \cdot \left[\lambda^{FR} \cdot B_{t+1,p^{B_{t+1}}} - \lambda_{t+1}^{DR} \cdot \left(B_{t+1,p^{B_{t+1}}} - e \right) \right]^2 \middle| B_{t-1} = \acute{B}, \right\} \tag{6.5}$$

where the values of B_t and B_{t+1} in this case have probability distributions $\left[B_{t,1}, B_{t,2}, \dots, B_{t,p^{B_t}}, \dots\right]$ and $\left[B_{t+1,1}, B_{t+1,2}, \dots, B_{t+1,p^{B_{t+1}}}, \dots\right]$ with previous-state transition probabilities $\left[P_1^{t-1:t}, P_2^{t-1:t}, \dots, P_{p^{B_t}}^{t-1:t}, \dots\right]$ and $\left[P_1^{t:t+1}, P_2^{t:t+1}, \dots, P_{p^{B_{t+1}}}^{t:t+1}, \dots\right]$, given that the value of B_{t-1} is known, since it had already occurred in the previous time step. The optimal solution, e, in such case is defined as the solution satisfying all possible scenarios weighted by their probabilities. Using discretized historical demand data, the state transition probabilities are estimated using the maximum likelihood estimate method. We have used the same method for estimating energy price transition probabilities in [100].

Quadratic Form

Problem (6.1), as well as its stochastic form (6.5), is convex. This is concluded from taking the second derivative with respect to the DVs. Furthermore, the constraints (i.e. bound constraints) are linear. Therefore, the problem can be transformed into the quadratic form:

$$\underset{e}{argmin}\ \theta_1 \cdot e^2 + \theta_2 \cdot e + \theta_3 \tag{6.6}$$

where:

$$\theta_1 = {\lambda_t^{DR}}^2 + {\lambda_{t+1}^{DR}}^2 \tag{6.7}$$

$$\theta_2 = 2 \cdot \left({\lambda_t^{DR}}^2 \cdot B_t - \lambda^{FR} \cdot \lambda_t^{DR} \cdot B_t - {\lambda_{t+1}^{DR}}^2 \cdot B_{t+1} + \lambda^{FR} \cdot \lambda_{t+1}^{DR} \cdot B_{t+1} \right) \tag{6.8}$$

$$\theta_3 = {B_t}^2 \cdot (\lambda^{FR} - \lambda_t^{DR})^2 + {B_{t+1}}^2 \cdot (\lambda^{FR} - \lambda_{t+1}^{DR})^2 \tag{6.9}$$

for the non-stochastic problem. The last coefficient, θ_3, can be dropped since it does not affect the optimization process (i.e. its value does not affect the DV choice). For the stochastic problem the quadratic form becomes:

$$\underset{e}{argmin}\ [I]^{1\times 2}\times[P\theta_1]^{2\times\dots}\times[e^2]^{\dots\times 1} + [I]^{1\times 2}\times 2\cdot[P\theta_2]^{2\times\dots}\times[e]^{\dots\times 1} \tag{6.10}$$

where:

$$[I]^{1\times 2} = [1 \quad 1] \tag{6.11}$$

$$[P\theta_1]^{2\times\dots} = \begin{bmatrix} P_{1^{B_t}}^{t-1:t}\cdot\lambda_t^{DR^2} & P_{2^{B_t}}^{t-1:t}\cdot\lambda_t^{DR^2} & \dots & P_{p^{B_t}}^{t-1:t}\cdot\lambda_t^{DR^2} & \dots \\ P_{1^{B_{t+1}}}^{t:t+1}\cdot\lambda_{t+1}^{DR\ 2} & P_{2^{B_{t+1}}}^{t:t+1}\cdot\lambda_{t+1}^{DR\ 2} & \dots & P_{p^{B_{t+1}}}^{t:t+1}\cdot\lambda_{t+1}^{DR\ 2} & \dots \end{bmatrix} \tag{6.12}$$

$$[e^2]^{\dots\times 1} = \begin{bmatrix} e \\ e \\ \vdots \end{bmatrix} \tag{6.13}$$

$$[P\theta_2]^{2\times\dots} = \begin{bmatrix} P_{1^{B_t}}^{t-1:t}\cdot\left(\lambda_t^{DR^2}\cdot B_t - \lambda^{FR}\cdot\lambda_t^{DR}\cdot B_t\right) & P_{2^{B_t}}^{t-1:t}\cdot(\dots) & \dots \\ P_{1^{B_{t+1}}}^{t:t+1}\left(\lambda^{FR}\cdot\lambda_{t+1}^{DR}\cdot B_{t+1} - \lambda_{t+1}^{DR\ 2}\cdot B_{t+1}\right) & P_{2^{B_{t+1}}}^{t:t+1}\cdot(\dots) & \dots \end{bmatrix} \tag{6.14}$$

The functions above are quadratic and can be solved in polynomial time using quadratic programming with the interior-point-convex algorithm [101]. These quadratic problems are easily solvable in real time and thus momentary DR can be achieved, given that another system (e.g. the regulator discussed in chapter 4) is present to transform controller output to equipment in real time. At each additional time step $t+1$, information for $t+2$ become available and new load shifting goals between $t+1$ and $t+2$ are determined. Equilibrium throughout the planning horizon is maintained by propagating the $t+1$ target, obtained from the shifting between t and $t+1$, to the next optimization step, which calculates targets between $t+1$ and $t+2$. This strategy is demonstrated by the pseudo-code in Figure 6.1.

Initial State ($t = 0$):
    User sets λ^{FR};
    $e_0 = 0$;

Stage 1 (Discrete: non-stochastic/stochastic optimization):
    for $t = 1{:}H$
        read λ_t^{DR}, λ_{t+1}^{DR};
        forecast B_t, B_{t+1};
        register M controllable loads at time t: Compute C;
        optimize e_t =-e_{t+1};
        adjust e_t=e_t+e_{t-1};
        while $t < t + 1$
            jump to **Stage 2 (Continuous: real-time optimization)**
        end
    end

Figure 6.1. Pseudo-code for the hierarchical optimization scheme (showing only stage-1 in detail), where H is the planning horizon (e.g. $H = 24$ hours).

Utility Functions for Controllable Loads

Defining Utility Functions

Before discussing the second stage of the hierarchical optimization process, let us present a paramount variable to satisfying the stage's multi-objective outcome. The Consumer's utility functions for tasks (i.e. loads) are measures of his relative satisfactions of completing these tasks [102]. Due to the tasks' timeliness nature, the utility is modeled as a function of time [103], they are assumed to be non-decreasing with a maximum limit [104]. A load's (e.g. HVAC unit) utility value is zero when it does not bring a benefit to the consumer. Likewise, a load's utility value is non-zero when it bring benefit and it reaches a maximum utility value when its operation is critical to the consumer. Utility functions can thus be model using linear or quadratic equations [99]. By assigning weights to utility functions of various loads, the consumer can select which loads to operate in response to a given cost and thus maximize his welfare [104].

In accordance with the above statements, we derive task-specific quadratic utility functions. We formulate these utility functions for three types of loads: multistage chiller

system, EV charging, and EV discharging for building's demand support (V2B). Additional task load types, whether load consuming or supplying tasks, can be integrated in the 2 stage approach. For example demand for heat pumps, variable speed motors, heaters, thermal storage, lighting, curtailment generators, or even some manufacturing processes can be modeled with utility functions. We leave these opportunities for future work. The three utility function models are described in the sections below.

Utility Function for Multistage HVAC System

For thermostatic loads, the consumer's comfort is maximized when the temperature is kept at his preferred setpoint T^s. Thus, in the case of an HVAC load (e.g. Air chiller), his utility for the load increases or decreases with the positive or negative deviation from the desired setpoint. Therefore, his HVAC utility is a function of both time t and temperature T. The maximum utility value corresponds with temperatures higher than his maximum tolerance level, $T^s + TOL^+$, and the zero utility corresponds with temperatures less than his minimum tolerance level, $T^s - TOL^-$.

Assuming an HVAC system with S operational stages (i.e. 25%, 50%, 75%, and 100% loading options), the utility for the ordered stage s, where $s \in \{1,2,\dots,S\}$, is $U_s\{t,T\}$. To derive $U_s\{t,T\}$, we identify the following two conditions:

- $U_s\{t,T\}$ is at maximum (i.e. $U_s\{t,T\} = U_s^{max}$) when the temperature reaches or exceeds the maximum tolerated temperature (i.e. $T \geq T^s + TOL^+$).
- $U_s\{t,T\}$ is zero when the temperature is $T \leq T^s - TOL^- + (s-1)\cdot\tau$, where $\tau = \frac{TOL^-}{S}$ is the incremental change in minimum tolerated temperature by each HVAC stage.

Accordingly, we can assume the following two conditions:

$$\frac{dU_s\{t, T \geq T^s + TOL^+\}}{dT} = 0 \tag{6.15}$$

$$U_s\{t, T \leq T^s - TOL^- + (s-1) \cdot \tau\} = 0 \tag{6.16}$$

From (6.15), $U_s\{t, T\}$ can be derived as:

$$U_s\{t, T\} = \int_{T^s - TOL^-}^{T^s + TOL^+} (T^s + TOL^+ - T) \, . \, dT \tag{6.17}$$

$$U_s\{t, T\} = \begin{cases} T^s \cdot T + TOL^+ \cdot T - \dfrac{T^2}{2} + Constant, & if\ T \leq T^s + TOL^+ \\ \dfrac{(T^s + TOL^+)^2}{2} + Constant, & Otherwise\ (U_s^{max}) \end{cases} \tag{6.18}$$

We substitute in condition (6.16) to find the $Constant$ as:

$$Constant = \begin{cases} \vartheta_1 \cdot (s-1)^2 + \vartheta_2 \cdot (s-1) + \vartheta_3, & if\ T > T^s - TOL^- + (s-1) \cdot \tau \\ -T^s \cdot T - TOL^+ \cdot T + \dfrac{T^2}{2}, & Otherwise \end{cases} \tag{6.19}$$

where:

$$\vartheta_1 = \frac{\tau^2}{2} \tag{6.20}$$

$$\vartheta_2 = -\tau \cdot (TOL^+ + TOL^-) \tag{6.21}$$

$$\vartheta_3 = -\frac{T^{s\,2}}{2} - T^s \cdot TOL^+ + TOL^- \cdot TOL^+ + \frac{TOL^{-2}}{2} \tag{6.22}$$

Finally, we can summary the multistage HVAC utility function, for cooling tasks only, as:

$$U_s\{t, T\} = \begin{cases} U_s^{max}, & if\ T \geq T^s + TOL^+ \\ 0, & if\ T \leq T^s - TOL^- + (s-1).\tau \\ T^s \cdot T + TOL^+ \cdot T - \dfrac{T^2}{2} + \vartheta_1 \cdot (s-1)^2 + \vartheta_2 \cdot (s-1) + \vartheta_3, & Otherwise \end{cases} \tag{6.23}$$

Note that T is a variable in time t. The correct notation should be T_t, however, we neglect the correct notation for simplification and the utility is computed in continuous time (i.e. t is non-discrete). Also, the notation definitions for $Constant$ throughout the chapter are independent in each subsection.

Utility values must be scaled for application in DR (i.e. for comparability), therefore, we normalize the utility functions through division by the load's maximum utility, $\grave{U}_s\{t,T\} = \frac{U_s\{t,T\}}{U_s^{max}}$. Examples of the normalized utility graphs for multistage cooling unit are shown in Figure 6.2. The graphs demonstrate the impacts different parameters' values have on the consumer's utility function.

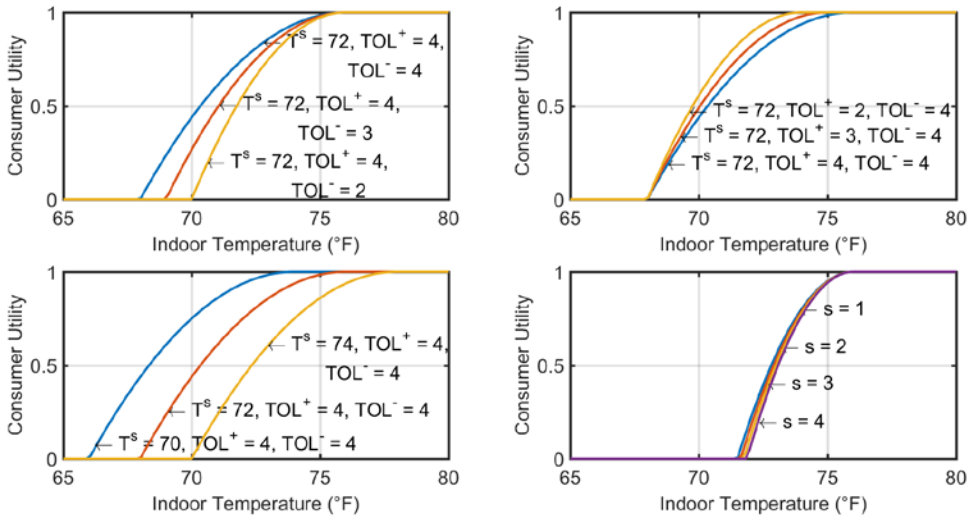

Figure 6.2. Multistage cooling unit utility function charts for various settings.

Utility Function for EV Charging (B2V)

When an employee or service EV parks at the industrial consumer's building, the EV owner expects his EV to be fully charged by his departure time. Thus, as the departure time approaches and as the state of charge (SOC) decreases, an EV will have a higher utility for power than another EV with delayed departure time or higher SOC. Therefore, the utility for EV charging is a function of both time and SOC.

Assuming V commercial EVs, the vth EV, such that $v \in \{1,2,\dots,V\}$, is scheduled to arrive at time a_v and depart at time b_v. That is the EV v will be plugged in during the interval $t \in \{a_v : b_v\}$. The SOC at any given time during the interval is $SOC_{v,t}$ and the battery capacity is Q_v. If the charging power is P^{EV}, then the period required to reach full charge is given by $t_{f_v}\{t\} = \frac{Q_v - SOC_{v,t}}{P^{EV}}$. The consumer's utility for charging the EV is $U_v\{t, SOC_{v,t}\}$. We can identify the following two conditions:

- $U_v\{t, SOC_{v,t}\}$ is maximum (i.e. $U_v\{t, SOC_{v,t}\} = U_v^{max}$), when the remaining time to departure is less than or equal the needed charging duration (i.e. $t \leq b_i - t_{f_v}\{t\}$).
- $U_v\{t, SOC_{v,t}\}$ is zero when the EV had just arrived (i.e. at $t = a_v$), on the condition that the EV will spend more than the time required to fully charge in the system (i.e. $t_{f_v}\{a\} < b_v - a_v$).

According to the previous statements, we assume the following two conditions:

$$\frac{dU_v\left\{t \leq b_v - t_{f_v}\{t\}, SOC_{v,t}\right\}}{dT} = 0 \tag{6.24}$$

$$U_v\left\{t = a_v | t_{f_v}\{a\} < b_v - a_v, SOC_{v,t}\right\} = 0 \tag{6.25}$$

From condition (6.24), we derive $U_v\{t, SOC_{v,t}\}$ as:

$$U_v\{t, SOC_{v,t}\} = \int_{a_v}^{b_v} \left(b_v - t_{f_v}\{t\} - t\right).dt \tag{6.26}$$

$$U_v\{t, SOC_{v,t}\} = \begin{cases} b_v \cdot t - t_{f_v}\{t\} \cdot t - \dfrac{t^2}{2} + Constant, & if \;\; t \leq b_v - t_{f_v}\{t\} \\ \dfrac{\left(b_v - t_{f_v}\{t\}\right)^2}{2} + Constant, & Otherwise \; (U_v^{max}) \end{cases} \tag{6.27}$$

We substitute in condition (6.25) to find the $Constant$ as:

$$Constant = \frac{{a_v}^2}{2} + t_{f_v}\{t\} \cdot a_v - b_v \cdot a_v \tag{6.28}$$

Finally, we can summary the EV utility function, for charging tasks only, as:

$$U_v\{t, SOC_{v,t}\} = \begin{cases} U_v^{max}, & if \;\; t \le b_v - t_{f_v}\{t\} \\ 0, & if \;\; t \le a_v \; and \; t_{f_v}\{a\} < b_v - a_v \\ \left(b_v - t_{f_v}\{t\}\right) \cdot (t - a_v) - \dfrac{t^2}{2} + \dfrac{{a_v}^2}{2}, & Otherwise \end{cases} \tag{6.29}$$

In line with the previous subsection utility values must be scaled, therefore, the utility functions are normalized through division by the load's maximum utility (i.e. $\grave{U}_v\{t, SOC_{v,t}\} = \frac{U_v\{t, SOC_{v,t}\}}{U_v^{max}}$). Examples of the normalized utility graphs for EV B2V are shown in Figure 6.3.

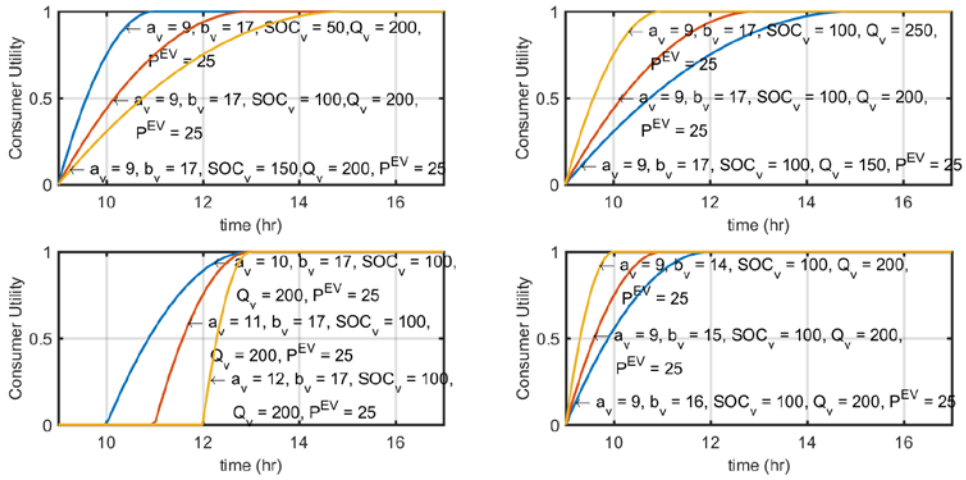

Figure 6.3. EV charging utility function charts for various EV attributes.

Utility Function for EV Discharging (V2B)

The utility function concept was first applied in microeconomics. It defines the value of a product to the user. Accordingly, researchers have adopted the concept in prioritizing energy-consuming tasks according to the trade-off between their utility values and costs. Therefore, with EV loads, utility functions constituted the interruptible charging of EVs

but neglected the opportunity of bidirectional charging control [105]. We take the utility functions concept one step further in our work by incorporating the value for the consumer to sell back load or support his peak demand. Since the consumer would still be required to purchase the energy at a different time in order to make up for the sold amount during V2B, we logically model his V2B utility as a function of energy price. In other words, the consumer's value for V2B occurs when his profit is higher than the cost of B2V at a different time. The complete V2B utility then becomes a function of time, SOC, and price. The consumer's utility function for utilizing his vth EV battery storage as an energy source is given by $U_v^{V2B}\{t, SOC_{v,t}, \lambda_t^{DR}\}$. Based on these logical assumptions, we can deduce the following two conditions:

- $U_v^{V2B}\{t, SOC_{v,t}, \lambda_t^{DR}\}$ is at maximum (i.e. $U_v^{V2B}\{t, SOC_{v,t}, \lambda_t^{DR}\} = U_i^{V2B,max}$) when a desired price incentive, λ^{max}, is reached.
- $U_v^{V2B}\{t, SOC_{v,t}, \lambda_t^{DR}\}$ is zero when any of the following states occur: the price is equal to or below the threshold price (i.e. $\lambda_t^{DR} \leq \lambda^{FR}$), the SOC hits the minimum allowed level for battery conservation (i.e. $SOC_{v,t} \leq \varkappa \cdot Q_v$), or there is insufficient time to reach full charge (i.e. $t_{f_i}\{t\} \geq b_i - t$).

Hence, we apply the following two conditions:

$$\frac{dU_v^{V2B}\left\{\lambda_t^{DR} \geq \lambda^{max} \cap SOC_{v,t} > \varkappa \cdot Q_v \cap t \geq b_i - t_{f_v}\{t\}\right\}}{d\lambda_t^{DR}} = 0 \tag{6.30}$$

$$U_v^{V2B}\left\{\lambda_t^{DR} \leq \lambda^{FR} \cup SOC_{v,t} \leq \varkappa \cdot Q_v \cup t \geq b_v - t_{f_v}\{t\}\right\} = 0 \tag{6.31}$$

From condition (6.30), we can derive $U_v^{V2B}\{t, SOC_{v,t}, \lambda_t^{DR}\}$ as:

$$U_v^{V2B}\{t, SOC_{v,t}, \lambda_t^{DR}\} = \int_{\lambda^{FR}}^{\lambda^{max}} (\lambda^{max} - \lambda_t^{DR}) \,.\, d\lambda_t^{DR} \tag{6.32}$$

$$U_v^{V2B}\{t, SOC_{v,t}, \lambda_t^{DR}\} = \begin{cases} \lambda^{max} \cdot \lambda_t^{DR} - \dfrac{{\lambda_t^{DR}}^2}{2} + Constant, \;\; if\; \lambda_t^{DR} < \lambda^{max} \\ \dfrac{{\lambda^{max}}^2}{2} + Constant, \;\; if\; \lambda_t^{DR} \geq \lambda^{max} \; (U_v^{V2B,max}) \\ 0, \;\; if\; SOC_{v,t} \leq \varkappa \cdot Q_v \\ 0, \;\; if\; t_{f_v}\{t\} \geq b_v - t \end{cases} \tag{6.33}$$

We substitute in condition (6.31) to obtain the $Constant$ as:

$$Constant = \begin{cases} \dfrac{{\lambda^{FR}}^2}{2} - \lambda^{max} \cdot \lambda^{FR}, \;\; if\; \lambda^{FR} < \lambda_t^{DR} < \lambda^{max} \\ \dfrac{{\lambda_t^{DR}}^2}{2} - \lambda^{max} \cdot \lambda_t^{DR}, \;\; if\; \lambda_t^{DR} \leq \lambda^{FR} \end{cases} \tag{6.34}$$

Finally, we can summary the EV utility function, for building support (V2B) tasks only, as:

$$U_v^{V2B}\{t, SOC_{v,t}, \lambda_t^{DR}\}$$

$$= \begin{cases} U_v^{V2B,max}, \quad if\; \left\{\lambda_t^{DR} \geq \lambda^{max} \cap SOC_{v,t} > \varkappa \cdot Q_v \cap t \geq b_v - t_{f_v}\{t\}\right\} \\ 0, \quad if\; \left\{\lambda_t^{DR} \leq \lambda^{FR} \cup SOC_{v,t} \leq \varkappa \cdot Q_v \cup t \geq b_v - t_{f_v}\{t\}\right\} \\ \lambda^{max} \cdot (\lambda_t^{DR} - \lambda^{FR}) - \dfrac{{\lambda_t^{DR}}^2}{2} + \dfrac{{\lambda^{FR}}^2}{2}, \;\; Otherwise \end{cases} \tag{6.35}$$

Similar to the previously derived utility functions, $U_v^{V2B}\{t, SOC_{v,t}, \lambda_t^{DR}\}$ is normalized in order to be scaled with the various tasks' utility functions. This is accomplished by computing $\grave{U}_i^{V2B}\{t, SOC_{i,t}, \lambda_t^{DR}\} = \frac{U_i^{V2B}\{t, SOC_{i,t}, \lambda_t^{DR}\}}{U_i^{V2B,max}}$. Examples of the normalized utility graphs for EV V2B when the SOC and time are held constant are shown in Figure 6.4, which demonstrates the impacts of λ^{FR} and λ^{max} on the utility function.

Another suggestion would be to include the building's demand level as a variable in the utility function, since V2B can be utilized in shedding high demand costs. However, we leave this part to future work and we also consider that higher energy prices usually coincide with high demand periods. Therefore, we assume that the impact of demand is mitigated through the price and can be omitted from the function for simplicity. In some instances, V2B and B2V may have high utility values. Because both activities cannot simultaneously be practiced for the same EV, careful modeling of the prioritization algorithm is required. This is addressed in the upcoming sections.

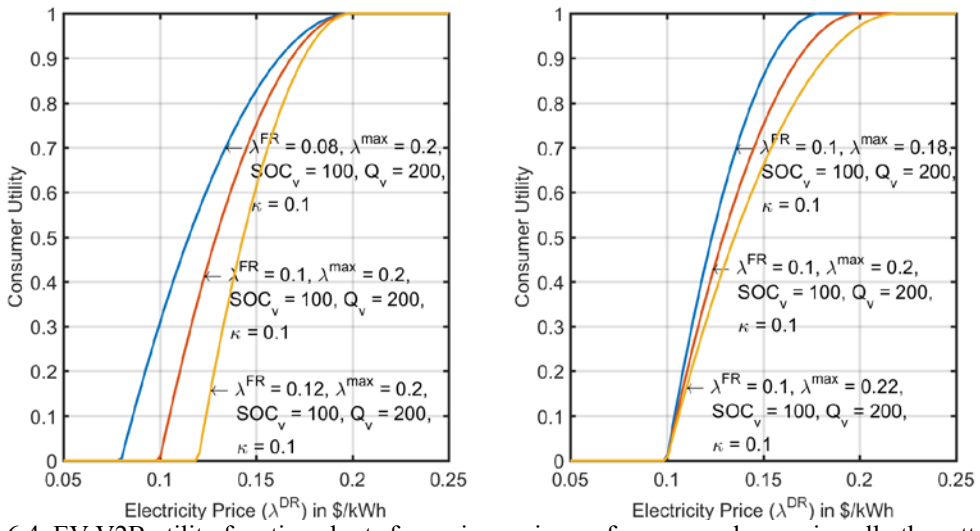

Figure 6.4. EV V2B utility function charts for various price preferences and assuming all other attributes are held constant.

Stage 2: Dynamic Multi-Objective Load Management in Real-Time

Pareto Optimization Approach

After the load shifting target had been identified for the hour in stage 1, several loads must be continuously managed during the same hour in order to accomplish this identified target. Choices are made concerning which loads to switch on or off based on two objectives: maximizing the consumer's utility from all loads and maintaining a lumped load level within close range to the identified load targets. In contrast to previous

work by other researchers, our work does not model the multi-objective problem by combining objectives using weights in a single function. Alternatively, we use a Pareto optimization approach. This may yield one or more Pareto-optimal solutions in the continuous simulation time, which we discuss how to deal with in later sections. Our approach is superior to having a single objective function because the optimality of the latter method's solution is questionable, where it is difficult to prove that the objective weighting strategy is proper enough or that it achieves perfect comparability among objectives. In contrast, the Pareto frontier presents neutral-compromise solutions independent of preference weights or scalarization errors Therefore, it is more valid to call a solution optimal only if it exists on the Pareto frontier.

Mathematical Formulation

If we consider a set F of controllable loads with index $f \in \{s \cup v \cup \dots\}$ such that $F = \{\{1,2,\dots,s,\dots,S\} \cup \{1,2,\dots,v,\dots,V\} \cup \dots\}$ for an S-stage cooling unit, V EVs, and other loads. If M is the total number of available individual loads at a particular time instance (e.g. $A\ 4\ stage\ cooling\ unit + 5\ EVs + 3\ heaters = 12\ total\ loads = M$), then. $L = \{l_1, l_2, \dots, l_f, \dots, l_M\}$ is the set of load capacities and $W = \{w_1, w_2, \dots, w_f, \dots, w_M\}$ is the set of weights assigned to each load, such that each w_f is determined relatively with the other loads using the analytic hierarchy process (AHP) [106]. The objective is to decide which loads to switch on or off. This is modeled using the set of DVs $X = \{x_1, x_2, \dots, x_f, \dots, x_M\}$, where:

$$x_f = \begin{cases} 1, & If\ load\ j\ is\ turned\ on \\ 0, & If\ load\ j\ is\ turned\ off \end{cases} \tag{6.36}$$

In the Pareto multi-objective optimization context, optimality at any instance is achieved when the set values of X satisfy two objectives: The first objective, $f_1(X)$, is to maximize the consumer's wellbeing (i.e. utility/ comfort/ satisfaction), and the second objective, $f_2(X)$, is to minimize the deviation from the lumped operation target e_t set in stage 1. Thus, we can formulate the two objectives as:

$$f_1(X) = \underset{x_f \in X}{argmax} \left(X \cdot WI_M \cdot \left[\grave{U}\right]^T \right) \tag{6.37}$$

$$f_2(X) = \underset{x_f \in X}{argmin} (e_t - X.L^T)^2 \tag{6.38}$$

where:

$$WI_M = \begin{bmatrix} w_1 & 0 & \dots & 0 & \dots & 0 \\ 0 & w_2 & \dots & 0 & \dots & 0 \\ \vdots & \vdots & \ddots & \vdots & \dots & \vdots \\ 0 & 0 & \dots & w_f & \dots & 0 \\ \vdots & \vdots & \vdots & \vdots & \ddots & \vdots \\ 0 & 0 & \dots & 0 & 0 & w_M \end{bmatrix} \tag{6.39}$$

$$\left[\grave{U}\right]^T = \begin{bmatrix} \grave{U}_1\{t, \dots\} \\ \grave{U}_2\{t, \dots\} \\ \vdots \\ \grave{U}_f\{t, \dots\} \\ \vdots \\ \grave{U}_M\{t, \dots\} \end{bmatrix} \tag{6.40}$$

All the notations above represent dynamic variables or parameters. The subscript t is omitted from some parameters or variables for mathematical convenience, except in e_t because its values change in discrete time (i.e. every hour). The superscript T denotes the transpose of a vector and should not to be confused with T for temperature. Also the subscript f denotes the index of the selected load and should not be confused with f for function.

Finally, we can express the multi-objective Pareto optimization problem as:

$$\underset{x_m \in X}{argmin}\left(-f_1(X), f_2(X)\right) \tag{6.41}$$

Subject to:

$$x_f = \begin{cases} 1, & \forall\, \grave{U}_f = 1 \\ 0, & \forall\, \grave{U}_f = 0 \end{cases} \tag{6.42}$$

where constraint (6.42) enforces the on/off switching of loads when critical conditions are reached. This constraint guarantees that all the optimal solutions on the Pareto frontier comply with the consumer's wellbeing range.

Special Loads

We presented the multi-objective optimization problem (6.41) for the general load. However, some load types need parameter modification or additional constraint in order to be modeled correctly. Some of these examples are:

- *Thermostatic Loads:* For HVAC loads (e.g. air conditioners, heaters, chillers, etc.), the definition of $\left[\grave{U}\right]^T$ in (6.40) is invalid, because $\grave{U}_f\{t, T\}$ is not an accurate indication of the consumer's comfort level. In the multistage cooling unit case, $\grave{U}_f$ is zero when T reaches the consumer's lowest limit for acceptable temperature. Similarly, $\grave{U}_f$ is maximum when T reaches his upper limit. This explanation is valid for the utility value because it is critical for the consumer to switch the system off or on according to his lower and upper limits for thermal comfort. However, this does not explain the degree of his wellbeing. Differently, his wellbeing is logically maximized when T is maintained at the T^s level and any deviation from T^s results in a decreased wellbeing. Therefore, his true utility should have a positive increasing value when $T > T^s$ and a negative decreasing value when $T < T^s$, otherwise, the

solution for (6.37) can be biased towards operating the chillers even when $T < T^s$. For this special load type, we redefine $\grave{U}_f\{t,T\}$ as:

$$\grave{U}_f\{t,T\} = \frac{U_f\{t,T\} - U_f\{t,T^s\}}{U_f^{max}}, \qquad \forall\, f \in \{1,2,\dots,s,\dots,S\} \tag{6.43}$$

- *EV loads:* For battery storage, EVs, or similar type of loads, the calculation of C used in (6.2) as the summation of loads' capacities is invalid, because the capacity for an EV is represented by Q_v and $SOC_{v,t}$. However, the useful power at any given moment is P^{EV}. Assuming that the V EVs are all plugged in, then we can calculate C as:

$$C = V \cdot P^{EV} + \sum_{f \in F \setminus \{1,2,\dots,i,\dots,V\}} l_f \tag{6.44}$$

- *Bidirectional loads:* Other considerations must be made for battery loads operating in the bidirectional control mode as in B2V and V2B. First, we duplicate the EV elements of F to model separate DVs for V2B from B2V tasks. Second, we assign negative signs to the values for the V2B duplicate (i.e. dummy) subset in L, which is used in (6.38), to represent the power flow in the opposite direction. Following the same condition discussed in the paragraph above, the subsets of L representing bidirectional load elements become $\{[P^{EV}]^{1\times V}, [-P^{EV}]^{1\times V}\}$. Third, because the power cannot flow in both directions at the same instance, we must add the following constraint to problem (6.39):

$$x_f + x_g \leq 1, \qquad \forall\, f \in \{1,2,\dots,v,\dots,V\} \mid f = g \tag{6.45}$$

where g is the index for the duplicated (i.e. dummy) EV subset of F.

Evolutionary Programming for Real-Time Nonlinear Optimization

The multi-objective problem (6.39) is a mixed-integer nonlinear programming (MINLP) type of problem, where the DVs, (6.40), are binary. However, both objectives (6.37) and (6.38) are convex and a solution may be found through the use of linear approximation techniques or other exact methods. Nevertheless, for any time instance, we are not interested in finding a dominated optimal solution, which is a feasible solution the problem may converge towards, although it is not actually a Pareto-optimal solution. We are interested in finding all nondominated solutions, where neither of the objective functions can further improve without degrading the other. These are called Pareto-optimal solutions. Linear approximation techniques will not guarantee finding the nondominated solutions, while the exact techniques efforts increase exponentially with respect to the dimensions of the problem. Therefore, we seek non-exact solution techniques that are customized for this specific type of problem to solve efficiently in real-tme. We rely on evolutionary algorithms due to their ability of finding a set of evenly distributed nondominated optimal solutions through computing an approximation of the entire Pareto frontier. We develop a customized GA solver based on intelligent and adaptive chromosome coding. GA is also a good fit for non-smooth problems without bound and linear constraints. GA is inspired by the natural selection process from biological evolution. We customize the evolutions stages of GA to our problem as explained in the following subsections.

Chromosome Coding

We define the chromosome for the general case such that its length represents the number of registered loads, which varies throughout the simulation as loads are added or

removed. We utilize binary chromosome coding where the 1s and 0s identify the operation signals for loads. In other words, the genome of the chromosome models the DV (6.36). In special cases like that of bidirectional loads, the chromosome identifies the type of registered loads and duplicates genomes for bidirectional loads. We include special codes to insure that the values of the original genomes and the duplicates satisfy constraint (6.45). We also include additional codes to read out utility values in real time, so that if the utility value for a particular load reaches the lower or upper bounds, then the corresponding genomes are hard coded to 0 or 1, then these hard-coded values pass unchanged throughout the evolution process. Through our custom lines of codes, we satisfy rules (6.36), (6.42), and (6.45) within the creation function of the GA, and pass all the information throughout to the crossover and mutation functions. This is more efficient than defining separate constraint functions prior to calling the solver as in classical programming techniques. The chromosome coding structure is graphically represented in Figure 6.5.

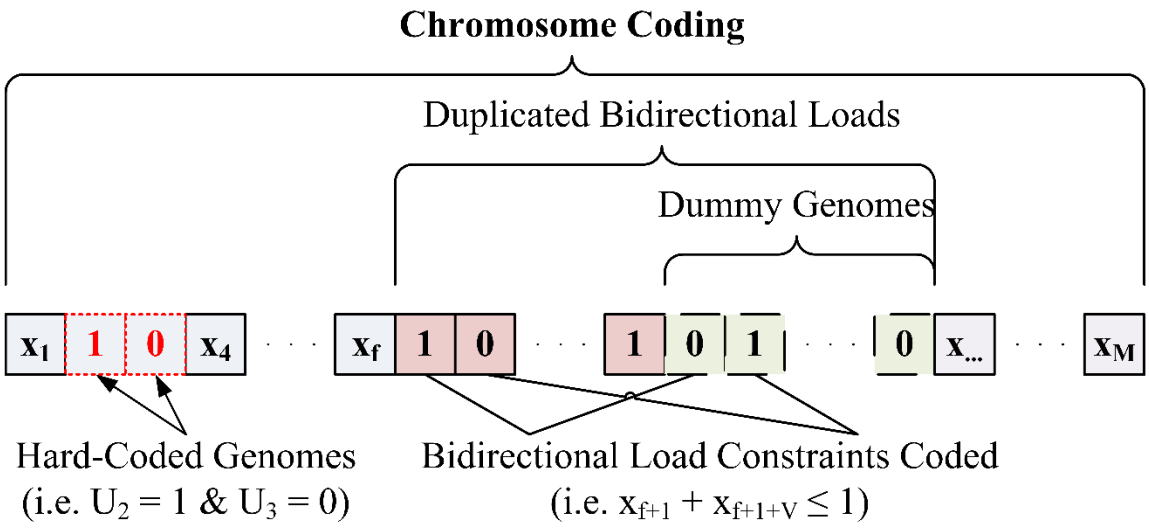

Figure 6.5. Chromosome coding for customized binary GA.

Crossover Coding

We give the crossover process a higher preference of execution during the evolution process; 80% of chromosomes undergo crossover. In crossover, we join two pairs of chromosomes, called the parents, in order to form a new chromosome, called the crossover child. The child is thus formed by combining genomes from both parents, with one parent, the dominant, who usually holds a better score, passing on more genomes. We add integrity codes to adjust children, if necessary, after crossover. For example, to ensure that bidirectional loads constraints, if any, are not violated in the process. Figure 6.6 illustrates the crossover process graphically.

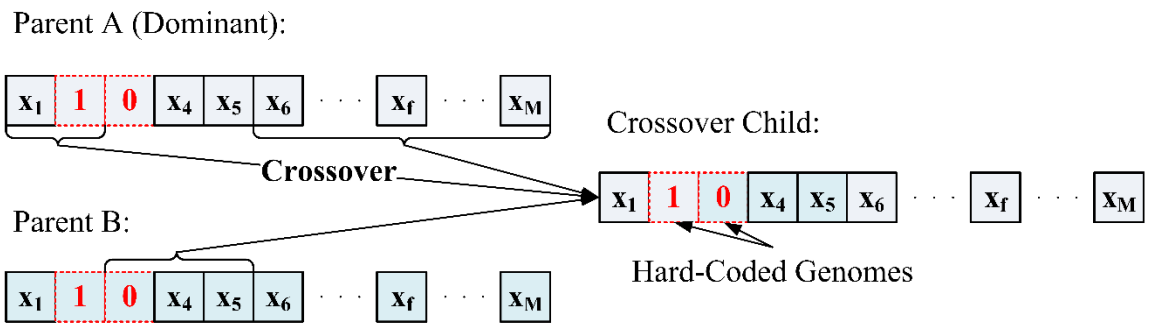

Figure 6.6. Chromosomes combination during crossover.

Mutation Coding

We give the mutation process the lowest order of execution during evolution. We mutate a parent chromosome by switching two randomly selected genomes in order to create the mutation child. Similar to the crossover process, we add integrity lines of code to make adjustments, if necessary, when bidirectional loads are registered. The mutation process is illustrated graphically in Figure 6.7.

Figure 6.7. Chromosome alteration during mutation.

Elite Coding

The solver, which we customized, uses a variant of the controlled elitist GA [107], which favors individuals increasing the population's diversity even if they possess a lower score. Thus, the solver tends to limit the number of individuals on the Pareto frontier. Maintaining this diversity is important for convergence to an optimal Pareto front.

Scores are assigned to the population chromosomes using the fitness (i.e. objective) function (6.41). According to the computed scores, elites, crossovers, and mutations are selected for the following generations in the evolution process. The coding of the solver mechanism is one of the contributions of this study. It must be noted that the constraint hard-coding process within the chromosome development functions provides key values to the computational process. For instances, the classical solver consumes more memory due to the iterative process of validating chromosomes with respect to constraints, then regenerating chromosomes, accordingly, the classical solver requires larger population sizes and higher number of generations as several chromosomes are usually deemed infeasible, especially when the problem is of high complexity. Therefore, our proposed solver is intelligent because it identifies and considers all requirements during all processes, requires less memory and fewer generations to convergences, and produces only feasible chromosomes (i.e. no rejected/recreated chromosomes are generated).

Pareto Frontier Analysis

Rather than solving a function of linearly scalarized objectives as in surveyed literature, our work finds Pareto optimal solutions using evolutionary programming. Consequently, there may exist more than a single solution on the Pareto frontier.

Therefore, we propose a programmable tool to guide the consumer through the Pareto optimal solution choice without the requirement of his frequent interference. The underlying principle is that the solution choice depends on the shape of the Pareto frontier (i.e. convex or concave) and the consumer's preset solution settings. Thus, we provide the consumer with higher flexibility in his DR participation, rather than enforcing a fully balanced load shifting between 2 successive hours as we had assumed in chapter 4.

The consumer presets his controller by selecting from 4 solution settings: extreme objective 1 solution, extreme objective 2 solution, centric solution leaning towards objective 1, or centric solution leaning towards objective 2. The consumer is also free to change his settings at any time during the operation period. It must be noted that regardless of the choice of either extreme solutions, acceptable values for both objectives (i.e. load shifting and comfort objectives) shall remain satisfied at all times due to the use of utility functions with boundary limits and hard-coded solutions. We explain the 4 proposed Pareto frontier solution selection methods in the following subsections.

Setting 1: Maximum Load Shifting

We define this setting as a greedy DR solution because it selects the solution from the Pareto frontier with the best value only for the DR objective; (6.37).

Setting 2: Maximum Utility

In complete contrast to setting 1, this setting results in a greedy wellbeing solution, which selects the solution from the Pareto frontier with the best value for the comfort objective, (6.38), only.

Setting 3: Biased Load Shifting

If more than 3 solutions exist, this setting results in Pareto frontier solution choice from the region close to the maximum load shifting solution. If only 3 solutions exist, this setting will results in the center solution.

Setting 4: Biased Utility

Similar to the biased load shifting, this setting allows the controller to select a solution from the region close to the maximum utility solution, if more than 3 solutions exist.

Chapter 7: Simulation Modeling and Results

Chapter Introductory Remarks

In chapter 4, we introduced a simple DR mechanism and we have demonstrated its functionality using a SIMULINK model fit with real data. This mechanism was modified in chapter 6 to include additional and more complex features like nonlinear optimization, consumer utility models, Pareto optimization in real time (i.e. continuous time), and support for bidirectional loads (e.g. B2V and V2B). For validating the proposed methods, a new simulation model is required to incorporate all the additional features. Additionally, when fitting the simple model in chapter 4, we neglected factors like solar loading and human-related activity. In this chapter, we address all these factors and develop a model for the proposed 2-stage DR approach. The model presented in this chapter assumes an industrial consumer with the following controllable load types: a 4-stage chiller unit and a dynamic traffic of logistic EVs. We demonstrate the proposed 2-stage methodology in this chapter through simulation and realistic data. The work in this chapter was accepted for publication in [108]

Chapter Motivation and Objective

The objective of this chapter is to develop a realistic simulation model to implement and test the methods proposed in the previous chapter. However, due to the complexity and high dimensionality of the problem, many challenges must be overcome, which motivates this work. For instance, the model is to apply hierarchical 2-stage solutions, where one solution is designed for a discrete system simulation, and the other solution requires real-time optimization. Thus, both discrete-event driven simulation and system dynamics simulation paradigms must be integrated. We also need to develop control tools

to allow for real-time user interference where the user is given more flexibility in his DR participation, logging tools for real-time extraction of information (e.g. temperature, SOC, loads, etc) and calculation of utility values, and design a communication platform for transferring information among load entities, EMS (i.e. logging controls), utility provider, user, EVs, proposed controllers, etc.

Real Environment Data Collection

We utilized data for building the new simulation model from a real manufacturer as we have done in chapter 4; Data were collected during an energy assessment conducted by the MIIAC team. Through a series of data loggers, current transducers, temperature sensors, among other equipment, the MIIAC logged various data for the facility based in Florida including: the 3 phase current amperage drawn at each main electrical panel, the current drawn by each HVAC unit, the conditioned space temperatures for several zones of the facility, and the outdoor temperature. The logging session extended to 1 month with 1 minute of data collection intervals. For outdoor conditions, we utilized environmental data specific to the consumer's location from the National Oceanic and Atmospheric Administration (NOAA) online repositories. In this model, we utilize data for only 1 consumer, therefore, we do not simulate prices using the model presented in chapter 3. Instead, we use real RTP data obtained from PJM Interconnection LLC, which is a regional transmission organization (RTO). Knowing the voltage for each piece of equipment, all amperage readings were converted into load data. While the actual facility utilizes both water-based chillers and rooftop packaged units, we fit the data into an assumed single multistage large chiller system for simplification. From examining the logged data, we conclude that the combined cooling load of the facility fluctuates

between 375 kW and 500 kW, which represents 75% and 100% loading. The combined logged cooling and the assumed load are shown in FIGURE. In addition to conducting DR simulation studies using the real data, the developed model can be used for comparing HVAC systems efficiencies, insulation quality, and other energy-related studies.

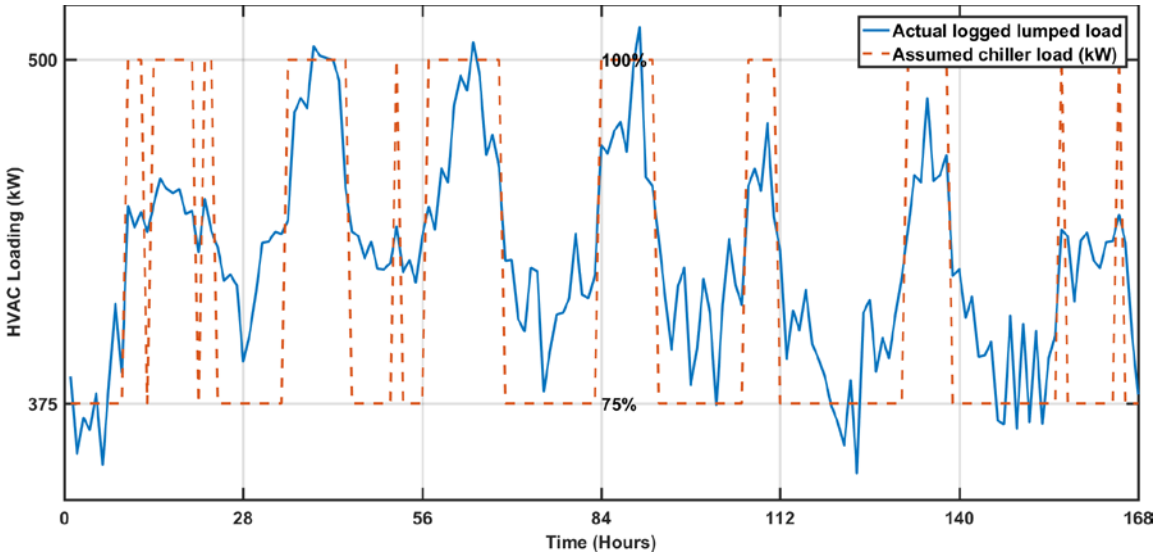

Figure 7.1. Logged cooling loads vs. fitted 4-stage chiller system.

Model Parameter Estimation

In order to create a thermal model for the facility, we must consider all heat sources including: heat conducted through the building envelope, solar loading during the day time, and heat emitted from human traffic and machinery. From data logging and NOAA resources, we obtained real data for: both outdoor and indoor climate conditions, the HVAC system operation, and the energy consumed by industrial machinery, lights, and equipment within the manufacturing facility. We reasonably presume that the heat produced by the indoor operations is directly proportional to the lumped electric power drawn by the various machinery, lights, etc. Thus, knowing the HVAC specifications and

the volume of the air-conditioned space, we build the parameter estimation model shown in Figure 7.2. Using this model, we estimate the following model parameters:

- The building's equivalent thermal resistance (Req), which models the heat amount conducted from the outdoor environment to the conditioned space through walls, ceilings, doors, and windows.
- The presumed coefficient of internal load gains (ILG), which relates power consumed by the facility to internal heat generated.
- The coefficient of heat gained through solar radiation (SLG), which is similar to (Req) except that it models the heat gained during high solar radiation periods of the day, where part of the solar radiations are reflected off the ceiling and the remainder part is absorbed by the building as heat.

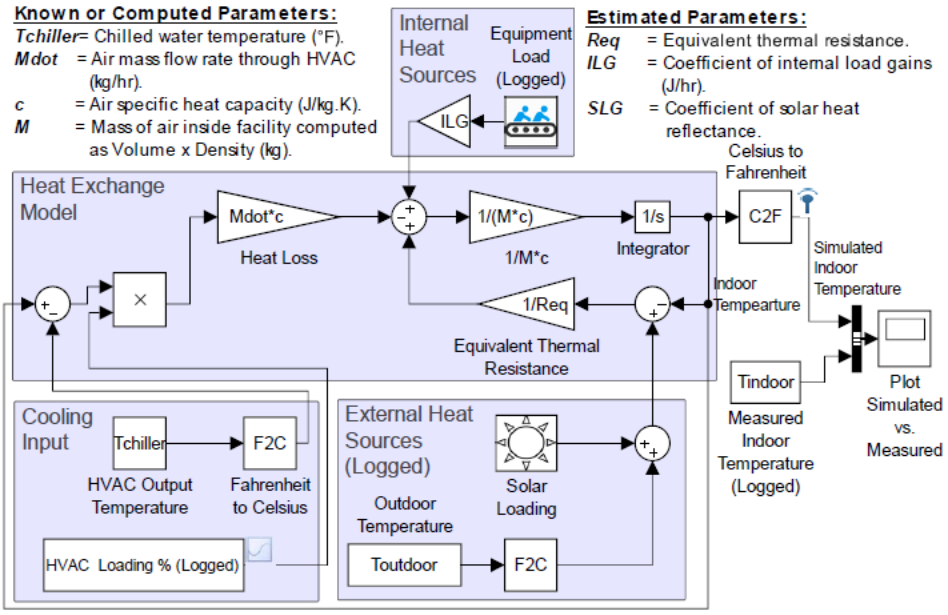

Figure 7.2. SIMULINK thermal parameters estimation model.

We assume and relax parameter bounds based on educated guesses. Finally, we use the Levenberg Marquardt algorithm [109] to optimize the model parameters iteratively through simulation. Thus, the thermal model is validated using real data and the

differences between guessed parameters and optimized parameters compared to measured data are illustrated in Figure 7.3, which demonstrates the simulation model's goodness of fit. We carried out all processes using MATLAB and SIMULINK.

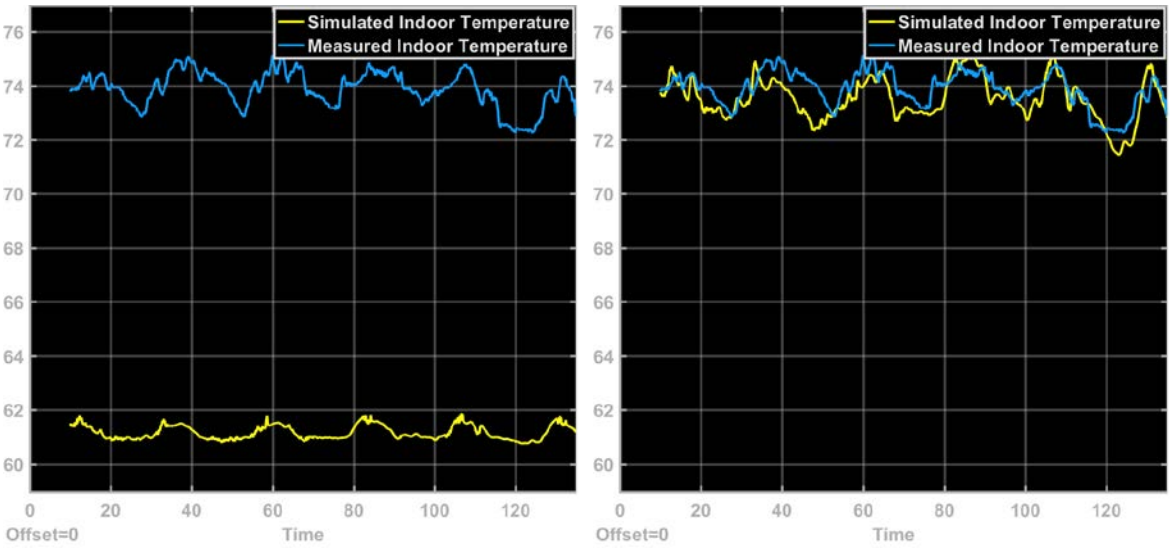

(a) (b)

Figure 7.3. Simulated vs. measured indoor temperature: (a) Before parameter optimization. (b) After parameter optimization.

Model Communications Architecture

To simulate the realistic scenario, we utilize both the continuous system dynamics and event-driven discrete simulation paradigms. For instance, we practically model the HVAC loads in continuous time, where the loads are activated or deactivated through an EMS control system (e.g. thermostats and switches) and a chiller feedback control system (e.g. relays for selecting operational stages based on water temperature). When an HVAC load is activated, it then registers to our proposed controller to determine the number of DVs M and the capacity C at the specific time instance. For example, if the EMS and Chiller controller determines that 3 out of the 4 operational stages (e.g. 3 chiller compressors) are required, assuming that there are no other controllable loads (e.g. EVs) in the system, then $M = 3$, $C = l_1 + l_2 + l_3$, and the stage 2 DVs after computing e are

x_1, x_2, and x_3. The continuous optimization phase means that DVs are allowed to change indefinitely during the interval for which the load shifting target e is constant (i.e. 1 hour). In the continuous time system, time steps are variable and very small in size. The model's state at the next time step is computed using temporal discretization methods for the approximate solutions of ordinary differential equations [110]. Differently, realistic modeling of the commercial EVs requires a different setting because the shipping EVs arrive and depart at various time instances independent of the system dynamics simulation model. Therefore, they cannot register based on any control loop (e.g. EMS, thermostat, etc). Additionaly, each EV is independent with respect to its SOC, battery capacity, required service time, etc. Therefore modeling of the EVs traffic requires an event-driven discrete simulation paradigm. Similar to the multi-agent based modeling scheme, where several independent entities interact in order to satisfy their independent goals. We define the entities (e.g. agents) and their attributes for our event-driven model below.

Utility Supplier Entity

The utility supplier entity is responsible for clearing the energy price for the next hour of operation (i.e. $t + 1$) at each discrete 1-hour step t. We assume that the cost of energy reflects the supplier's objectives for economical dispatch and DR.

Chiller Stage Entities

There are 4 entities in this group (i.e. $S = 4$) for the multistage chiller system. Each entity may exit or enter/reenter the system as many times as directed by the system dynamic control signals; an entity (i.e. stage) s is activated by the chiller feedback control system based on the incoming water temperature. Once s is activated, it enters the event-

driven system and registers at the main controller which decides on its operation. The independent objective of each entity is to maximize its operation time while it is activated (i.e. maximize its utility).

EV Entities

Different than chiller stage entities, we assume an infinite pool of EVs from which EV entities are summoned. This means that when a registered EV leaves, it does not return at a future date. At any instance in time, the number of total EV entities in the system is a variable V. Each EV v acts as an independent agent with the following set of attributes upon arrival: arrival time stamp a_v, expected departure time b_v, expected service time t_v^s, battery capacity Q_v, and SOC SOC_{v,a_v}. The objective of each v is to maximize its SOC (i.e. $SOC_{v,b_v} \approx Q_v$) through charging while in the system. If the charging costs were to be incurred by the EV, then, a profit maximization or a cost minimization objective would be added to the EV. We assume only large commercial EVs (e.g. shipping and pickup trucks) in our model. Future work may include employee EVs as well.

Stage 1 Entity: Load Shifting Optimizer

The load shifter entity enters at discrete 1-hour time steps, where it receives the energy price for the upcoming hour period, the forecasted, and optimizes objective (6.6). Then it sends the new objective values to the stage 2 controller.

Stage 2 Entity: Multi-Objective Optimizer

Perhaps this is the most complex entity in the model as it is the point of connection between the system dynamics model outputs/inputs and the discrete event-driven model outputs/inputs; all activated load entities HVAC or EV, registers to the stage 2 entity and

remains connected for real-time optimization (i.e. continuous simulation) until an entity departure event occurs (i.e. discrete-event simulation). It also receives and updates discrete data from the stage 1 entity. The objective of this entity is to defined by (6.41), which is to both satisfy the received load shifting targets and to maximize the independent objectives of each registered load entity. This is also the entity responsible for managing V2B options as a buffer for energy needed beyond the received targets. Also assigned weights through the AHP and consumer-defined settings are communicated through this entity.

In this context, the number of load entities, M, in the system varies throughout the simulation as entities are allowed to leave once their objectives are achieved, thus, creating an event-trigger. Like in the multi-agent models, the load entities are engaged in a competition for achieving their independent objectives, which are prioritized through their utility function values.

Integration of Discrete and Continuous Systems

We modeled EV entities using SimEvents package tool, which is a discrete-event simulation engine for analyzing event-driven systems and supports agent-based modeling. However, we modeled the system dynamics (i.e. continuous model) in SIMULINK, which includes the thermal model, feedback control systems, etc. One challenge was to integrate SimEvents with the system dynamics simulation paradigm. We accomplished this integration through event-triggered function blocks; In SimEvents, an event occurs once an entity enters or leaves the system. Based on the entity and event type, a corresponding function block is triggered which activates a MATLAB function. This function is scripted to read the entity's unique ID, add an attribute to the entity to

determine when the entity is present or absent from the system, then saves or reads its related information to a memory matrix in MATLAB's workspace. The memory matrix stores all present and past entities with their details. The entity's unique ID defines its row location in the matrix. The matrix data are continuously updated throughout the simulation to output information in real-time. For example, through the workspace matrix, an EV's SOC is continuously monitored, recorded and allowed to vary in real-time, which wouldn't have been possible in SimEvents alone because it is discrete-event-based and cannot communicate in real-time with the continuous system dynamics model. However, the memory matrix can be called in both systems simultaneously; it is called and updated continuously in the continuous model, while it is called and updated as triggered by discrete-events in the discrete model. This integration is illustrated schematically in Figure 7.4. The full SIMULINK model is shown in Figure 7.5.

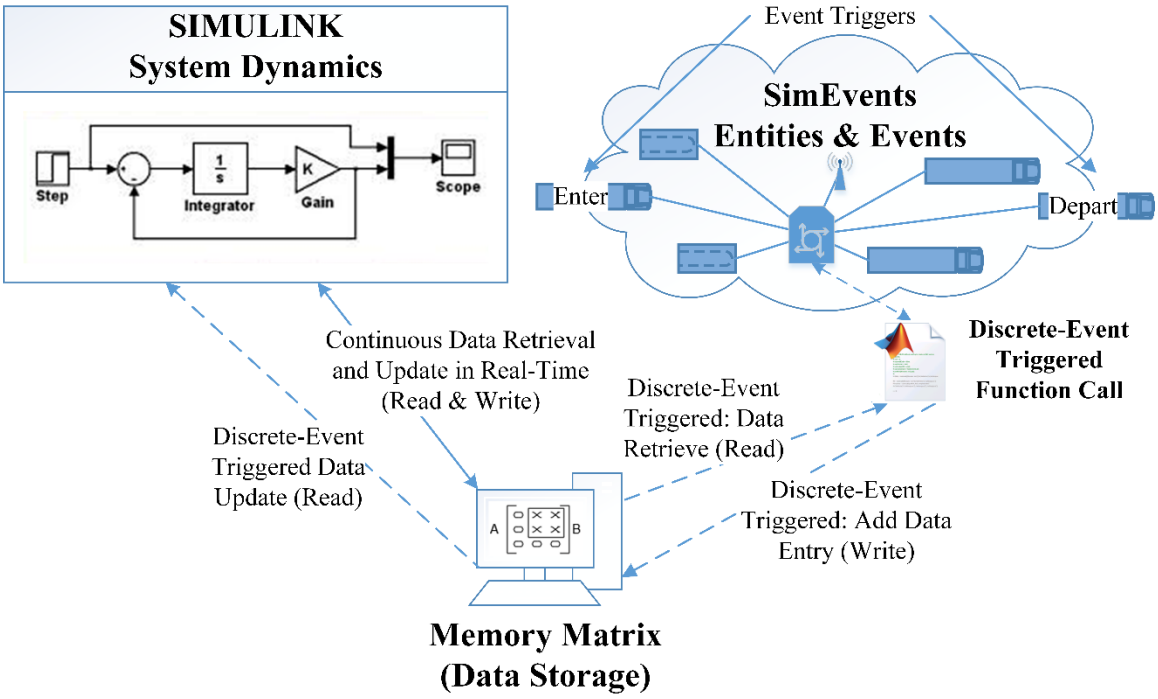

Figure 7.4. Schematic illustration of the integration between the continuous model and the event-driven model.

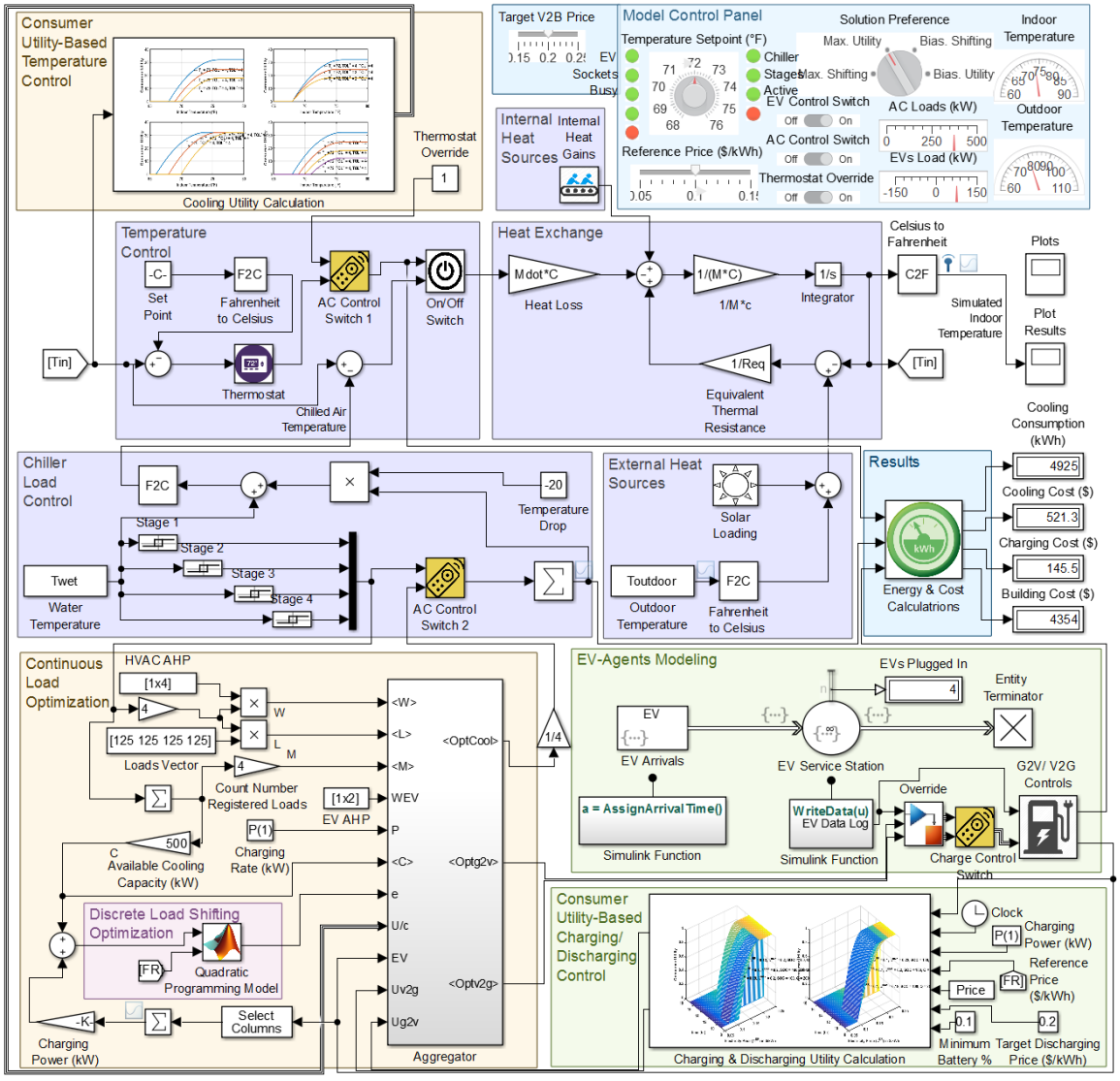

Figure 7.5. SIMULINK diagram for entire simulation model.

AHP for Weights Assignment

We have utilized task-specific utility functions to model the consumer's value for each task independently of all other tasks. However, to appropriately make decisions based on the independent utility values, we assign weights to each task in order to consider the consumer's comparative preferences among tasks. We utilize a simple AHP for assigning comparative weights according to a typical consumer's preferences; three attributes are assumed for the task choices: Cost, comfort, and security. The consumer's attribute for cost gives higher ranks for loads of lowest cost impacts or highest profit , his

comfort attributes promotes only HVAC loads with higher ranks given to base stages than the ramp up stages, while his security attribute prioritize charging and assigns the lowest rank to discharging. Thus, we can rank loads by importance with respect to each attribute as shown in Table 7.1. Realistically, we assume that most consumers value comfort slightly more than security and both comfort and security more than cost. Accordingly, the AHP constructs an attribute pairwise comparison matrix, determines each load's score for each attribute, and finally, through problem decomposition and hierarchical computations, comparative weighs are determined.

Table 7.1. Load types ranked by their importance to each attribute.

Order of importance (i.e. Rank)	**Attributes**		
	Cost	**Comfort**	**Security**
1	All V2B loads	Stage 1 of HVAC loads	All B2V loads
2	All B2V loads	Stage 2 of HVAC loads	All HVAC loads
3	All HVAC loads	Stage 3 of HVAC loads	All V2B
4		Stage 4 of HVAC loads	
5		All V2B and B2V loads	

Simulation Model Input Data

HVAC Model Parameters

For the simulation case study, we use the multi-stage chiller loads and the user's preset parameters given in Table 7.2; The multistage chiller operates at a maximum of 4 stages with 125 kW of power drawn by each stage, the consumer adjusts his set-point temperature to 72°F with ±4 tolerance, and the consumer's threshold for price is \$0.1/kWh.

Table 7.2. Model parameters.

Parameter	S	l_1, l_2, l_3, l_4	T_s	TOL^+	TOL^-	P^{EV}	λ^{FR}	λ^{max}	$\varkappa$
Value	4	125 kW	72°F	4	4	24 kW	\$0.1/kWh	\$0.2/kWh	10%

EV Model Parameters

As mentioned before, in our case study, we assume only large capacity commercial EVs used for shipping or receiving, while we leave employee or visitor EVs to future work. We realistically define the EV entities' interarrival distribution function such that EV traffic is higher during the midday than during the day or evening periods. Therefore, for the interarrival rate, we utilize a Poisson distribution with a sinusoidal function of time as the mean. Each arriving EV obtains a unique ID and random values for its attributes upon arrival. The recorded attributes for the arriving EVs during a random 24-hour simulation time period are shown in Table 7.3. Other parameters are given in Table 7.2; the charging and discharging rates are 25 kW, the consumer's desired incentive for discharging is \$0.2/kWh, and the minimum SOC allowed for battery health reservation is 10%.

Table 7.3. EV entity attributes during 1 day of simulation.

Arrival number (i.e. ID)	Q_{ID}	$SOC_{ID,a_{ID}}$	a_{ID}	b_{ID}
1	250	41	3.372	11.37
2	150	49	4.431	10.43
3	250	48	7.386	15.39
4	200	163	9.726	12.73
5	250	201	10.1	18.1
6	150	129	10.82	18.82
7	250	189	11.58	16.58
8	150	109	12.29	15.29
9	150	24	12.5	19.5
10	150	144	13.3	16.3
11	200	156	13.69	20.69
12	200	95	13.84	19.84
13	250	77	14.69	21.69
14	150	27	15.45	20.45
15	200	122	17.81	21.81
16	150	81	19.02	26.02
17	250	142	21.2	24.2
18	150	128	21.41	25.41

Load Preference Weights

The weights set according to the consumer's AHP are given in Table 7.4.

Table 7.4. AHP weights assignment.

Load (i.e. Task)	l_1	l_1	l_1	l_1	$l_{v\in V}$ for any B2V	$l_{v\in V}$ for any V2B
Weight	0.23	0.17	0.14	0.11	0.18	0.17

Results and Analysis

We run the simulation for a period of 1 week using real climate, price, and consumer base load data. The hour-ahead base load forecasts were obtained using the artificial neural network described in
with less than 2% error. Attributed to the quadratic programming and proposed GA solver's efficiency, the simulation for the whole week is completed in less than 15 minutes on an Intel Core i7 machine with processing unit clock speed of 2.2 GHz and 12 GB of memory. This demonstrates the method's suitability for real-time application and for achieving autonomous, instantaneous, and momentary DR. Figure 7.6 shows the discrete RTP-HA and the corresponding identified load targets using quadratic programming in stage 1. Our observations are discussed in the following subsections. For clarity, the figures shown below present the simulation results for only day 1 of the simulation. These figures show the cooling loads, the lumped loads from B2V and V2B, the indoor temperature, and the overall building consumption.

Pareto Optimal Solutions

As mentioned in the previous chapter, this is the first study to consider Pareto optimization for the conflicting objectives of satisfying DR and maximizing consumer's comfort. Throughout the case study simulation, we observed that, at some time instances, a single solution existed which optimizes both objectives, but for most time instance, multiple nondominated optimal solutions were identified like the those found for the time

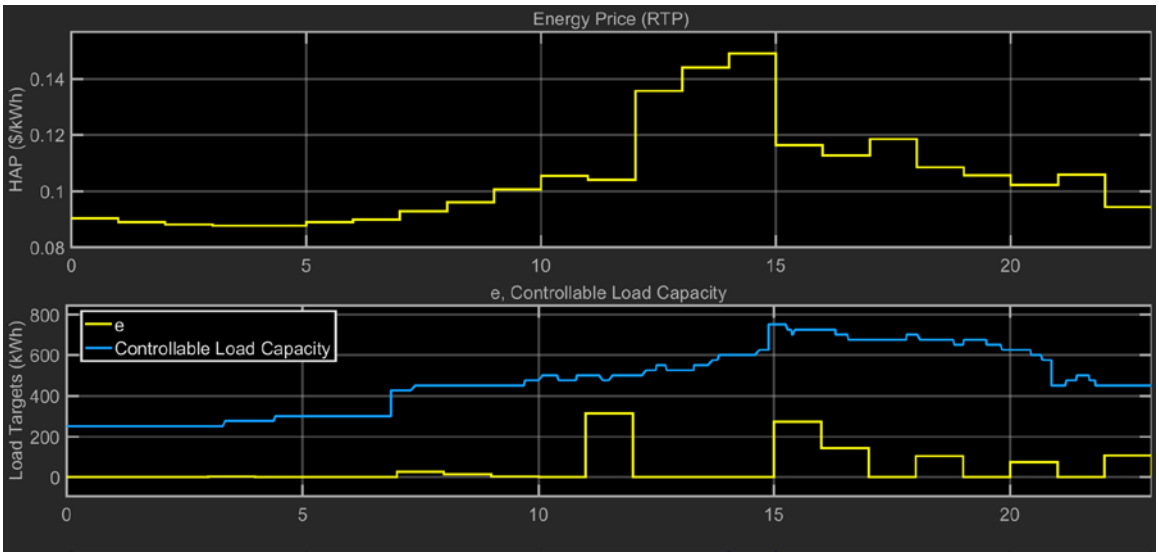

Figure 7.6. RTP-HA, controllable load capacity (i.e.C), and stage 1 optimized load shifting targets (i.e. e).

instant 19.2 shown in Figure 7.7. The solution choice was made using the consumer's preset criteria described in the previous chapter. It must be noted that the user is given the flexibility to change his settings at any time during the simulation. We discuss and compare the results obtained for each of the available settings in the subsection below.

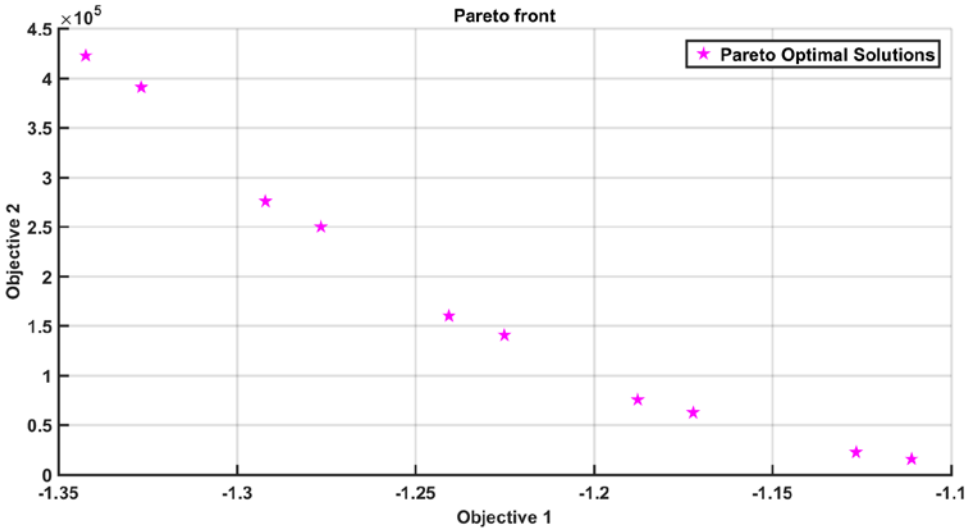

Figure 7.7. Pareto frontier for the real-time optimization at simulation time instance 19.2 hours.

Scenario 0: Controller Turned Off

In the case of opting out from using the proposed controller, then static thermostat settings are utilized, which maintains the temperature at the desired 72°F level without

allowing further deviations beyond the deadband width. The EVs draw charging power when they are plugged in without utilizing smart bidirectional power controls. As for the chiller, the loading stages are only controlled by the feedback control system (i.e. incoming water temperature). The results for only the first day of simulation are shown in Figure 7.8, which demonstrates the Maintained temperature level and the one-way power flow to EVs.

Scenario 1: Maximum Load Shifting Consumer Settings

In the case where the consumer presets the controller for the maximum load shifting settings, about 6% savings are achieved at the cost of maintaining a temperature closer to the consumer's upper tolerance level. If more load types were included in the system or larger number of EVs, then the savings could have been substantially higher and the impact to the temperature should become lower. As Figure 7.9 shows, we observed that the cooling loads operated at a much lower frequency than in scenario 0, hence the higher temperature and the higher savings.

Scenario 2: Maximum Utility Consumer Settings

When the consumer presets the controller for the maximum utility settings, which is perhaps the option with the highest chance of acceptance among industrial consumers because they tend to value comfort or security higher than cost, we observed that higher cooling load was demanded. However, thanks to the bidirectional EV charging controls, overall saving of approximately 2% were achieved. EVs acted as an energy buffer during higher peak periods, where if more EVs or additional energy storage loads were utilized, this controller setting could become even more favorable. Figure 7.10 shows the higher cooling loads and the higher regard to maintaining the 72°F temperature level.

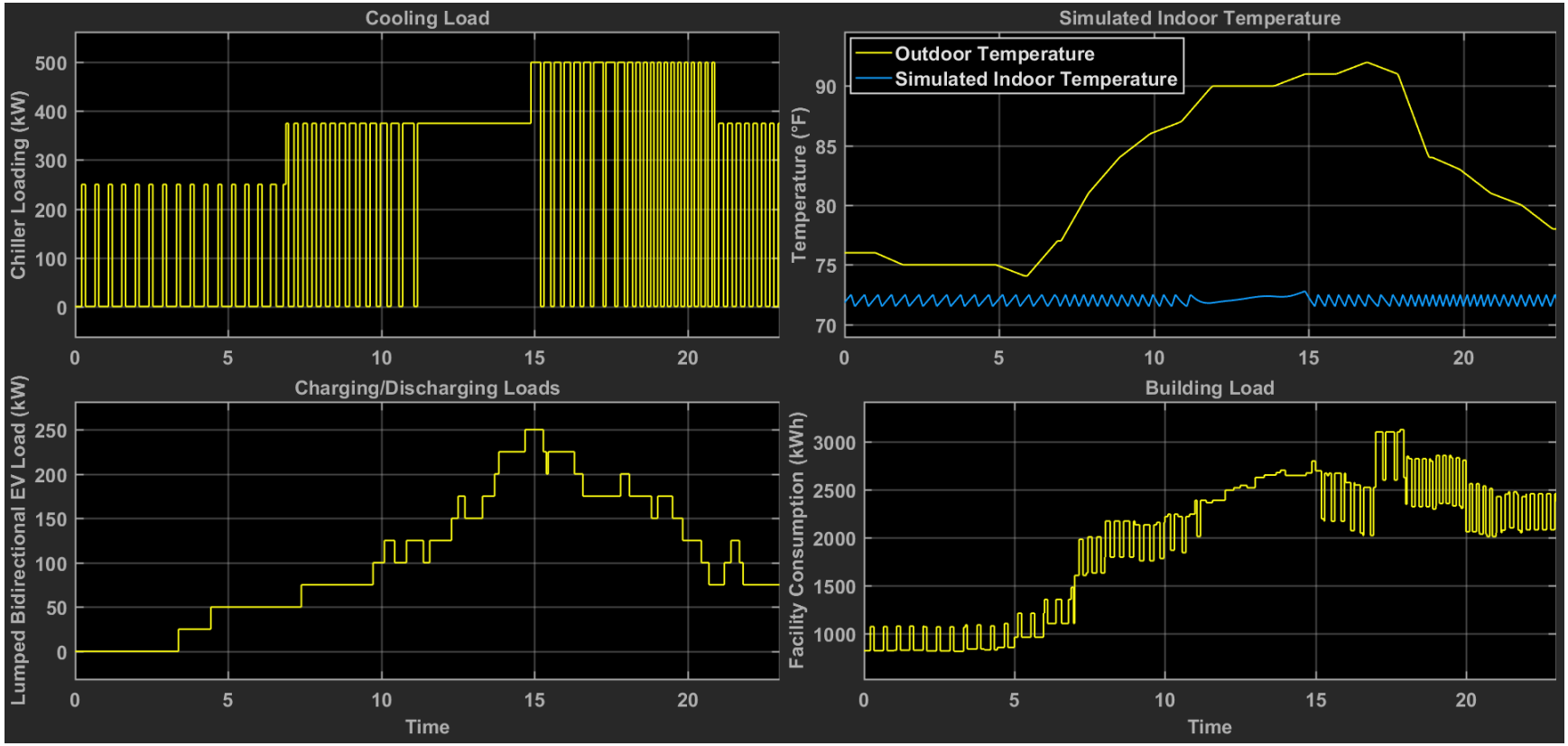

Figure 7.8. Simulation results for day 1 when the consumer does not participate in DR.

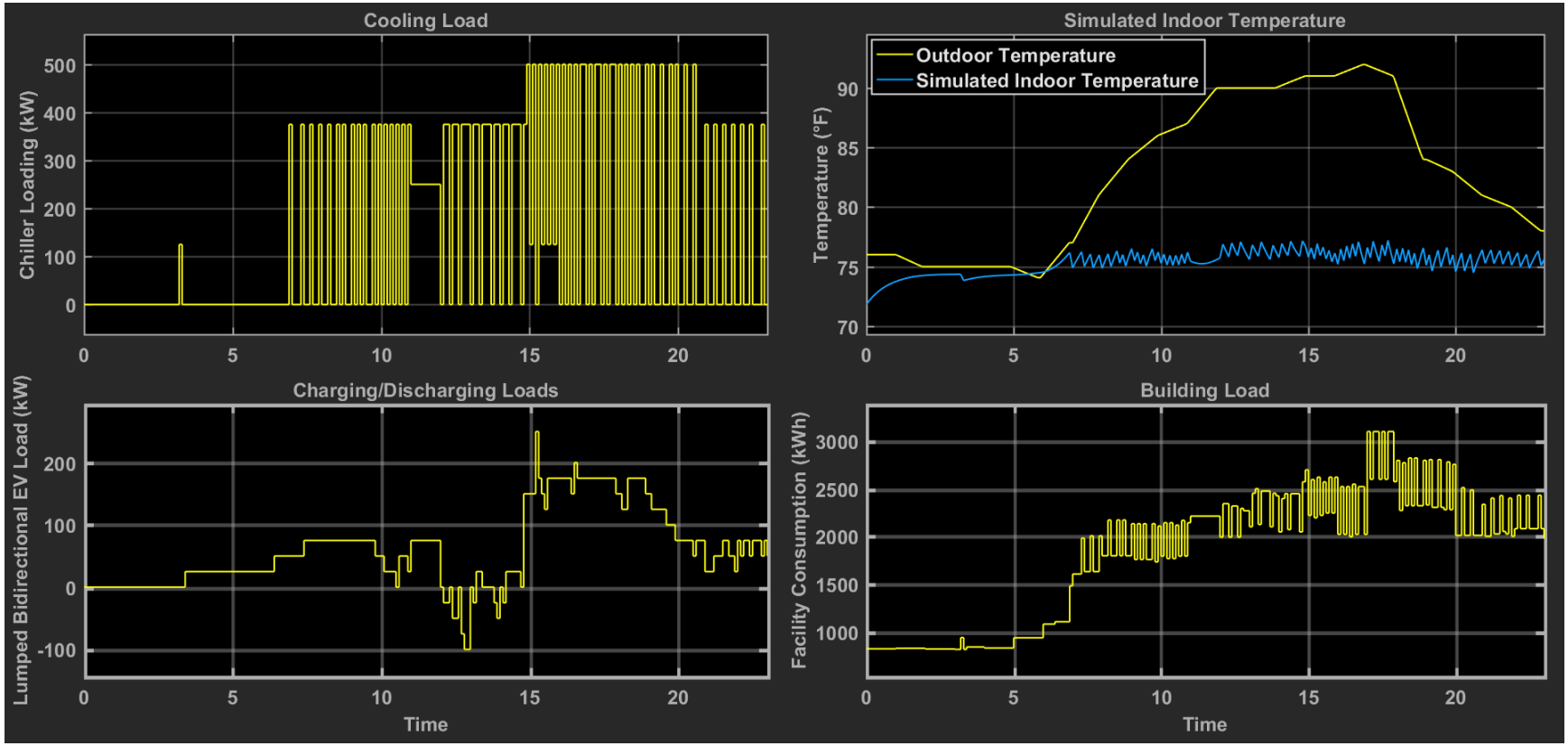

Figure 7.9. Simulation results for day 1 when the consumer selects the maximum load shifting setting.

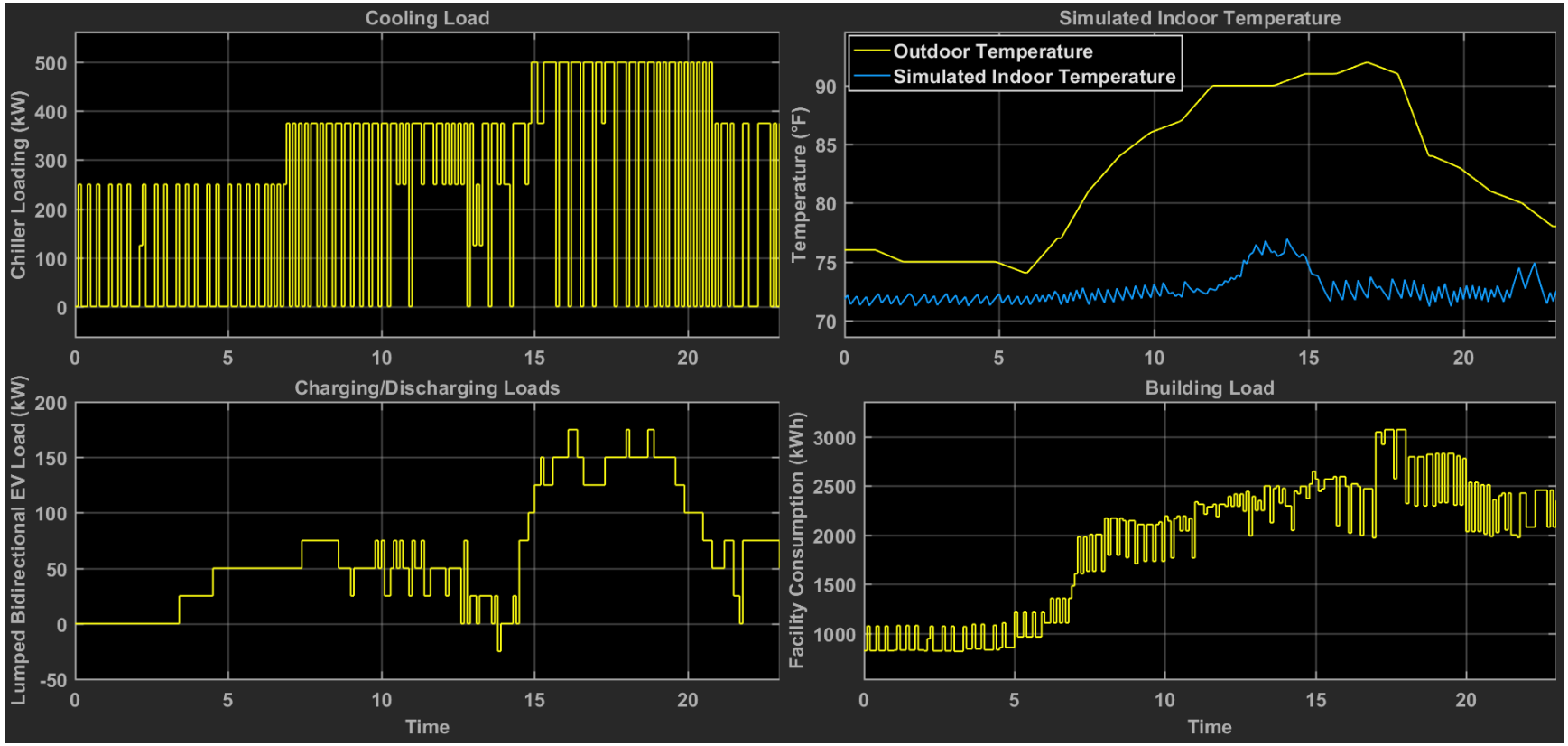

Figure 7.10. Simulation results for day 1 when the consumer selects the maximum utility setting.

Scenario 3: Biased Load Shifting Consumer Settings

In the case where the consumer presets the controller for the biased load shifting settings, we observe that there is no realizable differences in consumption or savings between this setting and the maximum load shifting setting as shown in Figure 7.11. Discrepancies may have been noticed, if larger load varieties were incorporated in the model.

Scenario 4: Biased Utility Consumer Settings

In the case where the consumer presets the controller for the biased utility setting, which is perhaps the most superior and the recommended setting, we observe that the achieved savings are close to 5% and the impact on the desired temperature level is minimal in comparison to both the maximum load shifting and the biased load shifting settings. This is evident in the plots shown in Figure 7.12.

Summary of Results

The simulation was run for a period of 1 week using real climate, price, and consumer base load data. It is concluded that the consumer can lower his overall utility bill from 2% to 6%, depending on his selected solution criterion (i.e. Pareto frontier preferences). These results are attributed to about -4% to 30% savings in HVAC costs combined with an average 40% savings in EV load costs. It must be noted that the achieved savings would have been substantially higher, had we considered more and larger EVs or additional types of controllable loads. Additionally, the shifting towards the microgrid and the increasing deregulations could result in higher price volatility and thus leverage the proposed method to produce higher savings. Table 7.5 breaks down the average daily savings for each solution criteria. All solutions preferences satisfied the consumer's

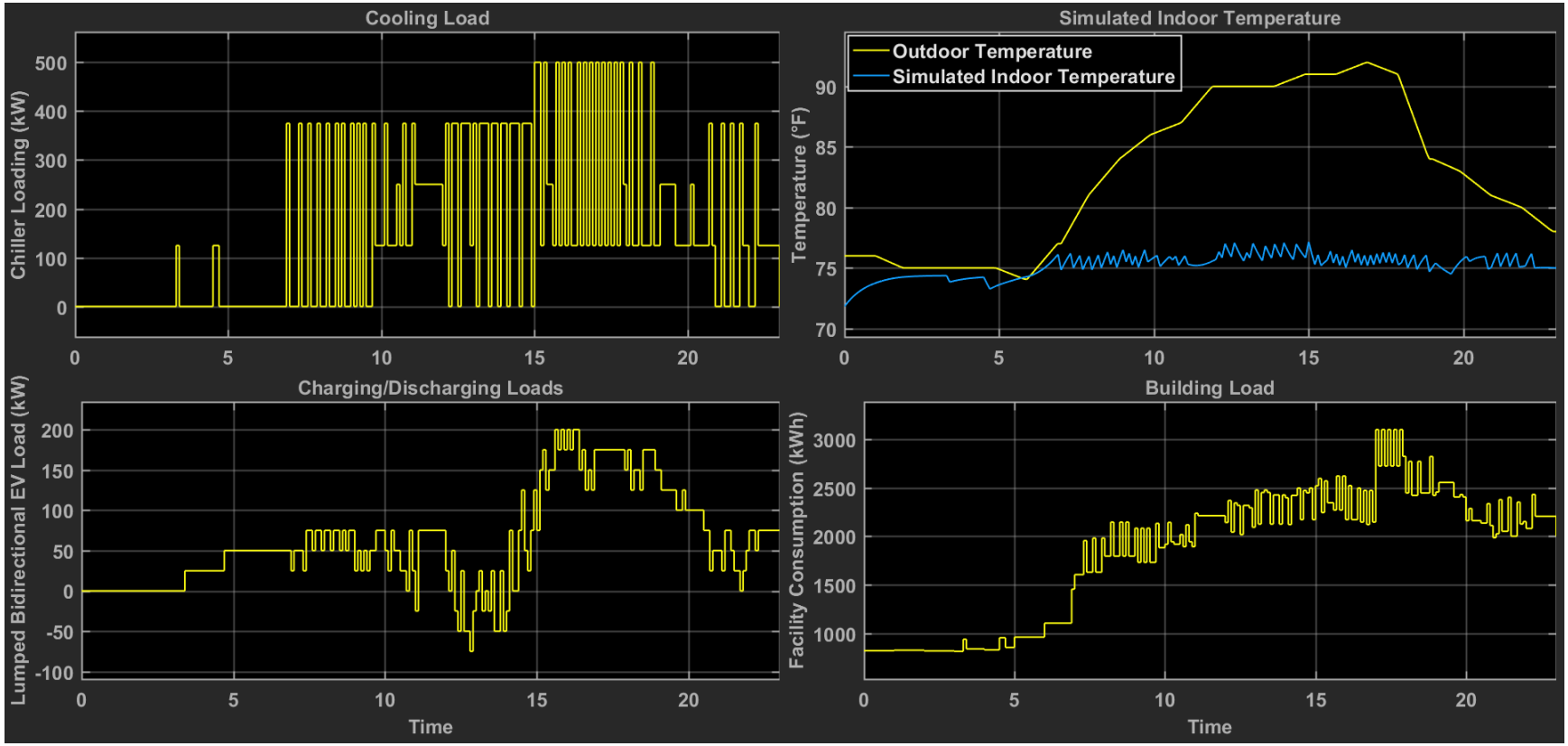

Figure 7.11. Simulation results for day 1 when the consumer selects the biased load shifting settings.

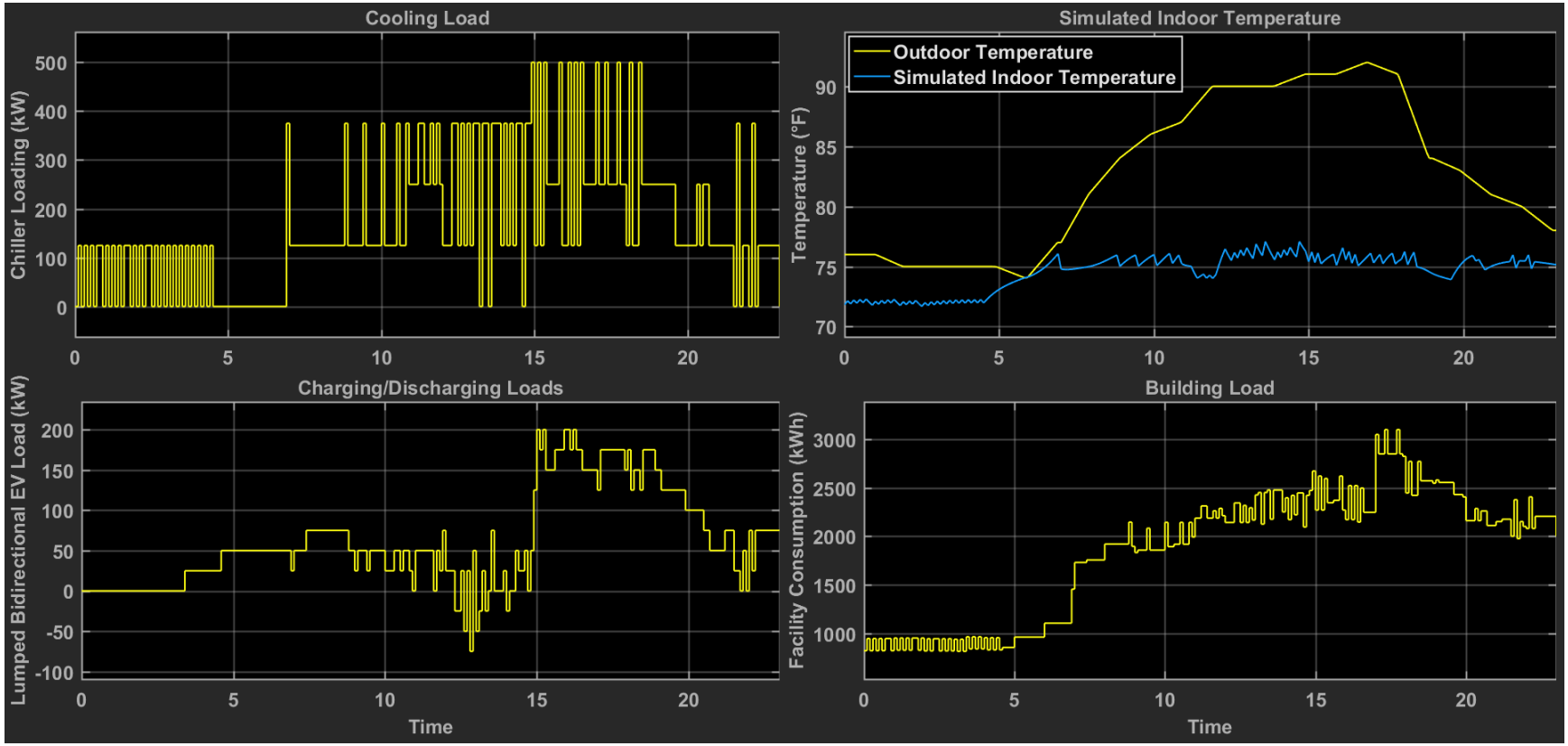

Figure 7.12. Simulation results for day 1 when the consumer selects the biased utility setting.

tolerance for comfort as shown in the previous subsections and figures. When the consumer chooses the maximum comfort solution criteria, he ends up using more energy for HVAC, yet, his overall energy bill decreases by approximately 2%, because the controller utilizes the V2B as buffer for the cooling energy required. If there EVs or other storage systems weren't included, then we can expect that the maximum utility scenario would not produce savings. Overall, it is expected that most consumers would find that the biased utility solution is the best since it achieves realizable savings while maintaining a better thermal comfort than the other extreme options. Furthermore, it was concluded that proposed controller allocates higher load targets to the hours prior and post to high price hours, thus leveraging the building's thermal inertia or the EVs charge capacity to maximize the utilization of DR and maintain comfort.

Table 7.5. Average daily savings from applying the proposed DR controller with 4 adjustable settings.

Savings category	**Pareto solution selection criteria**			
	Maximum load shifting	**Maximum utility**	**Biased load shifting**	**Biased utility**
Building energy costs ($)	$245	$67	$235	$198
Building energy costs (%)	5.9%	1.6%	5.6%	4.7%
HVAC consumption (kWh)	1630 kWh	-208 kWh	1543 kWh	1155 kWh
B2V/V2B net savings ($)	$92.8	$86.7	$90.5	$89.8

Chapter 8: Conclusion

Summary

In this dissertation, we presented a novel approach to addressing the consumer-side DR problem, with focus on the industrial consumer. We argued that highly dynamic energy pricings can uncover potentials for load balancing and grid stability, if the consumer is able to respond in a wise and timely manner. Hence, we directed our research effort to creating and testing an intelligent, autonomous, and instantaneous DR controller method, which omits the dependency on frequent user interference, long term planning or forecasting, and thus eliminates the errors associated with these approaches.

In chapter 3, we presented a price-simulation model for the purpose of mimicking volatile dynamic energy tariffs. The model generates prices for each upcoming hour in the system as in the RTP-HA system. This is significant because a truly dynamic tariff, which represents the actual cost of energy, cannot be accurately estimated before the energy is actually consumed. As several researchers had concluded, the less dynamic tariffs, like TOU or DAP, do not capture the full potentials of DR, whereas a highly dynamic tariff, like RTP-HA, is superior for the utilization of DR as the utility supplier benefits from decreased forecast uncertainties in the short term. Our price-simulation model was used for DR simulation analysis in chapter 4.

In chapter 4, we presented the first DR control methodology to instantaneously shift loads between two successive hours, guided by the price differences among these hours. We defined two strategies for shifting loads, BDS and FDS, where in the first strategy the load is shifted from an upcoming hour to the current out, and the opposite is achieved in the latter strategy. Once load shifting values were identified, we proposed a regulator to

carry out the load shifting objectives through a series of switches, relays, and thermostat controls. We considered 8 realistic industrial buildings' simulation models, which were fit using real measured data, to test the controller. It was concluded that modest savings in mostly HVAC loads can be accomplished at the consumer-side. However, the utility supplier-side faces new and higher load spikes in the aggregate system due to the synchronization of loads during cheap energy periods.

Although the supplier-side impact was not our main focus, we discussed a machine learning approach in chapter 5 to disaggregate the loads by consumer-side and according restructure the RTP-HA tariff. First, we suggested a clustering strategy of energy consumers with focus on DR applications. Second, in order to achieve prompt consumer classification for assigning the right tariff to the right consumer, we developed a classification algorithm which achieves better results than classical methods. Without getting into price optimization research, we demonstrated through simulation that the disaggregate system would result in fewer load synchronization spikes.

In Chapter 6, we added features to the DR controller. The result is a 2-stage hierarchical DR approach with options for higher consumer flexibility. A consumer-task utility model was developed in order to identify load preferences for the controller to turn on or off. In addition, we enabled the utilization of energy storage systems or bidirectional loads as part of the DR optimization function. The controller solves a nonlinear and a Pareto multi-objective problem in real time. Therefore, we developed a evolutionary programming tool with creative customized coding scheme for efficiently cutting down the dimensionality of the problem and producing instantaneous solutions in

real time. Finally, we provided the consumer with a tool to adjust the controller objective settings at any time during the controller operation, guided by his preferences.

We developed a virtual testbed for the aforementioned 2-stage controller in chapter 7. This includes an industrial building's thermal model fit with real data, a multi-stage HVAC unit, and commercial-sized EVs which behave independently of the building's model. The testbed is characterized by incorporating both a continuous system dynamics control model and an event-driven (i.e. discrete) simulation model, which behaves as a multi-agent simulation model. We demonstrate that the loads, also named as entities, tasks, or agents throughout the dissertation, engage in a competition, where each load is an independent entity. Most loads have conflicting objectives and their competitive advantages (i.e. bidding powers) are given by the consumer's time-varying utility value for each task. The optimization of these loads occurs in a continuous real-time manner. Finally, we conclude from the simulation results that the consumer can achieve realizable savings, where the savings quantity depends on whether he prioritizes comfort or cost. The user is given 4 settings to choose from with respect to prioritizing cost or comfort, and he is allowed to interact with the model in real time to alter his settings. We also note that we have used a very conservative testbed with very limited load amounts. In a realistic application, several loads can contribute to DR as well as standby fuel generators, thermal storage systems, employee EVs, etc. Thus, the realized savings would be much higher in reality than in our assumed model.

In conclusion, we demonstrated our method's suitability for real-time application and for successfully achieving autonomous, instantaneous, and momentary DR.

Contributions

We can list the contributions of this study as following:

- This study develops a realistic price-simulation model, which can be useful for research purposes when a system's load is known but realistically volatile RTP are required.
- This study formulates a practical linearized demand control algorithm, which is the first DR approach, among the surveyed literature, to adopt frequent and instantaneous actions as new hourly price signals become available.
- Additional contribution is in designing a framework for the conjunction between demand controllers at the equipment level, building EMS, utility and smart meters,
- This study demonstrates the proposed methodologies using real measured data in simulation models, different than many work in literature where user-generated data are relied on.
- To best of the authors' knowledge, this study is the first to utilize the hour-ahead RTP tariff in DR for industrial buildings, which omits the reliance on price estimation or long period scheduling approaches unsuitable for the industrial buildings' dynamics. The surveyed work in literature had either utilized TOU, DAP, or forecasted tariffs.
- New methods for industrial consumer load clustering, which considers the unique periodic behaviors of industrial consumer and the ultimate goal of DR applications, are discussed with real field data in this study.

- A fuzzy genetic algorithm-based classifier is proposed in this study which outperforms classical methods for high dimensionality problems. The classifier is intended for the industrial consumer load profiling only.
- A 2-stage approach to DR is adopted in this study, which utilizes optimization methods from quadratic programming in discrete time and evolutionary programming in real-time. Both real DVs and integer DVs are modeled in this study, whereas, the DR problem in surveyed literature was solved as MILP or as a linearly approximated MINLP only for discrete time simulation.
- This is the first study to derive and utilize utility functions for task prioritization in DR. Previously, utility functions were mostly used in related-research for optimizing energy tariffs.
- In contrast to previous DR work, this study does not solve a single function of weighted objectives of cost and comfort. Alternatively, the second stage of the problem finds Pareto optimal solutions using evolutionary programming.
- Additionally, this study proposes a modification of the genetic algorithm (GA) for solving the multi-objective problem of the second stage. The customized solver is necessary due to the complexity of the nonlinear problem and the difficulty of implementing constraints to existing solvers. The creative coding structure for the solver reduces the dimensionality of the problem, the recursive process, and achieves convergence in real-time (i.e. instantaneously).
- The study develops a virtual testbed with a creative approach for integrating two independent simulation engines: a discrete agent-based simulation tool

and the system dynamics simulation paradigm where the handling of time is continuous.

Limitations

The work and results presented in this study have the following limitations:

- First, the discussed approaches are designed for medium to large industrial buildings, where large, variable, and bidirectional loads can be utilized in DR. Although the same methods can be adjusted and applied for the smaller residential buildings, we have not conducted such investigations or collected residential data.
- Second, this study uniquely considers the RTP-HA tariff for driving DR. However, we have not considered other tariff types or tariff-free signals as options for DR. It must be noted that the RTP-HA is not as popular as the DAP or other tariffs in the deregulated energy markets.
- Third, the definition of "Optimality" in this study is limited to the attainable results in the current, short period of time (i.e. 2-hours). However, specifically with energy storage systems, if the impact of these optimal short-term solutions on future unforeseen solutions is to be taken into consideration, then the optimality of the current solutions may not hold. To consider the future impacts, high reliance on price and load forecasts would be required.
- Fourth, this study assumes that the consumer has already an automated building equipped with reliable EMS, which is capable of reading building data and communicating setpoints or operation signals to the various equipment in real-time. In reality, this level of advancement is only found at

very few and very large consumers. Therefore, the applicability of the proposed methodology to most consumers may first require a significant capital investment in building automation and state-of-the-art EMS.

Implementation and Future Work

Discussion for Implementation

Although real data and realistic building simulation models were utilized in this study, much of the work remained theoretical without physical experimentation. This section aims to define the conceptual design of our proposed system as it was intended; The system is to be applied as an add-on to large building with existing EMS. A schematic representation of the conceptual design is provided in Figure 8-1. The core of the system is implemented as a live software, which reads inputs from various devices and ports, calculates operation setpoint, and accordingly adjusts EMS settings, which would have alternatively needed frequent user interference. The first type of inputs is the RTP-HA data, which are available in real-time via a secure internet connection with the utility provider. The second type of inputs are the load states (e.g. indoor temperature, EV battery level, etc.), which would be provided from either the EMS or plug-and-play ports. The third type of inputs is the service schedules for EVs, which require manual entry from the shipping dock operator as new EVs enter or depart the system. This data can be provided wirelessly from the operator's smart device. The fourth type of inputs is the loads data, which require user-installed sub-metering devices with RFID wireless transmission. The sub-metering devices are essentially distributed to separate the building's base load from the controllable loads (e.g. HVAC and EV loads). The received load data are stored in data storage memory, which the software utilizes for forecasting

future loads and periodically adjusting the forecast model parameters. Given all the data and communications, the software can then perform all of the: Stage-1 aggregate load target optimization, the real-time disaggregate load utility calculations, and the final optimization of disaggregate loads.

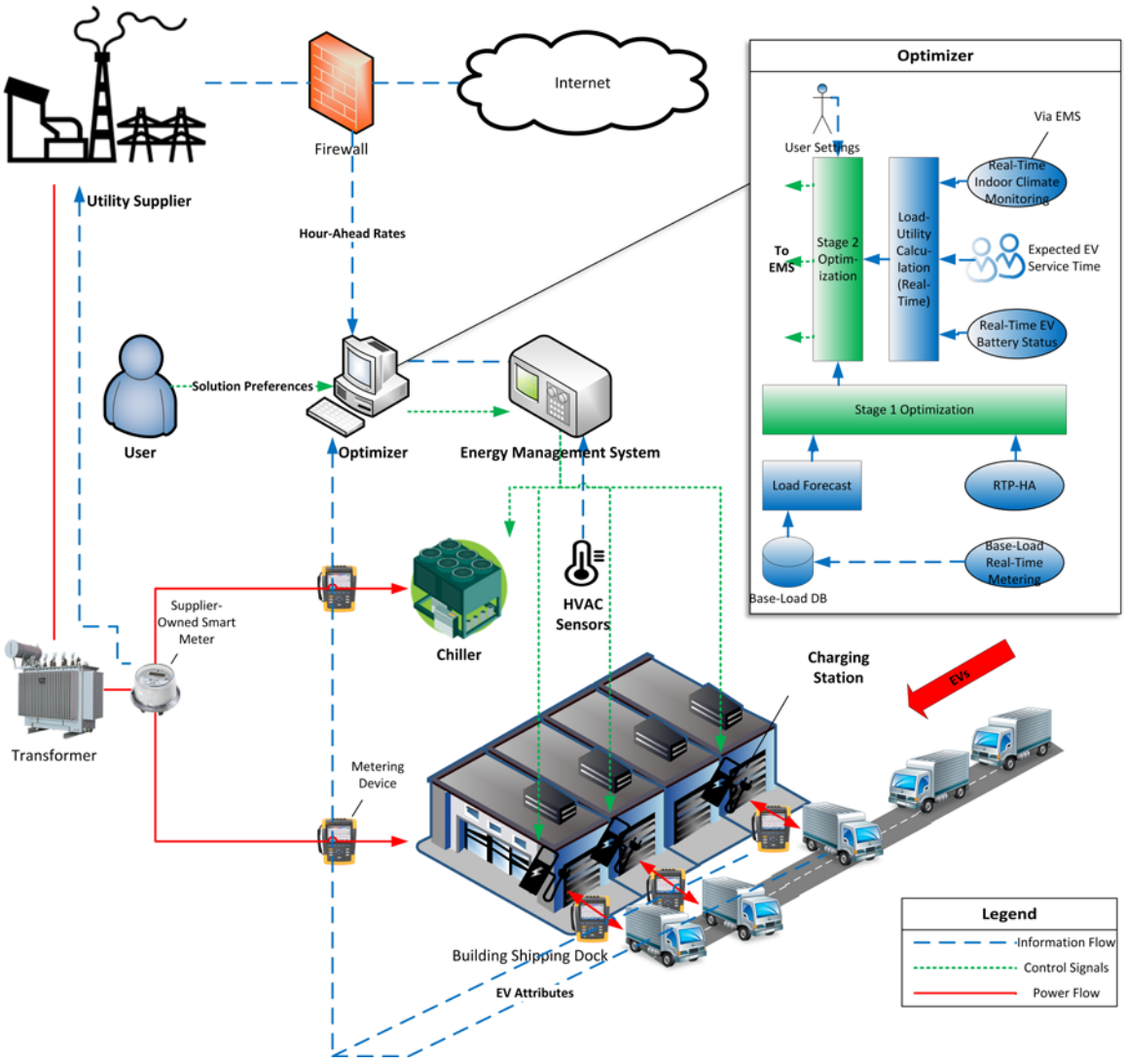

Figure 8.1. Implementation framework of the proposed system for a building with existing EMS.

Discussion for Future Work

Several opportunities for future work are identified in this study. First, practical experimentation of the proposed controller is missing, where we had only relied on

virtual models reinforced with real data. Second, the load synchronization problem is not fully addressed. In order to tackle the supplier-side impact, research focus on tariff optimization and DR programs or policies is required. Third, we had only considered three types of loads: cooling, B2V, and V2B. While the inclusion of V2B is a seldom addition to the DR research, several other DR opportunities were left to future work, including: standby generators, thermal storage systems, air compressors, employee EV, etc. Fourth, the controller assumes only one supplier, while distributed energy generation is expected to grow in the future and multiple suppliers mays coexist. Thus, the DR controller may also be utilized for optimizing the amount of purchased energy from each supply source. Finally, the controller is designed for the single facility loads. Alternatively, we may consider a community DR controller where several facilities collaborate together in their DR participation to achieve a mutual goal.

References

1. Armaroli, N. and V. Balzani, *Towards an electricity-powered world.* Energy & Environmental Science, 2011. **4**(9): p. 3193.

2. PJM. *Real-Time Energy Markets*. Available from: https://www.pjm.com/markets-and-operations/energy/.

3. Bajpai, P. and V. Dash, *Hybrid renewable energy systems for power generation in stand-alone applications: A review.* Renewable and Sustainable Energy Reviews, 2012. **16**(5): p. 2926-2939.

4. Chauhan, A. and R.P. Saini, *A review on Integrated Renewable Energy System based power generation for stand-alone applications: Configurations, storage options, sizing methodologies and control.* Renewable and Sustainable Energy Reviews, 2014. **38**(0): p. 99-120.

5. Erdinc, O. and M. Uzunoglu, *Optimum design of hybrid renewable energy systems: Overview of different approaches.* Renewable and Sustainable Energy Reviews, 2012. **16**(3): p. 1412-1425.

6. Reihani, E., et al., *A novel approach using flexible scheduling and aggregation to optimize demand response in the developing interactive grid market architecture.* Applied Energy, 2016. **183**: p. 445-455.

7. Barbose, G., C. Goldman, and B. Neenan, *Electricity in real time - A survey of utility experience with real time pricing.* Energy (Norwalk, Connecticut), 2005. **30**(1): p. 14-18.

8. Allcott, H., *Real time pricing and electricity markets.* Harvard University, 2009.

9. Anvari-Moghaddam, A., H. Monsef, and A. Rahimi-Kian, *Cost-effective and comfort-aware residential energy management under different pricing schemes and weather conditions.* Energy and Buildings, 2015. **86**(0): p. 782-793.

10. Avci, M., et al., *Model predictive HVAC load control in buildings using real-time electricity pricing.* Energy and Buildings, 2013. **60**(0): p. 199-209.

11. Burke, W.J., *Control of residential load management networks using real time pricing*. 2010, University of California, Berkeley: Ann Arbor. p. 91.

12. Conejo, A.J., J.M. Morales, and L. Baringo, *Real-time demand response model.* IEEE Transactions on Smart Grid, 2010. **1**(3): p. 236-242.

13. Di Giorgio, A. and F. Liberati, *Near real time load shifting control for residential electricity prosumers under designed and market indexed pricing models.* Applied Energy, 2014. **128**(0): p. 119-132.

14. Fernandes, F., et al., *Dynamic load management in a smart home to participate in demand response events.* Energy and Buildings, 2014. **82**(0): p. 592-606.

15. Horowitz, S. and L. Lave, *Equity in residential electricity pricing.* The Energy Journal, 2014. **35**(2): p. 1-23.

16. Kiaee, S.M.S., et al. *Home load and solar power management under real-time prices*. in *Environment and Electrical Engineering (EEEIC), 2014 14th International Conference on*. 2014. Krakow.

17. Missaoui, R., et al., *Managing energy smart homes according to energy prices: Analysis of a Building Energy Management System.* Energy and Buildings, 2014. **71**(0): p. 155-167.

18. Mohsenian-Rad, A.-H. and A. Leon-Garcia, *Optimal residential load control with price prediction in real-time electricity pricing environments.* IEEE Transactions on Smart Grid, 2010. **1**(2): p. 120-133.

19. Özkan, H.A., *A new real time home power management system.* Energy and Buildings, 2015. **97**(0): p. 56-64.

20. Roscoe, A.J. and G. Ault, *Supporting high penetrations of renewable generation via implementation of real-time electricity pricing and demand response.* IET Renewable Power Generation, 2010. **4**(4): p. 369.

21. Schibuola, L., M. Scarpa, and C. Tambani, *Demand response management by means of heat pumps controlled via real time pricing.* Energy and Buildings, 2015. **90**(0): p. 15-28.

22. Setlhaolo, D. and X. Xia, *Optimal scheduling of household appliances with a battery storage system and coordination.* Energy and Buildings, 2015. **94**(0): p. 61-70.

23. Spees, K. and L. Lave, *Impacts of responsive load in PJM: Load shifting and real time pricing.* The Energy Journal, 2008. **29**(2): p. 101-121.

24. Tiptipakorn, S., et al. *Price naming on home appliance load controls in real-time pricing environment*. in *Power and Energy Society General Meeting, 2010 IEEE*. 2010. Minneapolis, MN.

25. Wei, Z. and A. Feliachi. *Residential load control through real-time pricing signals*. in *System Theory, 2003. Proceedings of the 35th Southeastern Symposium on*. 2003.

26. Wolak, F.A., *Residential Customer Response to Real-time Pricing: The Anaheim Critical Peak Pricing Experiment*. 2007.

27. Yoon, J.H., R. Baldick, and A. Novoselac, *Dynamic demand response controller based on real-time retail price for residential buildings.* IEEE Transactions on Smart Grid, 2014. **5**(1): p. 121-129.

28. Yoon, J.H., R. Bladick, and A. Novoselac, *Demand response for residential buildings based on dynamic price of electricity.* Energy and Buildings, 2014. **80**(0): p. 531-541.

29. Bingjie, R., et al. *Demand response under real-time pricing for domestic energy system with DGs*. in *Power System Technology (POWERCON), 2014 International Conference on*. 2014.

30. Althaher, S.Z. and J. Mutale. *Management and control of residential energy through implementation of real time pricing and demand response*. in *Power and Energy Society General Meeting, 2012 IEEE*. 2012.

31. Dongdong, L., et al. *Design and load control strategy of smart domestic electric system*. in *Intelligent Green Building and Smart Grid (IGBSG), 2014 International Conference on*. 2014.

32. Shirazi, E. and S. Jadid, *Optimal residential appliance scheduling under dynamic pricing scheme via HEMDAS.* Energy and Buildings, 2015. **93**(0): p. 40-49.

33. Surles, W. and G.P. Henze, *Evaluation of automatic priced based thermostat control for peak energy reduction under residential time-of-use utility tariffs.* Energy and Buildings, 2012. **49**: p. 99-108.

34. Alimohammadisagvand, B., et al., *Cost-optimal thermal energy storage system for a residential building with heat pump heating and demand response control.* Applied Energy, 2016. **174**: p. 275-287.

35. Anees, A. and Y.-P.P. Chen, *True real time pricing and combined power scheduling of electric appliances in residential energy management system.* Applied Energy, 2016. **165**: p. 592-600.

36. Borenstein, S., *Customer risk from real-time retail electricity pricing: Bill volatility and hedgability.* The Energy Journal, 2007. **28**(2): p. 111-130.

37. Choi, W.H., A. Sen, and A. White, *Response of industrial customers to hourly pricing in Ontario's deregulated electricity market.* Journal of Regulatory Economics, 2011. **40**(3): p. 303-323.

38. Gomez-Villalva, E. and A. Ramos, *Optimal energy management of an industrial consumer in liberalized markets.* IEEE Transactions on Power Systems, 2003. **18**(2): p. 716-723.

39. Goyal, S. and P. Barooah, *A method for model-reduction of non-linear thermal dynamics of multi-zone buildings.* Energy and Buildings, 2012. **47**: p. 332-340.

40. Henze, G.P., et al., *Experimental analysis of model-based predictive optimal control for active and passive building thermal storage inventory.* HVAC&R Research, 2005. **11**(2): p. 189-213.

41. Kang, S.J., et al., *Scheduling-based real time energy flow control strategy for building energy management system.* Energy and Buildings, 2014. **75**(0): p. 239-248.

42. Pavlak, G.S., G.P. Henze, and V.J. Cushing, *Optimizing commercial building participation in energy and ancillary service markets.* Energy and Buildings, 2014. **81**: p. 115-126.

43. Bianchini, G., et al., *Demand-response in building heating systems: A Model Predictive Control approach.* Applied Energy, 2016. **168**: p. 159-170.

44. Yu, M., R. Lu, and S.H. Hong, *A real-time decision model for industrial load management in a smart grid.* Applied Energy, 2016. **183**: p. 1488-1497.

45. Zheng, T. and E. Litvinov, *On ex post pricing in the real-time electricity market.* IEEE Transactions on Power Systems, 2011. **26**(1): p. 153-164.

46. Kirschen, D.S., et al., *Factoring the elasticity of demand in electricity prices.* IEEE Transactions on Power Systems, 2000. **15**(2): p. 612-617.

47. Samadi, P., et al., *Real-time pricing for demand response based on stochastic approximation.* IEEE Transactions on Smart Grid, 2014. **5**(2): p. 789-798.

48. Jokic, A., P.P.J. Van den Bosch, and M. Lazar. *Distributed price-based optimal control of power systems*. in *Control Applications, 2007. CCA 2007. IEEE International Conference on*. 2007. Singapore.

49. Laboratory, L.L.N. *Energy Flow Chart*. Available from: https://www.llnl.gov/.

50. Olivieri, S.J., et al., *Evaluation of commercial building demand response potential using optimal short-term curtailment of heating, ventilation, and air-conditioning loads.* Journal of Building Performance Simulation, 2013. **7**(2): p. 100-118.

51. Barooah, P., A. Buic, and S. Meyn. *Spectral Decomposition of Demand-Side Flexibility for Reliable Ancillary Services in a Smart Grid*. in *System Sciences (HICSS), 2015 48th Hawaii International Conference on*. 2015.

52. Hao, H., et al., *Ancillary service to the grid through control of fans in commercial building HVAC systems.* IEEE Transactions on Smart Grid, 2014. **5**(4): p. 2066-2074.

53. Lin, Y., et al., *Demand Side Frequency Regulation from Commercial Building HVAC Systems: An Experimental Study.* 2015.

54. Meyn, S.P., et al., *Ancillary Service to the Grid Using Intelligent Deferrable Loads.* IEEE Transactions on Automatic Control, 2015. **60**(11): p. 2847-2862.

55. Yashen, L., P. Barooah, and J.L. Mathieu. *Ancillary services to the grid from commercial buildings through demand scheduling and control*. in *American Control Conference (ACC), 2015*. 2015.

56. Yashen, L., et al. *Demand side frequency regulation from commercial building HVAC systems: An experimental study*. in *American Control Conference (ACC), 2015*. 2015.

57. Lin, Y., et al., *Experimental evaluation of frequency regulation from commercial building HVAC systems.* IEEE Transactions on Smart Grid, 2015. **6**(2): p. 776-783.

58. Zhao, P., et al., *Dynamic frequency regulation resources of commercial buildings through combined building system resources using a supervisory control methodology.* Energy and Buildings, 2015. **86**: p. 137-150.

59. Zhao, P., et al., *Evaluation of commercial building HVAC systems as frequency regulation providers.* Energy and Buildings, 2013. **67**: p. 225-235.

60. Greensfelder, E.M., G.P. Henze, and C. Felsmann, *An investigation of optimal control of passive building thermal storage with real time pricing.* Journal of Building Performance Simulation, 2011. **4**(2): p. 91-104.

61. Borenstein, S., *The long-run efficiency of real-time electricity pricing.* The Energy Journal, 2005. **26**(3): p. 93-116.

62. Philpott, A.B. and E. Pettersen, *Optimizing demand-side bids in day-ahead electricity markets.* IEEE Transactions on Power Systems, 2006. **21**(2): p. 488-498.

63. Holland, S.P. and E.T. Mansur, *Is real-time pricing green? The environmental impacts of electricity demand variance.* The Review of Economics and Statistics, 2008. **90**(3): p. 550-561.

64. Faria, P. and Z. Vale, *Demand response in electrical energy supply: An optimal real time pricing approach.* Energy, 2011. **36**(8): p. 5374-5384.

65. Faruqui, A. and J. Palmer, *Dynamic Pricing and Its Discontents.* Regulation, 2011. **34**(3): p. 16-22.

66. Power, A. *Real-Time Pricing, Hour Ahead*. [cited 2015 8/2]; Available from: http://www.alabamapower.com/.

67. Power, G. *Real Time Pricing (RTP) – Day Ahead*. 8/2/2015]; Available from: http://www.georgiapower.com/.

68. Abdulaal, A. and S. Asfour, *A linear optimization based controller method for real-time load shifting in industrial and commercial buildings.* Energy and Buildings, 2016. **110**: p. 269-283.

69. CEC, *California energy demand 2014 - 2024 preliminary forecast*. 2013, California Energy Commission.

70. Park, D.C., et al., *Electric load forecasting using an artificial neural network.* Power Systems, IEEE Transactions on, 1991. **6**(2): p. 442-449.

71. Nan, F., et al., *The forecasting accuracy of electricity price formation models.* International Journal of Energy and Statistics, 2014. **02**(01): p. 1-26.

72. *Open Energy Information*. Available from: en.openei.org.

73. Chen, C.S., J.C. Hwang, and C.W. Huang, *Application of load survey systems to proper tariff design.* IEEE Transactions on Power Systems, 1997. **12**(4): p. 1746-1751.

74. Mahmoudi-Kohan, N., M.P. Moghaddam, and M.K. Sheikh-El-Eslami, *An annual framework for clustering-based pricing for an electricity retailer.* Electric Power Systems Research, 2010. **80**(9): p. 1042-1048.

75. Mahmoudi-Kohan, N., et al., *A three-stage strategy for optimal price offering by a retailer based on clustering techniques.* International Journal of Electrical Power & Energy Systems, 2010. **32**(10): p. 1135-1142.

76. Andersen, F.M., H.V. Larsen, and T.K. Boomsma, *Long-term forecasting of hourly electricity load: Identification of consumption profiles and segmentation of customers.* Energy Conversion and Management, 2013. **68**: p. 244-252.

77. Misiti, M., et al., *Optimized clusters for disaggregated electricity load forecasting.* Revstat-Statistical Journal, 2010. **8**(2): p. 105-+.

78. Sadeghi Keyno, H.R., et al., *Forecasting electricity consumption by clustering data in order to decline the periodic variable's affects and simplification the pattern.* Energy Conversion and Management, 2009. **50**(3): p. 829-836.

79. Bidoki, S.M., N. Mahmoudi-Kohan, and S. Gerami. *Comparison of several clustering methods in the case of electrical load curves classification*. in *Electrical Power Distribution Networks (EPDC), 2011 16th Conference on*. 2011. Bandar Abbas: IEEE.

80. Bidoki, S.M., et al. *Evaluating different clustering techniques for electricity customer classification*. in *Transmission and Distribution Conference and Exposition, 2010 IEEE PES*. 2010. New Orleans, LA, USA.

81. Binh, P.T.T. and L.D. Tuong. *Clustering the behaviour of electricity consumption*. in *IPEC, 2012 Conference on Power & Energy*. 2012. Ho Chi Minh City.

82. Chicco, G., *Overview and performance assessment of the clustering methods for electrical load pattern grouping.* Energy, 2012. **42**(1): p. 68-80.

83. Chicco, G., R. Napoli, and F. Piglione, *Comparisons among clustering techniques for electricity customer classification.* IEEE Transactions on Power Systems, 2006. **21**(2): p. 933-940.

84. Ford, V. and A. Siraj. *Clustering of smart meter data for disaggregation*. in *Global Conference on Signal and Information Processing (GlobalSIP), 2013 IEEE*. 2013. Austin, TX.

85. Hernández, L., et al., *Classification and clustering of electricity demand patterns in industrial parks.* Energies, 2012. **5**(12): p. 5215-5228.

86. In Hyeob, Y., et al. *A method for classification of electricity demands using load profile data*. in *Computer and Information Science, 2005. Fourth Annual ACIS International Conference on*. 2005. Jeju Island, South Korea.

87. McLoughlin, F., A. Duffy, and M. Conlon, *A clustering approach to domestic electricity load profile characterisation using smart metering data.* Applied Energy, 2015. **141**(0): p. 190-199.

88. Depuru, S.S.S.R., L. Wang, and V. Devabhaktuni, *Electricity theft: Overview, issues, prevention and a smart meter based approach to control theft.* Energy Policy, 2011. **39**(2): p. 1007-1015.

89. Abdulaal, A. and S. Asfour. *A Fuzzy Genetic Algorithm Classifier: The Impact of Time-Series Load Data Temporal Dimension on Classification Performance*. in *Machine Learning and Applications (ICMLA), 2016 15th IEEE International Conference on*. 2016. IEEE.

90. Abdulaal, A., J. Buitrago, and S. Asfour. *Electric Load Pattern Classification for Demand-side Management Planning: A Hybrid Approach*. in *Software Engineering and Applications: Advances in Power and Energy Systems; Press, A., Ed*. 2015. Marina del Rey, USA.

91. Buitrago, J., A. Abdulaal, and S. Asfour, *Electric load pattern classification using parameter estimation, clustering and artificial neural networks.* International Journal of Power and Energy Systems, 2015. **35**(4): p. 167-174.

92. Lagarias, J.C., et al., *Convergence properties of the Nelder--Mead simplex method in low dimensions.* SIAM Journal on Optimization, 1998. **9**(1): p. 112-147.

93. Lloyd, S., *Least squares quantization in PCM.* IEEE transactions on information theory, 1982. **28**(2): p. 129-137.

94. Rousseeuw, P.J., *Silhouettes: A graphical aid to the interpretation and validation of cluster analysis.* Journal of Computational and Applied Mathematics, 1987. **20**: p. 53-65.

95. Wang, P., *Pattern-recognition with fuzzy objective function algorithms-Bezdek, JC*. 1983, Siam Publications 3600 Univ City Science Center, Philadelphia, PA 19104-2688.

96. Yu, M. and S.H. Hong, *Supply–demand balancing for power management in smart grid: A Stackelberg game approach.* Applied Energy, 2016. **164**: p. 702-710.

97. Jin, M., et al., *MOD-DR: Microgrid optimal dispatch with demand response.* Applied Energy, 2017. **187**: p. 758-776.

98. Weckx, S., R. D'Hulst, and J. Driesen, *Primary and secondary frequency support by a multi-agent demand control system.* IEEE Transactions on Power Systems, 2015. **30**(3): p. 1394-1404.

99. Samadi, P., et al. *Optimal Real-Time Pricing Algorithm Based on Utility Maximization for Smart Grid*. in *Smart Grid Communications (SmartGridComm), 2010 First IEEE International Conference on*. 2010.

100. Abdulaal, A., et al., *Solving the multi-variant EV routing problem incorporating V2G and G2V options.* IEEE Transactions on Transportation Electrification, 2016. **PP**(99): p. 1-1.

101. Gould, N. and P.L. Toint, *Preprocessing for quadratic programming.* Mathematical Programming, 2004. **100**(1): p. 95-132.

102. Yu, R., W. Yang, and S. Rahardja, *A statistical demand-price model with its application in optimal real-time price.* IEEE Transactions on Smart Grid, 2012. **3**(4): p. 1734-1742.

103. Jensen, E.D., C.D. Locke, and H. Tokuda. *A Time-Driven Scheduling Model for Real-Time Operating Systems*. in *RTSS*. 1985.

104. Yoon, S.-G., et al., *Stackelberg-game-based demand response for at-home electric vehicle charging.* IEEE Transactions on Vehicular Technology, 2016. **65**(6): p. 4172-4184.

105. Tulabing, R., et al., *Modeling study on flexible load's demand response potentials for providing ancillary services at the substation level.* Electric Power Systems Research, 2016. **140**: p. 240-252.

106. Golden, B.L., E.A. Wasil, and P.T. Harker, *The analytic hierarchy process.* New York: Springier-Verlag, 1989.

107. Deb, K., *Multi-objective optimization using evolutionary algorithms*. Vol. 16. 2001: John Wiley & Sons.

108. Abdulaal, A., R. Moghaddass, and S. Asfour, *Two-Stage Discrete-Continuous Multi-Objective Load Optimization: An Industrial Consumer Utility Approach to Demand Response.* Applied Energy, 2017. **(Accepted for publication)**

109. Marquardt, D.W., *An algorithm for least-squares estimation of nonlinear parameters.* Journal of the Society for Industrial and Applied Mathematics, 1963. **11**(2): p. 431-441.

110. Press, W.H., *Numerical recipes 3rd edition: The art of scientific computing*. 2007: Cambridge University Press.

111. Buitrago, J. and S. Asfour, *Short-term forecasting of electric loads using nonlinear autoregressive artificial neural networks with exogenous vector inputs.* Energies, 2017. **10**(1): p. 40.